Study of triboelectric kinetic energy harvester with an asymmetric double variable capacitor implemented in a bennet doubler

Naida Hodzic

Université Gustave Eiffel

École doctorale MSTIC

Mathématiques, Sciences, et Technologies de l'information et de la communication

DOCTORAL THESIS

Thèse de doctorat

Specialty: Electronics, photonics and system

Génie électrique, électronique, photonique et systèmes

Presented by

NAIDA HODZIC

Study of a Triboelectric Kinetic Energy Harvester With an Asymmetric Double Variable Capacitor Implemented in a Bennet Doubler

Étude d'un convertisseur d'énergie mécanique par effet triboélectrique avec un double condensateur variable asymétrique mis en œuvre dans un doubleur de Bennet

---

Supervised by

Prof. Philippe BASSET

Soutenue le 7 décembre 2022

Jury:

Rapporteurs:	Prof. Elie LEFEUVRE	Université Paris-Saclay
	Assoc.Prof. Hatem SAMAALI	Université de Carthage
Examinatrice:	CdR Guylaine POULIN-VITTRANT	University of Tours
Directeur de thèse:	Prof. Philippe BASSET	Université Gustave Eiffel
Invités (co-encadrants):	MdC Dimitri GALAYKO	Sorbonne Université
	CdR Armine KARAMI	Université Gustave Eiffel

Acknowledgements

I would like to express my gratitude to all the people for their help and support throughout my Ph.D. First and foremost, I would like to thank my academic advisor Professor Philippe BASSET for his mentorship, council and support throughout my research. I deeply appreciate how you have been continuously encouraging and guiding me in the last three years, and also how you have always been supportive of all of my efforts and struggles. You gave me the opportunity to follow this path toward discovering research and science as a life call. It has been an honor and a privilege to work with you.

I would like to thank Mr. Armine Karami and Mr. Dimitri Galayko for advisory and assistance in carrying out the theoretical work that has been done during my Ph.D. The perspective that you brought changed my view on the theoretical part of this thesis.

I wish to thank members of the research team Ahmad Delbani and Srikumar Vaidyanathan; working with you has been a breeze and a great pleasure; and my office mates at ESIEE Paris Sreyash Sarkar and Mathieu Bourdeau for their kindness, help and talks that were truly necessary.

Amila, Arslana, Maida and Nedzla thank you for the unconditional support and patience that was needed throughout the years. I am eternally grateful for having you as friends. Without you, the past couple of years would not be possible.I am grateful for everything I have and for becoming the person I am today. All the challenges that this thesis has brought on have made me a stronger person.

I would like to sincerely thank my thesis defense committee members for agreeing to evaluate my work. Thanks to Professor Elie Lefeuvre and Mr. Hatem Samaali for agreeing to report my dissertation and improve my thesis with your thoughtful advice and valuable suggestions.

Finally, I dedicate this work to my mother.

Abstract

Energy harvesting is the process that involves converting otherwise unused energy present in our environment into usable electrical energy that can be used to power an electronic system. Electrostatic kinetic energy harvesters (eKEHs) utilize vastly present kinetic energy that originates either from an object in motion or vibrations and converts it into electrical energy. The employed principle is based on a polarized variable electrostatic capacitor. With an addition of a triboelectric layer between its plates and utilizing the triboelectrification effect, an eKEH is transformed into a triboelectric nanogenerator (TENG). This type of transducer accumulates charges by contact in the triboelectric layer which thus becomes an electret whose generated semi-permanent electric field allows a variation of the distribution of the electric charges in the electrodes by electrostatic induction.

Altering the architecture of a TENG by adding the third electrode, a single-capacitive transducer is converted into a double-capacitive TENG. Doubling the conversion element in a transducer is expected to increase the amount of converted energy. Chosen electronics circuit to condition obtained signal from the generator is Bennet's charge doubler. An increase without saturation point at the output of this circuit is the unique characteristic of this unstable charge pump. It reflects through an exponential increase of output voltage and a number of charges accumulated in the storage capacitor which increase (in theory) in an infinite way. This means that the surface of the charge-voltage cycle at the terminals of the TENG, and thus the converted energy of the mechanical domain, increases at each iteration of the mechanical cycle of the transducer.

The scope of this thesis encompasses the simulation, analytical and experimental research of Bennet's charge doubler with two asymmetric variable capacitors each containing a triboelectric layer. It is postulated that the performance of the "double TENG" - "double Bennet" system is superior to the classic Bennet's double. The results of analytical and simulation analysis have shown that the expected behavior of this circuit aligns with hypothesized performance results. The system has been tested experimentally. It is concluded that the results of the constructed system are relevant when compared with the reported performance of the classic "single-capacitive TENG" - "Bennet's doubler" system.

When compared with classic Bennet's doubler, double Bennet reaches the same voltage levels in less time. That is due to the advantage of double capacitive TENG which increases the number of accumulated charges per mechanical cycle. In analytical analysis, it was found that the two TENG capacitors are codependent and that in operation they affect one another.

The output signal of double Bennet is characterized by high voltages ranging from a few hundreds of volts to a few kilovolts (kV). To reduce the rectified output voltage to a level compatible with a commercial application, a Buck DC-DC converter is implemented. This requires a switch. This thesis proposes and studies the use of a high-voltage MEMS microplasma switch whose actuation voltages is defined by Paschen's law. Within the scope of this thesis, the theoretical and experimental studies of this law at the micrometer scale propose optimal actuation voltages for better management of the converted energy.

Résumé

La récupération de l'énergie est le processus qui consiste à convertir l'énergie inutilisée présente dans notre environnement en énergie électrique utilisable pour alimenter un système électronique. Les récupérateurs d'énergie cinétique à transduction électrostatique (eKEH) utilisent l'énergie cinétique présente dans l'environnement, qui provient d'un objet en mouvement ou de vibrations, afin de la convertir en énergie électrique. Le principe employé est basé sur un condensateur variable polarisé. En ajoutant une couche triboélectrique entre ses armatures et en créant un contact entre elles, un eKEH devient ce qui l'on appelle communément un nanogénérateur triboélectrique (TENG).

La modification de l'architecture d'un TENG par l'ajout d'une troisième électrode permet de transformer un transducteur à capacité simple en un TENG à capacité double. Le fait de doubler l'élément de conversion dans un transducteur doit permettre d'augmenter la quantité d'énergie convertie. Le circuit électronique choisi pour redresser le signal obtenu en sortie du générateur est le doubleur de Bennet. L'absence de tension de saturation en sortie de ce circuit est une caractéristique particulière de cette pompe de charge dite instable. Elle se traduit par une augmentation exponentielle de la tension de sortie et des charges accumulées dans le condensateur de stockage qui augmentent (en théorie) de manière infinie. Cela signifie que la surface du cycle charge-tension aux bornes du TENG, et donc l'énergie convertie du domaine mécanique, augmente à chaque itération du cycle mécanique du transducteur.

Cette thèse comprend l'analyse, la simulation et la démonstration expérimentale d'un doubleur de Bennet comportant deux capacités variables asymétriques incluant chacune une couche triboélectrique. Il est montré que les performances du système double TENG - double Bennet sont supérieures au doubleur de Bennet classique. L'étude analytique s'aligne sur les simulations. Le système a été testé expérimentalement. Il en est conclu que les résultats expérimentaux sont pertinents lorsqu'ils sont comparés aux performances du système classique d'un TENG mono-capacitif - Bennet simple. Par rapport au doubleur de Bennet classique, le double Bennet atteint les mêmes niveaux de tension en moins de temps. Cela est dû à l'avantage du double condensateur TENG qui augmente le nombre de charges accumulées par cycle mécanique. L'analyse a montré que les deux condensateurs TENG sont co-dépendants et qu'ils s'influencent mutuellement lorsqu'ils sont mis en fonction.

Le signal de sortie du double Bennet est caractérisé par des tensions élevées allant de plusieurs centaines à plusieurs milliers de volts. Pour abaisser la tension redressée en sortie à un niveau compatible avec une application commerciale, un convertisseur DC-DC de type Buck est implémenté. Celui-ci nécessite un interrupteur. Cette thèse propose et étudie l'utilisation d'un interrupteur haute-tension MEMS dit à micro-plasma dont la tension d'actionnement est définie par la loi de Paschen. Cette thèse se conclue par une étude théorique et expérimentale de cette loi à l'échelle micrométrique dans le but de proposer des tensions d'actionnement optimales pour une meilleure gestion de l'énergie captée.

Contents

List of Figures

List of Tables

1 Introduction to energy harvesting and power management

1.1 Introduction

This introduction chapter serves both as a general introduction to the field of electrostatic vibration energy harvesting (eKEH), and triboelectric nanogenerators (TENGs) as well as a presentation of the knowledge of electronics circuits used with the transducers that are going to be used throughout this manuscript. The chapter begins with an overview of the reasons for energy harvesting. It then proceeds to provide an example of the power management system that is used as a general guideline for adapting energy harvesters to commercial standards. Different energy harvesting systems have been identified and the focus is put on the eKEHs. The following sections proceed to explain the theoretical aspect of different modes of operations of an eKEH as well as a specific case of one using the triboelectric effect, the TENG. The chapter then goes on to describe the mechanical design of one and its electrical equivalent. Continuing, a theoretical overview of various charge pump circuits generally used in combination with eKEHs has been presented. Finally, the chapter concludes with a hypothesis of the study and a general overview of the research methods used to conduct it.

1.2 Energy harvesting and power management

The process of energy harvesting involves converting otherwise unused energy present in our environment into usable electrical energy. It is possible that this energy originated in the nature or was generated by a machine. Transducers are devices that convert energy from one form to another. They are guided by the energy conservation law that states that energy cannot be created nor destroyed, but transformed from one form to another. Based on the materials employed and the specificity of their design, they can harness different forms of energy and convert them into electrical one. The concept is based on the use of the rather redundant ambient energy that results in small amounts of electrical energy compared to traditional sources of it. Specifically designed transducers that convert energy and store it for later use like powering up commercially available electronic components are energy harvesters (EHs). To generate enough energy, continuous transduction is encouraged in energy harvesters, thus making them part of a self-sufficient electronic device.

There are numerous applications of energy harvesting from those in the buildings as part of assisted living systems and smart home systems [1], traffic monitoring [2], healthcare, wireless electronic devices [3], and in recent years the Internet of Things (IoT) [4] has been an area of significant advances. IoT represents a cluster of connected devices which communicate with one another and the cloud server which is then able to send and receive data to and from the end user. The connection between sensors, actuators, and other electronic devices is preferably wireless, which makes them independent of the network. To create stand-alone devices, most of them are powered by single-use batteries. With the advancements in energy harvesting, it is possible to expand the lifetime of these devices and make them truly stand-alone in the sense that each component of the network can power up itself.

1.3 Why energy harvesting?

Energy harvesters address important and extremely attractive topics such as energy efficiency, conservation of energy, waste management, and device maintenance. A single internet search reveals undeniable evidence about pollution and our ancestors' lifestyles, bringing global warming to our attention. In the present day, it is no longer acceptable to heavily rely on polluting energy sources. Increasingly, leading forces are turning to green energy and using as much of the non-invasive natural energy as possible.

In addition to becoming energy conscious, Moore's law kept us moving on the innova-

tion curve so fast that consumer electronics have become broadly accessible and replaceable. Changing a smartphone every year and buying a few new electronic gadgets for your home or yourself every year has become the norm. With fast production, the quality of available products is not guaranteed. Consequently, many products are simply discarded due to the trade-off between quality and price. The philosophy of today's leading companies does not include the repairability and serviceability of their products.

The management and reduction of waste is another burning issue of this generation. Moreover, specifically the chemical waste from batteries. Batteries provide energy to electronic devices is by a chemical reaction. Due to the volatile nature of chemical reactions and the potential faultiness of the packaging or assembly process, a single battery can cause a disaster due to its flammability and toxicity. No standardized procedures are in place worldwide to address handling battery waste.

Secondly, batteries have spatial issues. They tend to be bulky if they are to support the operation of devices for a long time. If a battery-operated sensor can work for a long time, and the manufacturer can assure that maintenance will not be necessary too frequently, or if electronic device requires a lot of energy to operate, the batteries have to be large. In most cases is not an acceptable situation. Today's trend is to have devices with multiple features which can only be done by the contracting size of the components to fit a size-restricted packaging. To suffice the energy demands of all components and meet lifespan expectancy, batteries show a tendency to be large.

In IoT and industrial environments, harsh conditions are ever-present. Devices placed in those environments will stay untouched after being added to the network. It is not practical nor advised to access them for a battery change every 5 years, or less [5]. This may be due to possible interference with system's performance because of its sensitivity or placement. In industry, sensors that operate on batteries are often placed in hard-to-get places or are even embedded in structures, which means that their maintenance requires specifically trained people.

The aforementioned issues are addressed by energy harvesting. The purpose of energy harvesting is to create continuous sources of energy that do not need to be replaced, charged or maintained. Physically, EH tends to occupy small areas, smaller than batteries that are generally used as reported by Holmes et al. in [6] and more recently by Du et al. in [7]. Fabrication materials are chosen so that their performance is maximized over long periods (years in this case). With new advancements, it is possible to upgrade already existing sensors to be powered by an EH, especially if the sensor is mobile or placed in a high concentration

of ambient energy. This has been the inspiration and starting point for the research.

The success and promise of future endeavors in the field of energy harvesting can be seen through a few successful companies that are placing their products on the market. For example, Kinetron [8] in the Netherlands produces gravity based weight systems as well as linear and rotational generator systems, and electromagnetic devices, and Perpetuum [9] in the UK works on vibration electromagnetic generators.

1.4 Power and energy management in energy harvesting

Energy harvesters work on the principle of continuous, but not regular, energy conversion whose output must be compliant with commercial standards for input signals. Consequently, it is necessary to manage the harvested power in a way that is compatible with the load it supplies. If the energy harvester's signal is not treated correctly, the input signal for the electronics component will not be in the correct form and transduction will be without any use. Therefore, it is very important to get the signal treated. There are a few steps that need to be taken to ensure that the output signal is compatible with commercially available electronics.

The first stage is the energy harvesting step at which a signal from the transducer is obtained. The signal produced at the output of the EH is a raw and uneven signal which, in most cases, tends to be nonlinear signal with high current or voltage peak values [10]. Ideally, the obtained signal would be rectified with a conditioning circuit, however, usually that is not sufficient to obtain a compatible signal with the load application. To shape the signal to an adequate form, a few stages are necessary which should include conditioning circuits like AC-DC converter and a DC stabilization module.

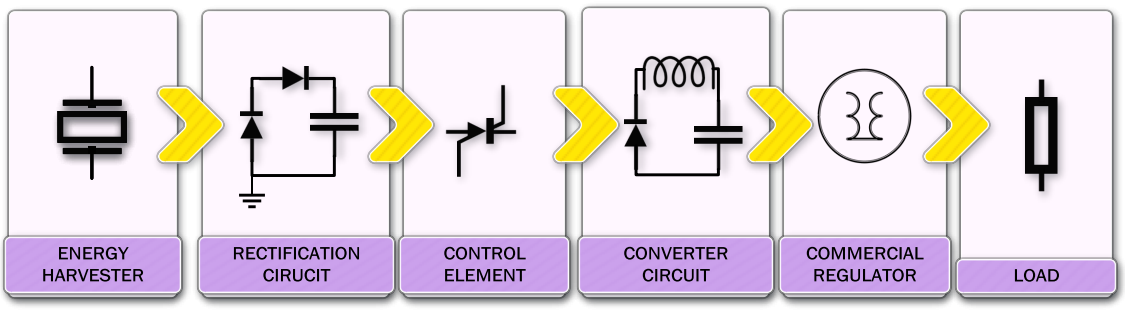

Figure 1: *Proposed 6-stage system for energy harvesting and management adapted for use with commercial components.*

Hence, conditioning of the obtained signal from an EH aims for the optimum signal that provides the maximum power is the second stage. The selection of the electronic circuit in this stage depends on the power level that is at its input and constraints criteria set by the shape of the signal. For example, whether the input signal is current or voltage dominant, or if it necessary to treat it. This can be done by:

- impedance matching [11]
- controlled switching with AC signals like Synchronized Switch Harvesting on Inductor (SSHI) [12] or Synchronous Electric Charge Extraction (SECE) circuits for piezoelectric and electromagnetic [13] EHs
- or basic conditioning circuits like diode-bridge rectifiers for eKEHs.

For eKEHs, that are the devices under study in this work, diode-bridge rectifiers should charge a small buffer capacitor at their output to a high DC voltage, corresponding to the optimum voltage of the circuit with the objective of maximization of accumulating converted energy per cycle. For instance, for the stable charge pumps, it is equal to half of the saturation voltage of a stable charge pump (Vsat/2) [14].

If optimal signal shape is obtained after this step, the signal can be supplied to the load. Otherwise, voltage signal leveling is necessary. With eKEH, a charged buffer capacitor reaches quickly high voltages for maximum conversion, and then a DC–DC converter stabilizes voltage and transfers the energy to a larger storage capacitor with low voltage. To safely and efficiently transfer energy from conditioning to conversion phase, the third stage in the signal treatment process is control circuit. It may include a motion-triggered mechanical switches [15] or an electrical [16] or electrostatic switches [17].

The fourth stage in the chain is the conversion or leveling stage. Pretreated signal fed to the input of this stage may need to be additionally rectified or its levels adjusted for the needs of the load. Input voltage or current signal is treated with DC-DC converters [18][17] for step-up or step-down adjustments to its levels that are supported by the load. After this stage the treated signal can be fed into an electronic component like a regulator that is attached to the load. In the following sections, the first three stages of energy and power management process will the examined in detail with attention put on the conditioning circuit and its performance.

1.5 The classification

Light, heat, airflow, vehicle or human movement, chemical reaction, and electromagnetic waves are some of the diverse sources of ambient energy. Energy harvesters differ one from another by their source of energy such that, they can be segmented into the following categories:

- photovoltaic,
- thermoelectric,
- electromagnetic
- induction,
- and kinetic energy harvesters. [1]

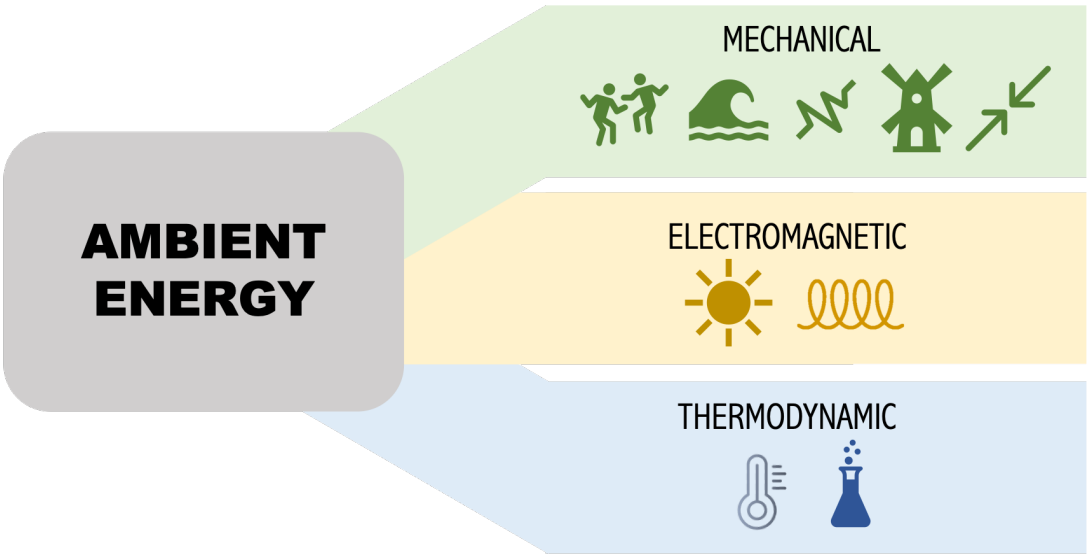

Figure 2: *The three forms of ambient energy used in energy harvesting: mechanical (human movement, bodies of water, vibrations, wind and pressure), electromagnetic (solar energy and induction) and thermodynamic (temperature gradient and chemical reactions).*

All of the said energy harvesters use different physical phenomena from nature and in the end, give the same output – electrical energy. To do so, each system is tailored with its design and use of distinctive materials to meet the needs that are set by said conversion mechanism.

Photovoltaics are a family of energy harvesters that utilize light, natural sunlight or ambient light as a source of energy that is then transformed into electrical with the use of a photovoltaic (PV) cells. This EH cluster has a very high scientific and commercial interest as they are studied a lot and widely implemented. The efficiency of one such unit depends on its sensitivity,

size, incident angle of light and type of cell – there is a difference between ambient and sunlight PV cells. These types of EHs have harvesting power in the range of tens of micro-Watts to a few milli-Watts. [1]

A specific configuration of two dissimilar semiconductors or conductors, i.e., n- and p-type semiconductors, when exposed to the temperature gradient engage in the Seebeck effect and convert thermal energy into electrical. The difference in temperature between the two sides of the transduction module is directly proportional to the amount of converted energy. Different configurations of two types of semiconductors target different outputs, voltage or current. Similar to photovoltaics, thermoelectric devices are commercially available in different sizes, from the centimeter scale to a millimeter size for provisioned applications and conversion rates. The power density of such EH is approximately 10 $\mu W/cm^3$.[1]

All electronic devices that are around us, emit electromagnetic (EM) waves. Most waves that are present in an average living or work environment are on the radio frequency and are therefore known as RF waves. Waves produced by computer networks (Wi-Fi, smartphones, tablets and laptops), radio and television and telecommunications (GSM, 4G and 5G) are picked up by a system of dedicated RF antennas and rectifiers, called RF energy harvesters, which convert them into AC currents that are later rectified into usable DC signals. The relevance of this family of harvesters is brought into question as they have low-efficiency rates. Some report rates as low as 0,8% to about 20% at most, where the sensitivity of the transducer to a certain frequency band plays an important role. Reports state that converted power is on the scale of a few hundred micro-Watts.[1]

Another energy type that is largely present in our surroundings is kinetic energy or energy of movement. Bodies in motion are used as kinetic energy sources caused by human body in motion, waves, airflow, vibrations or pressure. Kinetic energy harvesters are a type of EHs specifically constructed to convert mechanical movement when placed in such environments. Energy sources can be harmonic like an object that oscillates, or non-harmonic, like a moving car. Kinetic energy harvesters can be separated into three groups: piezoelectric, electromagnetic, and electrostatic EHs. [3]

Based on the concept of piezoelectricity discovered by Jacques and Pierre Curie which states that electricity is to be generated when mechanical stress, either tension or compression, is applied to crystallographic structures, piezoelectric generators are engineered. They vary in size, from micrometer to centimeter scale and are constrained by the direction of the mechanical stress applied as well as the durability of used materials like PZT [19] or PVDF [20]. [21] reports that a piezoelectric generator driven by human walking can generate up to

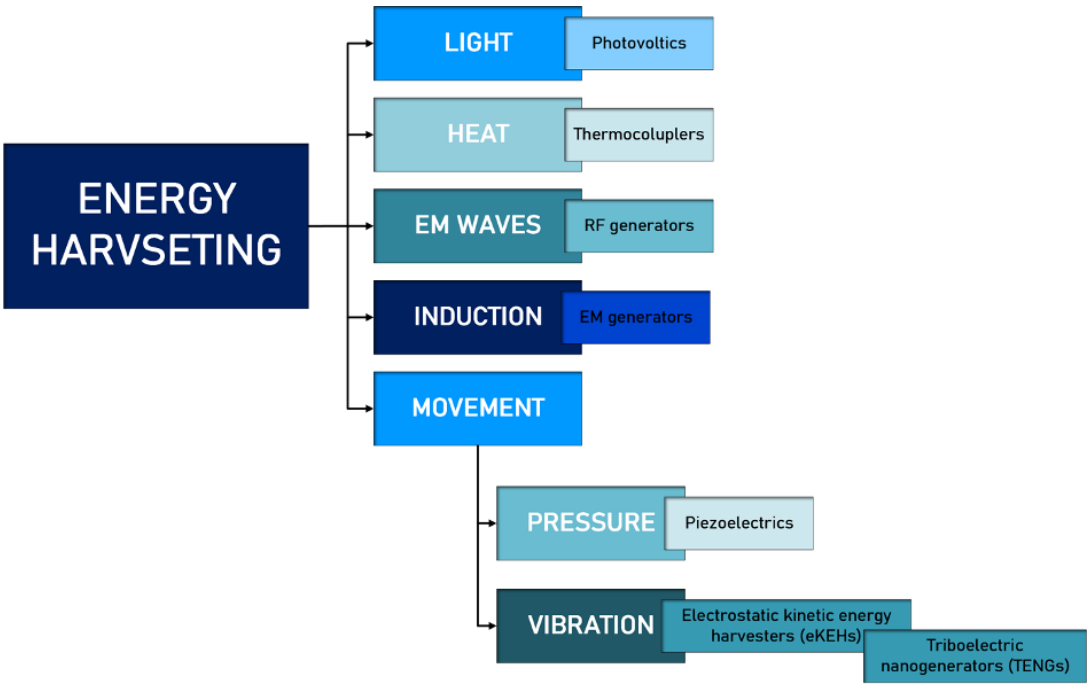

Figure 3: *A map of energy harvesting based on energy source. It includes: light, hear, electromagnetic waves, induction and movement. Movement can come in a form of pressure (piezoelectric) and vibrations (eKEHs).*

tens of milli-watts, while a smaller device like the one reported by [22] that is in the micrometer range generates up to a couple of micro-watts. It is important to note here that power output is highly dependent on the materials used.

Electromagnetic generators are based on Faraday's induction principle which states that an alternating magnetic field induces a current in an inductor. EH on this principle can be made with a beam oscillating coil and a magnet. A few commercial options from Europe are available which are targeting very specific applications or specific operating conditions. EHs can produce from a couple of hunters of micro-Watts to tens of milli-watts of power, depending on their design.[3]

Electrostatic kinetic energy harvesters (eKEHs) are based on the concept of a biased capacitor and its variable parameters inducing energy conversion. They are efficient mostly at small scale; thus, a large focus is on implementing them as microelectromechanical systems (MEMS). [22] reports the predictions of conversion in tens of micro-watts, whereas the practical devices reported in [23] have a rate of 450 nanojoules per cycle. A detailed description of the operation mechanisms of eKEHs is presented in the following sections.

1.6 Concept of an electrostatic kinetic energy harvester (eKEH)

Kinetic energy harvesters, as previously mentioned, work on the principle of a variable capacitor. It refers to the fact that the structure of the capacitor is used for transduction. Typically, they are composed of two conductive plates that are placed face-to-face. The plates are positioned at a controlled distance that can be filled with air, vacuum or a specifically chosen dielectric material. An expression defining the fundamental behavior of a capacitor is the following:

$$C = \varepsilon_0 \varepsilon_r \frac{A}{d} \tag{1}$$

where ε_0 is the dielectric permittivity of vacuum, ε_r represents the relative permittivity of medium between conductive plates, A is the effective surface area of the capacitor's overapping electrodes and d is the distance between conductive plates.

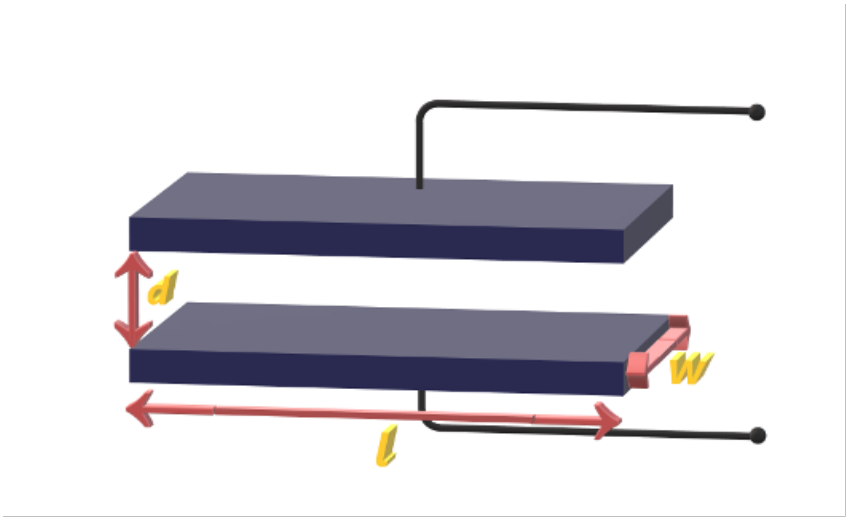

Figure 4: *Physical parameters necessary to calculate the capacitance of one: length of a plate, l, width w of it and distance d between two parallel plates.*

An inert capacitor, from an electrostatic point of view, is considered a charge-neutral element. There is an equal amount of change on both conductive plates. One plate is positively charged and the other one is negatively charged. The initial stability of the capacitance is electrically relevant for the assessment of potential and charge levels during the transduction process as a known initial condition. A charge stored in a capacitor can be expressed as a product of its capacitance and voltage over it:

$$Q = CV. \tag{2}$$

External force, caused by the excitation of kinetic energy near the transducer or directly to it, affects the transduction capacitor in the way that a property which defines its capacitance is varied. To do so, the design of the classic capacitor is modified so that one of the plates of the capacitor is fixed and the other one is mobile. The mobility of one of the electrodes allows for the external force to make an effect on the capacitor value. The two parameters that can be modified by a force applied to the structure are A, the effective surface area of the electrodes, and d, the distance between them. The change in either of those results in a change of capacitance which allows the form of electromechanical transduction.

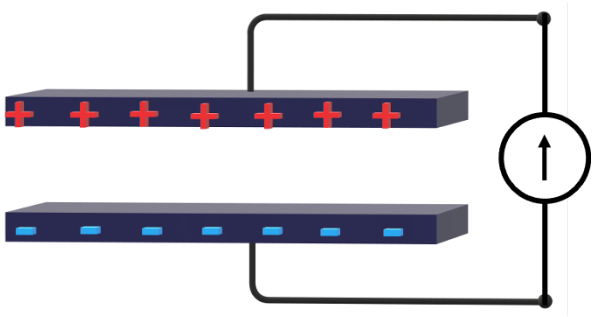

Figure 5: *Polarization of capacitor's plates, one plate concentrating all positive charges while the other plate contains all negative charges.*

Nevertheless, a necessary initial condition needs to be satisfied for a variable capacitor to be called an eKEH. To start the transduction process, the capacitor needs to be biased by a DC voltage source. This is to create a potential difference between the two capacitor plates and create varying electric fields with the capacitor variation. Supplying a transducer with a DC voltage in the applicative stage of the research and implementation might be presented as an inconvenience. Consequently, researchers opted for a construction solution so that eKEHs have a built-in voltage that is integrated. That is accomplished with materials that have good charge accumulating and storing properties. Those materials are called electrets. On account of their charge storing property can act as permanent voltage sources. The concept of these materials and their specific usage are detailed in the following sections. [14]

1.6.1 Classification of eKEHs

An eKEH can be subjected to external stimuli from any direction. Based on its design, the stimulus propagates to a transduction mechanism in different ways resulting in the force applied to it being lateral, transversal or rotational. Derived from the direction of the applied force, KEHs can be divided into the following categories:

- in-plane overlapping,

- gap-closing, and
- rotational KEHs

each having unique design properties specific to it. The following sections explain in great detail the modes of operation of each of the three types of KEHs.

1.6.2 Physics of in-plane overlapping eKEHs

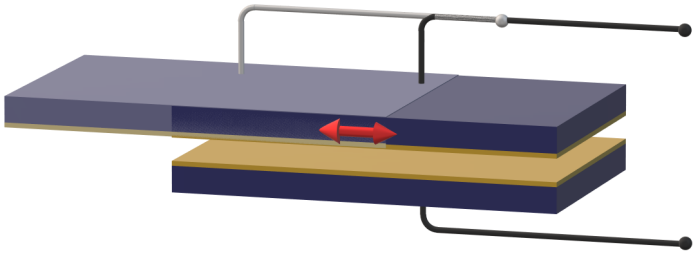

Figure 6: *A model of an in-plane overlapping eKEH demonstrating the sliding movement of the mobile electrode.*

In-plane overlapping KEHs, or as referred to in [24] as sliding KEHs, are the eKEHs based on the capacitor that has one of its plates moving in one of the directions of the two-dimensional system. In this case, the changing parameter of the capacitance expression is the effective surface area of the capacitor, A. Based on the shape of electrodes, for example, a rectangular shape, the two components calculated are the length of the electrode, l, and width of it, w, the capacitance expression can be rewritten to:

$$C = \varepsilon_0 \varepsilon_r \frac{l(w_0 \pm w)}{d} \tag{3}$$

where w_0 is the initial overlapping width of the electrodes when the capacitor is at rest and w is the change in the width that can be added or subtracted from the initial value based on the direction of the movement of the electrode. This formula is only valid if the distance between electrodes is significantly smaller than a possible change of the width in the electrode or other words displacement, $d \ll w_0 \pm w$.

When $\Delta w = w_0 \pm w = 0$, the overlapping area is equal to zero, capacitance is the smallest for that system, $C_{\min}$. Based on the physical parameters of the eKEH, when Δw is maximum, capacitance is equal to $C_{\max}$. If occurring phenomena were additionally neglected, $C_{\min}$ would be equal to zero. Nevertheless, this case would be considered flawed because of the significance of impact of the fringe effect, coplanar capacitance and diagonal capacitance.

To maximize the variation of area, electrodes of sliding eKEHs are designed as arrays of connected strips. The top and the bottom electrodes form a three-dimensional (3D) comb-like structure. The space between two fingers is defined by the technology used for fabrication (or my design to maximize device performance) to fit the maximum and minimum capacitance criteria for the transducer. Once a mobile electrode is subjected to the external stimulus, it moves between states of complete overlap to complete the misalignment of two capacitors' electrodes. It was quickly realized that the space between the fingers of the fixed electrode could be used to create another counter electrode. This led to the development of three electrode systems. The benefit of the additional electrode can be interpreted as the presence of a second transduction system within the same space of the device, increasing the amount of recovered energy.

1.6.3 Physics of rotational eKEHs

Rotational eKEHs have been around since self-winding watches were invented. Nevertheless, the concept was popularized as an energy harvesting system in the last two decades by a research group from the University of Tokyo group [25]. There were a few variations of this eKEH's design, thus the one that has been developed the most is one reported by [26]. This class of eKEHs is a variation of the in-plane overlapping harvesters with the change of direction of applied force. They are often placed in environments with significant rolling like running water like rivers, or on pendulum-like structures which is a human hand.

For the effective and sustainable energy conversion of applied rotational force, design adjustments to the transducer are required. Both mobile and fixed plates are attached to the central axis of rotation. When the rotational force is applied to the transducer its mobile electrode will rotate resulting in capacitance variation and therefore charge induction. The expression for the capacitance of this class of eKEHs is more complex as the shape of the electrodes cannot be taken as simple rectangles. To fit the largest number of electrodes, it is necessary to fabricate triangular electrodes that will fill up the circular space the best.

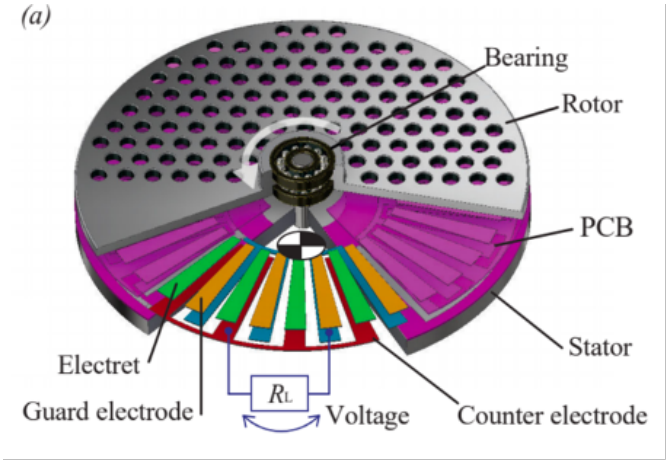

Figure 7: *An example of a rotary eKEH reported by T. Miyoshi, et al., [27]*

1.6.4 Physics of gap-closing eKEHs

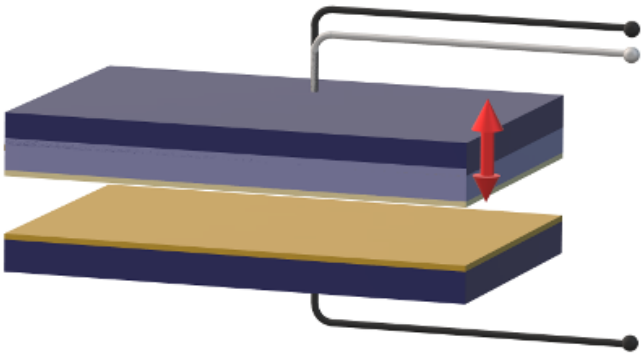

Figure 8: *A model of gap-closing eKEH demonstrating the misplacement of mobile electrode.*

Contrary to the two systems presented in previous subsections, gap-closing eKEHs are subjected to the force applied in the y-direction in a two-dimensional system. In this case, the varying parameter of the capacitance expression is d, the distance between the capacitor's plates. We can consider that one plate of the capacitor, for example, the bottom one, is affixed to the structure of the transducer, while the other one is mobile. When an external force is applied to the system transversally, the mobile plate is displaced from its inert position. The displacement causes the change in distance between the plates which is inversely proportional to the capacitance. The capacitance expression can be rewritten to:

$$C = \varepsilon_0 \varepsilon_r \frac{A}{d_0 \pm d} \tag{4}$$

where d_0 is the initial distance between electrodes when the capacitor is at rest and d is the change in the distance. d is added or subtracted from the initial value based on the direction of the movement of the electrode which can be upwards or downwards.

Firstly, when two plates are brought in the state of a minimum distance between them, without being in contact, the capacitance will be the largest ($C_{\max}$). When the plates are brought closer than critical proximity an occurrence of the pull-in effect is possible. That is the phenomenon that materializes if two conductors at different potentials are placed in close proximity to one another. Then the electric field formed by potential difference results in conducts being physically pulled to contact.

Secondly, when the mobile plate is forced to the maximum allowed distance (that is defined by the physical parameters and limitations of the transducer) from the other plate, the smallest capacitance ($C_{\min}$) is measured. Taking a mobile plate infinitely far away from the fixed one would give the absolute minimum capacitance value i.e., the parasitic one; thus, the realistic and measured values are defined. The two extrema show the inverse proportionality of the distance between plates and eKEH's capacitance.

If the nature of the applied force is known, its effects can be directly added to the equation by defining the change of the distance through time in the shape that the force is taking. Additionally, the effects of a possible change of the medium between the plates are accounted for by a relative distance which is a ratio between d and ε_r.

These systems are often implemented in environments where up and down movements are common, for example in mechanical (light) switches, roads, sidewalks, etc. Based on the size of them and the frequency of their movement, they generate different power levels.

1.7 Introduction to triboelectric nanogenerators (TENGs)

One of the directions that is taken to improve the performance of eKEHs is the addition of built-in voltage. It is done by adding the electret layer to the structure of the transducers. For the energy conversion to happen, the layer has to be pre-charged either by, for instance, using a soft x-ray, e-beam or by corona discharge. That way the electret layer can store charge in its structure. Soon, scientists started exploring another way to charge the electret layer, which is by the natural mechanical movement of the eKEH and the use of the process of triboelectrification. This way, some eKEHs have evolved into triboelectric nanogenerators

(TENGs) which are a sub-family of eKEHs. A TENG can be described as a variable capacitive transducer with an additional triboelectric layer as electret.

1.7.1 The process of triboelectrification

Electret materials are specific dielectric materials with the ability to accumulate electric charge for a relatively long time, making them electrostatic equivalent to a permanent magnet. Some studies have shown that variations of electret can store the charge in it for as long as 10 years. As mentioned earlier, to store or inject charges in electret, triboelectrification phenomena can be used. It is a form of contract electrification during which two materials come in contact, and friction force between the two transfers charges from one to another, after which the two can be separated.

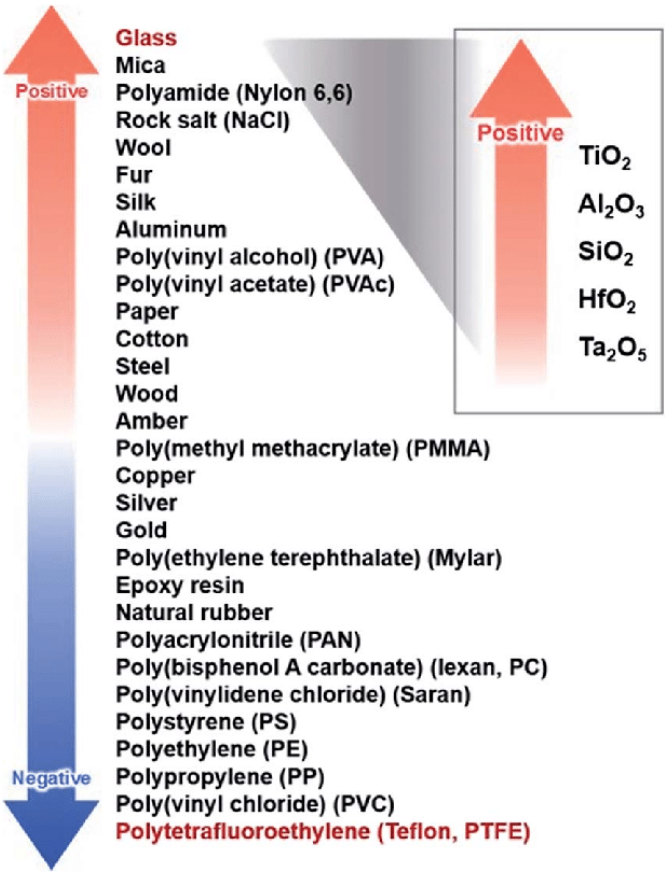

Figure 9: *A triboelectric scale defining positive and negative charge trapping capabilities of range of materials.[28]*

We have all witnessed this process at a young age with a science experiment with a balloon, scarf and hair. Firstly, a balloon is rubbed with a scarf. At this stage, the two materials are oppositely charged on the triboelectrification spectrum. The roughness of the surfaces causes surface friction resulting in the balloon being negatively charged. Once it is

brought close to the hair that is positively charged, the two attract and the result is frizzy hair. In the same way, the triboelectric effect is used to benefit the electromechanical energy conversion. Many materials have the ability to accumulate charge, hence a triboelectric scale is composed. On the triboelectric scale, one extreme is the materials which easily accumulate positive charges like polyurethane foam or glass. On the other side of the spectrum are the materials which are prone to accumulate negative charges like polypropylene and Teflon materials. The efficiency of the energy conversion in TENGs highly depends on the relationship between the two materials that come in contact, therefore materials from the opposite sides of the spectrum are chosen to be in contact. For an eKEH to become TENG, a specific modification in design is mandatory: the mobile electrode has to be allowed to touch the top most layer (the triboelectric layer) of the fixed electrode.

Once the oppositely charged materials came in contact and friction occurs, either positive or negative charges are stored inside it. Naturally, the majority of charges are stored at the surface layer. Hence the most relevant parameter of such material is its surface charge density expressed in C/m^2. As the depth of the material progresses the volume charge density decreases exponentially.

1.7.2 Materials used for TENGs

In the past 10 years, many materials from the triboelectric spectrum have been used to increase the energy conversion of electrostatic transducers. Firstly, development started with specifically engineered materials like diX-F films that can be charged to about 100V and [29] reported that the device with it had the power of 2 nW. Through the years, commercial materials started to be used, like CYTOP [30][31], Kapton [32], and Teflon-based materials [33]. [34] compared the performance of each of the materials by taking their charge densities. It was concluded that FEP, PE and cellulose have outperformed PVDF and rubber with charged densities above 10 $\mu C/m^2$. In addition, to be the ability to store high quantities of charge inside, the most relevant parameter for a TENG is the electret potential or surface potential of the triboelectric layer. Usually, it is measured using a non-contact voltmeter and ranges from a couple of tens of to volts to a couple of kilovolts (kV) for some materials. Based on data reported by Boisseau et al. in [35] surface potential directly correlates to the power throughput of the e-KEH.

1.7.3 Design of a TENG

When eKEH and TENG are structurally compared, it is concluded that the same design and fabrication methods are used with mitigation in the electret charging step as now it can be completely skipped. The electret is charged through contact and still has the purpose of providing the bias voltage thus it is now used as a (semi)permanent charge storage component of the transducer. For the TENG, the factor of the minimum distance between two electrodes before pull-in is completely omitted. Thus, it is made sure that the second electrode is in contact with the triboelectric layer as that is a necessary condition for triboelectrification to occur. Whether TENG is designed to be in-plane overlapping or gap-closing, the presence of electrode-dielectric contact is the crucial criterion for successful energy conversion.

1.7.4 An electrical equivalent of a physical device

Considering that the electromechanical energy conversion is occurring, it is crucial to assess the performance of the TENG electrically. Furthermore, an analogy between the mechanical and electrical models of the system is constructed. Firstly, it is evident that a variable electrostatic capacitor is represented by a variable capacitor. Its behavior is defined by the equations given in previous subsections.

Observing charge and potential distribution over a TENG, it is concluded that two capacitors are formed. One capacitor is the one that is there by design, the variable capacitor, and the other one is formed with the triboelectric layer and the electrode it is deposited on. It is formed because volume charge density, ρ, is not homogeneous through the thickness of the material. The majority of the charge that is trapped in the triboelectric layer is stored at its surface of contact and charge density reduces exponentially as the thickness of the material increases. Therefore, the contact surface of the triboelectric layer acts as another capacitor electrode forming the second capacitor with the transducer's electrode.

To represent the accumulated charge and kept surface voltage of the triboelectric layer, a voltage source is used. There are two approaches used to represent the same layer. Niu et al. in [36] report an equivalent circuit model of a triboelectric nanogenerator that uses a variable voltage source as an analogy for the triboelectric layer. The model is derived from the voltage-charge-displacement relationship, obtaining the following equation:

$$V = -\frac{1}{C_{TENG}}Q + V_{OC} \tag{5}$$

where the first term is the capacitive term and the second term, V_{OC} originates from contact-separation polarization of the triboelectric layer. The frequency of the movement of the system is reflected both in the frequency of V_{OC} 's and C_{TENG}'s operation. This indicates that structural properties and environmental stimulus (velocity and frequency of movement) are directly proportional to the open-circuit voltage term.

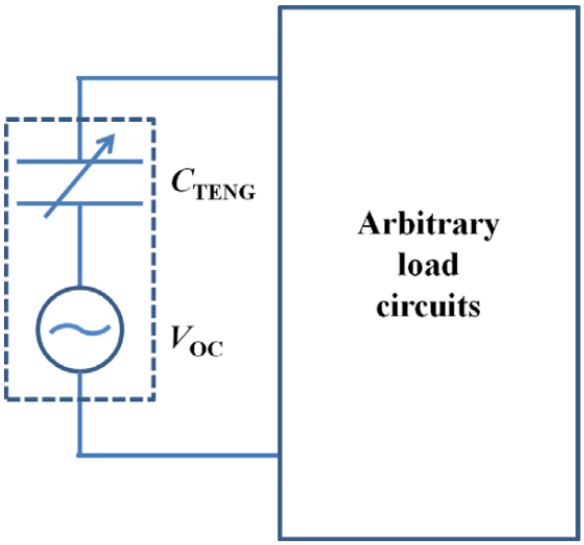

Figure 10: *An electric equivalent of a TENG composed of a variable capacitor and variable voltage source.[36]*

The second approach is reported by Hinchet et al. in [10] who utilized the same principles (Kirchhoff's and Gauss's laws) as in the previous model to derive TENG's voltage equation. After contact electrification of the triboelectric layer (the initialization of the device), it is considered electrically neutral. The equation defining the voltage is as follows:

$$V_{TENG} = -\frac{Q_{TE} d_{die}}{A\varepsilon_{die}} + \frac{Q_{var}}{A}\left(\frac{d_{var}}{\varepsilon_{air}} + \frac{d_{var}}{\varepsilon_{air}}\right) \tag{6}$$

where Q_{TE} is the charge of the triboelectric layer generated by contact electrification, d_{var} is the displacement of the device and d_{die} is the thickness of the triboelectric layer (the distance between electrodes on the fixed capacitor). Each part of the equation implies the voltage drop across a capacitor. The equation can be simplified as:

$$V_{TENG} = V_{TE} + \frac{Q_{var}}{C_{TENG}} \tag{7}$$

V_{TE} corresponds to the constant voltage source generated by triboelectrification. It solely depends on the characteristics of the triboelectric layer (thickness and charge density) and not on the design parameters of the TENG resulting in it being a constant value. For that reason, V_{TE} corresponds to a DC voltage source. The variable capacitor C_{TENG} comprises

the expression compensating for the mechanical movement as it directly affects the variation of it. The polarity of the attracted charge by the triboelectric layer is reflected in the polarity of the voltage source. If the material attracts negative charges and forms the dense potential layer of negative charges at its surface, the voltage source is to be negative too. On the other hand, when triboelectric material attracts and stores positive charges at its surface, the source will be oppositely polarized.

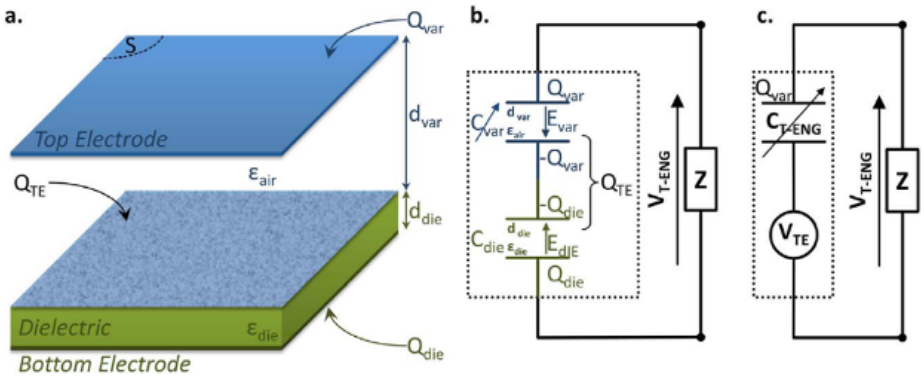

Figure 11: *An electrical model of the TENG based on charge distribution in a mechanical system composed of a variable capacitor and a DC source.[10]*

The difference between the two approaches is in the type of voltage source used. The first approach uses the AC source, while the second approach uses a DC voltage source. Even though both represent a capacitive TENG, the second model with a DC voltage source is only a faithful model of a gap-closing system, while the model utilizing the AC source is applicable to all mechanical configurations of the TENG.

1.7.5 Current and provisioned applications of TENGs

As mentioned earlier, energy harvesting has many applications. Nonetheless in some of those areas, TENGs are the dominant harvesters of choice. [22] reported three directions of TENGs' applications:

- sustainable micro-nano power sources for devices,
- active sensors as self-powered monitoring systems, and
- blue energy – kinetic and potential energy from the oceans. It is less dependent on environmental conditions and is broadly available.

1.8 The passive conditioning circuits

As mentioned in the introductory part, after the transducer has been selected and constructed and the energy conversion begins, it is necessary to treat obtained signal which is generally very uneven and not usable by commercial electronics. For that reason, the second step is the conditioning circuits. The circuits that are used to treat TENGs' outputs are commonly used for signal rectification in other fields too. They are used to process the output signal from a system to be suitable for the next stage of operation. They can be amplifying, rectifying or filtering circuits. Considering that obtained signal is usually present as a large voltage or current, there is no real need for it to be amplified. As the TENGs are oscillating systems and they have an operation frequency, most of the collected signals do not need frequency filtering. Moreover, the signal should be rectified. That is why rectifying circuits are used as the first step after transduction.

1.8.1 Rectifying circuits

Rectifying circuits are most often used in signal processing, where a signal is obtained from a measuring device or a sensor and needs to be smoothed out to generate a useful set of data points. If the signal at the start has a sinusoidal form, once it has been let through a rectifier (the shorter name for the rectifying circuit), it can have just positive peaks, or be closer to a DC signal of a certain amplitude. Electrically speaking, they can be constructed using diodes. The most commonly used rectifiers are half-wave (HW) and full-wave (FW) rectifiers, nevertheless, since the rectifier has a capacitor at its output, it is considered a charge pump. There is an abundance of variations of these circuits that will be mentioned in the following subsections.

1.8.2 Charge pumps

1.8.2.1 Stable charge pumps

Stable charge pumps (SCPs) are called stable because when they operate in combination with an oscillator like TENG, they bring energy conversion rates to the saturation point. It indicates that for each mechanical cycle of the TENG, an SCP goes through a series of variations of its topologies for it. Each iteration takes the energy from the TENG, smooths it out and stores it in the storage capacitor at the output of the circuit. At the beginning stages

of TENG-SCP operation, the amount of charge that is pumped to the storage capacitor is small and as the number of cycles increases, the conversion increases too, then decreases until the circuit reaches saturation. It means that at saturation, whatever excitation is given to the TENG, will not change the output of the SCP as it is now operating in a stable state, corresponding to a zero power generation.

HW and FW are the most popular rectifying circuits from SCP family. If output voltages of both are observed, it is clear that both saturate, thus at different voltage levels. The saturation voltages of both heavily depend on the ratio between the maximum and minimum capacitance of the TENG. The optimum conversion voltage for the HW and FW rectifiers is equal to half of the saturation voltage of the triboelectric layer.[37] It gives for the HW:

$$V_{opt\ HW} = \frac{1}{2} V_{TE}(\eta - 1) \tag{8}$$

where $\eta = \frac{C_{max}}{C_{min}}$, and for the FW:

$$V_{opt\ FW} = \frac{1}{2} V_{TE} \left(\frac{\eta - 1}{\eta + 1} \right) \tag{9}$$

Taking η the same for both cases, it is clear that HW operates optimally at higher voltages. At the start-up of the circuits, FW has a stronger start, denoting that voltages increase quickly and it reaches its ideal operation state in short amount of time, leading ti higher energy conversion.

Observing the QV cycles of the two SCPs, the effects of saturation are visible. For the HW, when the circuit reaches its maximum potential, it starts behaving like a constant-charge conditioning circuit. Secondly, when saturated, FW behaves as a constant-charge circuit. These circuits have a limit for saturation which reflects on the area of the QV cycle which degenerates into a line, thus converted energy per cycle tends to zero.

1.8.2.2 Unstable charge pumps

Stable charge pumps are a good choice of conditioning circuits to assess the working mechanisms of the transducer and to assess how it behaves when connected to different circuits. As the quantity of stored energy may have been limited by these circuits, it is questioned if transducers have greater conversion capabilities that can be managed otherwise. To solve the saturation problem, one of the proposed solutions is to use unstable charge pumps. They do not have any stable states, therefore, no saturation point. The main examples of

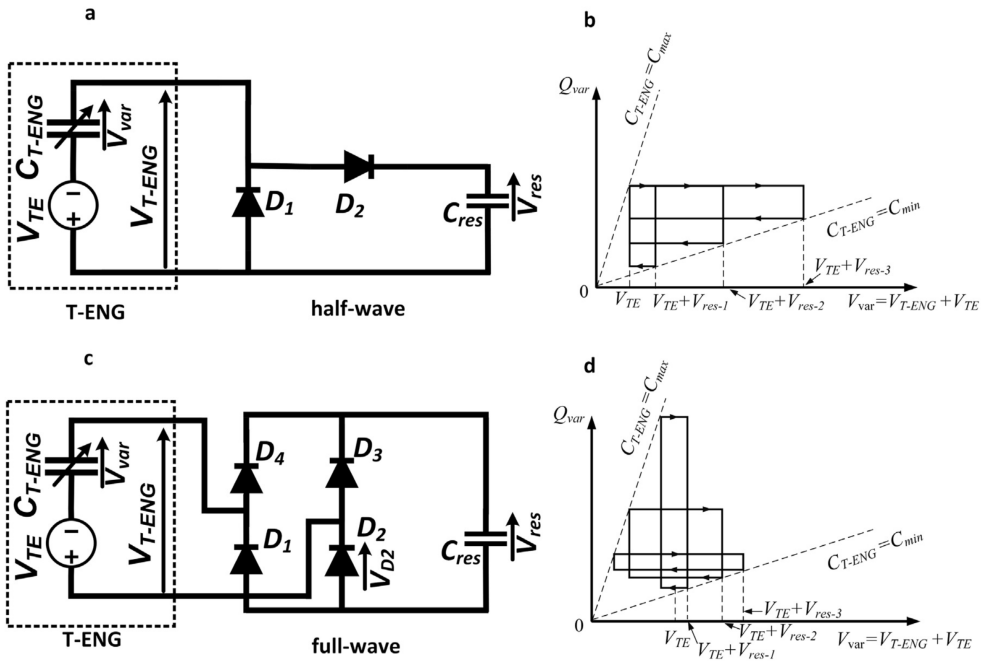

Figure 12: *Half-wave and full-wave rectifying circuits and their QV cycles. a) The schematic representation of the HW. and b) The QV cycle that yields from the HW operating. c) The schematic representation of established connection between TENG and diodes forming a FW. d) The QV cycle generated by operation of FW. The two QV diagrams are plotted with assumption of* $Cres >> Cmax$*.[37]*

such circuits are the derivation of Bennet's charge doubler like the cascade Bennet [38] and the USP with loss capacitance variation.

1.8.2.2.1 Bennet's charge doubler

Bennet's charge doubler is the mechanical system that was invented in year 1787 by Abraham Bennet [39]. He took 3 conductive plates and placed them parallel to each other, with dielectric layers between each. While two plates were stacked one over the other, one of the plates got charged with some q, while the other plate was grounded. This leaves the two plates charged oppositely. The grounded plate was removed and then the third plate is brought and placed on top of it charging it to the opposite charge from the ground. Now the removed plate is put back and the third electrode is brought in direct contact with the firstly charged plate. This doubled the charge of the first plate.

This mechanical system was reborn though its electrical equivalent first reported by de Queiroz in [40]. The first iteration of Bennet's charge doubler consisted of a variable capacitor, 3 switches, a reference capacitor and a storage capacitor. After its behavior has been studied from an electrical perspective, to reduce losses and increase the speed of the circuit, switches were replaced with diodes. They exhibit the same behavior with more sensitivity and stability

while operating. The simple model started to change each element for optimization purposes and the initial voltage source was replaced by a storage capacitor which made Bennet's charge doubler a possible conditioning circuit for energy harvesters. At this point, the circuit has been studied just from the electronics perspective, without any specific applications. In [17] one of the first applicative use of Bennet's doubler has been reported. Ben Ouanes et al. in [41] report the establishment of the TENG-Bennet combination for various transducers with different characteristics.

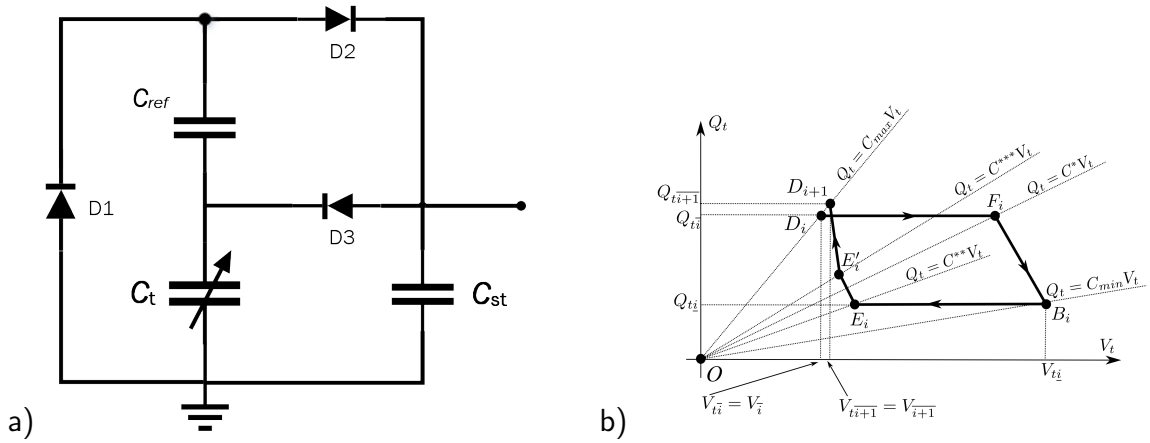

Figure 13: *a) Schematic of a classic Bennet's doubler.b) The geometry of the QV diagram implemented by one cycle of Bennet's doubler.*

Bennet's doubler has a necessary condition for η, which is, for instance, equal to 2 for the circuit in Figure 13a). It was first calculated by de Queiroz in [42]. The uniqueness of this circuit comes from the fact that it is unstable, meaning that it does not have an optimal state of operation for charge conversion. Its most notable characteristic is that it has an exponential voltage increase. It begins from its start-up of the circuit and continues infinitely, in theory, does not have a limit. In practice, the limiting factor is the maximum supported voltage of capacitors and diodes used or internal electrostatic discharge occurring in the transducer. An exponential increase of charge and voltage means that the QV cycles (shown in Figure 13b)) for Bennet's doubler are not floored by some voltage or some charge at any point. The QV cycles' area increases from one mechanical cycle to the other increasing converted energy per cycle.

1.8.2.2.2 History of Bennet's doubler - state of the art Bennet's doubler as a charge multiplying mechanism is the a mechanical system that has been firstly developed by Abraham Bennet in 1787. It is a system involving three plates forming two capacitors. Firstly, the middle plate is approached to the minimum distance from the lower plate while being connected to the ground. Secondly, the middle electrode is disconnected from the ground

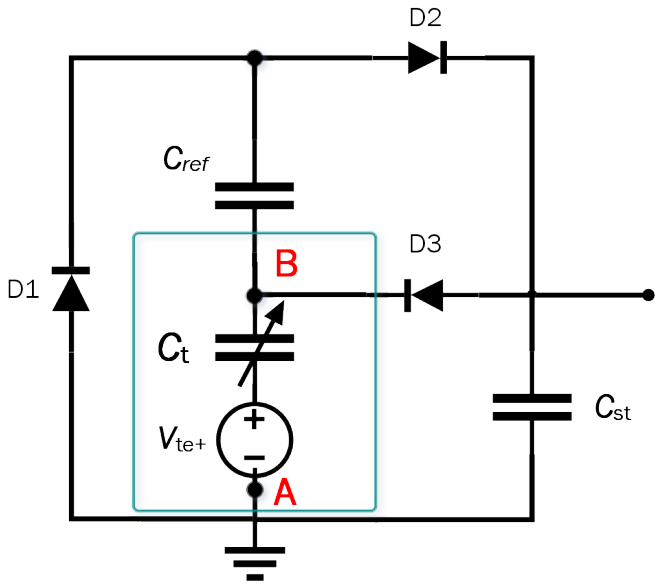

Figure 14: *Schematic of a classic Bennet's doubler with a single capacitor TENG.*

and is displaced to the other extreme approaching the top electrode which in now grounded. Thirdly, the top electrode is removed and middle electrode is brought back to its initial position - in closest possible contact with bottom electrode. The second step is the one at which it is recorded that some charges are redistributed in the system as conductive pendulum beads are repelling each other as negative charges are now introduced in the system.

This mechanical system has been reborn through its electrical equivalent developed by de Quairoz in 2010 [40]. The initial circuit was composed of two variable capacitors, three switches and a storage capacitor. At the early stages, the movement of charge through the circuit has been controlled by manual activation of the switches. The characterisation of newly formed circuit has given information about necessary initial conditions for its operation based on variable capacitance ratio ($\eta = 2$) and its output shape. It is reported that Bennet's doubler as a circuit has exponential increase of voltage over its output capacitor.

Over the next following years the variations of initially proposed circuit have been modified by various research groups to fit different applications. In 2014 in [43], E. Lefeuvre et al. reported that it is possible to structurally (by adding and removing cell elements of the circuit) modify Bennet's doubler to enable its operation for capacitance ratios below 2 ($\eta < 2$). On the other hand, in 2017, using a different structural approach developed by A. Karami et al. [38], a cascade Bennet is created and evaluated to accommodate the variable capacitors that are characterised with very high capacitance ratios.

In 2015, V. Dorzhiev et al. in [44] from the same research group reported that is possible to simplify the circuit by excluding one of the variable capacitors leaving Bennet operational with only one variable capacitor which in this case is a MEMS vibration energy harvester.

This report was the first introduction of the MEMS systems to the unstable charge pumps as circuits that are used to rectify raw signal generated by the MEMS transducer.

Exploration of possible applications of simplified Bennet's doubler circuit in domain of energy harvesting has been further explored and reported in 2018 by [37]. The focus of this study is application of such circuit in combination with a TENG. As TENGs have a particular electrical equivalents, either a variable capacitor and a DC voltage source, or the variable capacitor and an AC voltage source (chosen based on the physical characteristics of the transducer), the operation of the circuit has been redone as at this stage there has been modification in its topology.

Finally, in 2020 a research group from Russia published a very detailed theoretical analysis of the Bennet's doubler circuit with two variable capacitors, one of them being a TENG.[45] This study shows that there is space for development of the energy harvesters and circuits corresponding to their requirements in accordance to the commercial norms.

1.8.3 The QV cycle

To evaluate the performance of the circuit, we would derive Kirchhoff's equations and be able to see how one circuit compares to another. On the other hand, when the circuit is assessed in combination with the TENG, the quantity of converted energy per cycle should be assessed. Additionally, if the circuit goes through a series of changes in its topology during its operation, the complexity of the analysis and the number of unknown factors increase. To inspect TENG's behavior in an electrical sense, it is best to observe the behavior of the TENG through the evolution of charge and voltage at it during one cycle of operation, and later for the array of cycles to be able to follow the evolution of the cycle, therefore, the converted energy.

One cycle portrays one mechanical cycle for TENG, which as an oscillating system, coincides with an evolution $X_{max} - X_{min} - X_{max}$, for displacement or in terms of capacitance, $C_{min} - C_{max} - C_{min}$. As charge and voltage are 2 parameters that have a direct correlation with capacitance and can be translated in terms of Kirchhoff's law easily, it is best to use them as reference parameters.

Additionally, these two parameters are sufficient to calculate the energy of the capacitor. The area of the closed loop that forms after one mechanical cycle for any circuit, is equal to the energy converted during that cycle, as the equation states so. Some examples of the QV cycles have been shown in Figure 12.

1.9 The hypothesis

The hypothesis states that by an increase in total capacitance to vary and application of an efficient conditioning circuit, converted power is increased.

The increase of capacitance to be varied is done by increasing the transducer's size or by modifying the geometry. If the space is limited, which is the situation in most cases, increasing the size not is possible. The change of geometry can take a long time to perfect from the mechanical perspective, therefore it is not the most effective. By keeping the geometry and adding another plate of the same physical characteristics in the same confined space, a transducer with higher capacitance to varied can be designed. This new TENG has three output nodes, compared to the traditional two. The change in the number of outputs compels the implementation of different circuits that may not be suited for energy harvesters. Nevertheless, Bennet's charge doubler allows for possible substitutions in this topology which actually corresponds to its original one [40]. This thesis explores a design adjustment to the TENG transducer and adaptation of Bennet's charge doubler that significantly increase energy conversion rates and improve the performance of the energy conversion system.

1.9.1 Double TENG

1.9.1.1 Mechanical model/design

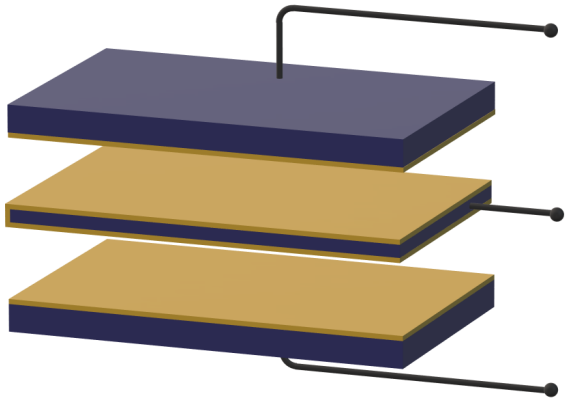

Figure 15: *A mechanical model of double capacitive eKEH.*

From a design perspective, double eKEHs consists of two fixed plates and one mobile plate. Comparing it to the single eKEH, an additional fixed plate is added. To form two capacitors

yet have three output nodes, the middle electrode is common for two capacitors. It is coated with the conductive material on both sides that are in contact. Electrodes A and C are fixed plates and electrode B is the mobile one. Double gap-closing eKEHs have a mobile plate is placed between the two fixed plates, while double in-plane sliding eKEHs have an additional set of fixed fingers in a comb-like structure.

It is necessary to add triboelectric layers to the variable capacitors for eKEHs to become TENGs. Because the new design has two capacitors and it is a transducer as a unit, two triboelectric layers have to be deposited. In the gap-closing case, layers can be deposited on two sides of the middle electrode or on the outside electrodes. In an in-plane sliding case, two fixed electrodes can be covered, or a single mobile electrode overlapping them can be covered in triboelectric material.

TENGs are not sustainable energy converters by themselves. They require other building blocks for successful energy conversion and storage. From the mechanical perspective, two placements of the triboelectric material are the same, thus the difference occurs when TENG is connected to the conditioning circuit. The performance of the TENG is graded based on the ratio of input energy and energy that is stored in the capacitor at the output of the conditioning circuit. Because of the electret's electrical properties and its connection to the conditioning circuit, two TENGs with the same geometry and different electret placement might have different efficiency rates. It is a criterion to be considered when choosing the placement of the triboelectric material.

a) b)

Figure 16: *Mechanical model of double TENG a) Triboelectric layer is placed of fixed plates. b) The triboelectric layer is placed on the middle mobile plate.*

1.9.1.2 Electrical model

The electrical model of double-capacitor TENG is based on the model of single-capacitor TENG. A series connection of a DC voltage source and a variable capacitor is a building block representing the classic single TENG. A block representing the double TENG is the block representing a classic TENG that is duplicated. The new block representing TENG consists

of two variable capacitors and two DC voltage sources representing two variable capacitors and two triboelectric layers in the system.

In the mechanical device, the three output nodes are always connected to the conductive capacitor's plates. In the electrical model, as it is the case of an analogy, the placement of the output nodes might differ for different placements of the triboelectric layer. If considering all feasible cases, there are four possibilities (as shown in Figure 17). Triboelectric layers on outer fixed plates resulting in mode number 1, the layers affixed to the middle plate which is mode 2, one layer on fixed and the other on mobile plate numbered as mode 3, and mode 3 on other remaining plates is mode 4. The last two modes are inferior to modes 1 and 2.

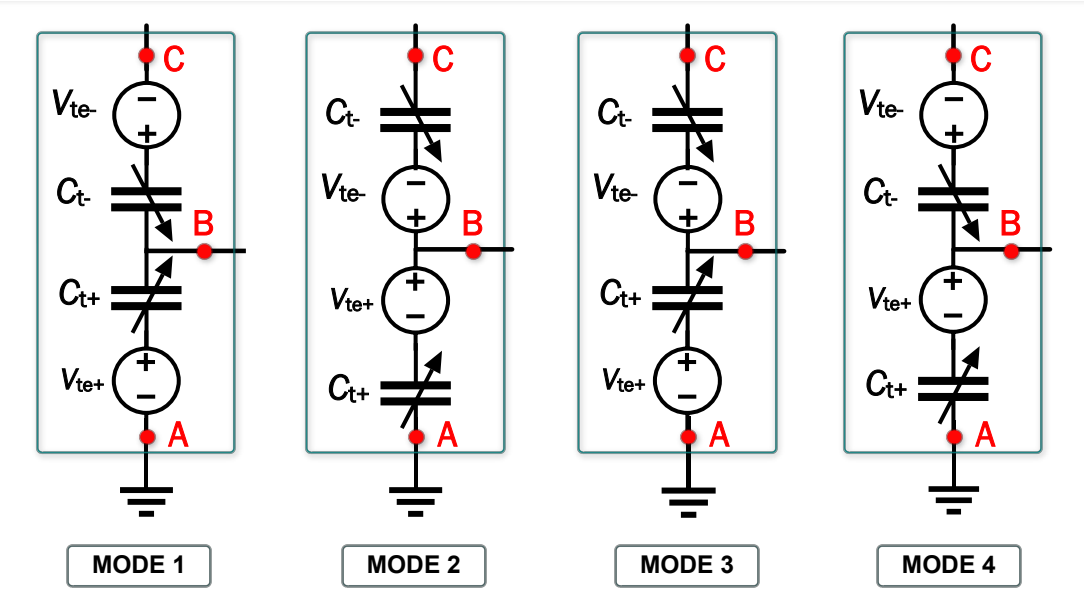

Figure 17: *The four models of possible TENG's electrical models based on its geometry.*

1.9.2 Double Bennet

1.9.2.1 Topology of double Bennet

A classic Bennet's charge doubler is constructed of an energy harvester block that is attached to a combination of diodes, a reference capacitor and a storage capacitor. Due to the unique location and role that the reference capacitor plays in this circuit, it can be replaced by another capacitive element. As double TENG contains the second variable capacitor, it is possible to substitute the reference capacitor with it.

As mentioned, it is possible to place triboelectric layers at different plates which results in a different electrical model of the double TENG. Based on the selected model, there are two possible ways that TENG can be connected to the circuit. In the first case, one of the voltage sources is connected to the ground and the other source is connected to diodes. The two variable capacitors are connected to each other with an output node extracted from their point of common potential. In the second case, variable capacitors are separated by two voltage sources. They have a common third node connected to the circuit. It is known that electrical connections within Bennet's doubler change as it operates. The placement of electret in physical device can have a direct impact on the operation of the Bennet's doubler as it defines the placement of DC voltage sources in the circuit. The voltage and current equations that are derived may differ in two cases.

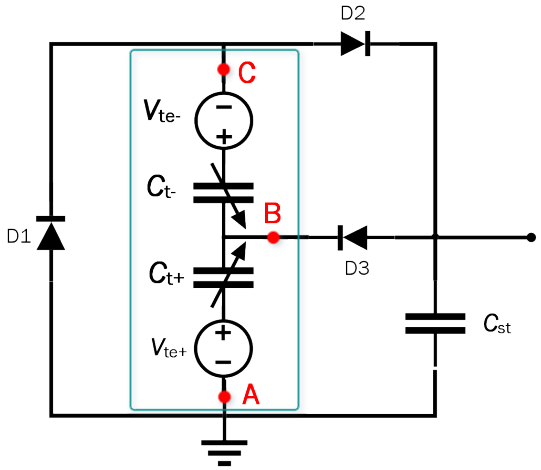

Figure 18: *Schematic of "double TENG" - "double Bennet" circuit system.*

The effects of change from one variable capacitor in the circuit to two are explored in great detail. This includes the distribution of charge and potential over a capacitor substituting reference capacitor as it plays the role of transduction capacitor and takes the functions that fixed capacitor had in the circuit and comparison of efficiency between "traditional" (single) and adapted (double) TENG and Bennet's doubler.

1.10 Research methods

1.10.1 Simulations

The stacking of conditioning circuits for improvement of energy harvester's performance is a concept that is reported by [38]. Conversely, Bennet's doubler with double capacitance is also a concept that had received some attention of de Queiroz [40]. Accordingly, the idea of modifying the conditioning circuit to better the performance of TENG and that being a Bennet's doubler that was not only stacked, but reconfigured, had to firstly be examined with a non-invasive method. Considering that the performance of the circuit is based on its electrical properties, SPICE simulators are chosen to do the analysis.

Selected tool used to execute the simulation is LTspice, a free high performance SPICE simulator software by Analog Devices. Netlists are used to define the circuit and set simulation parameters. They are text-based scripts that contain information necessary for software to conduct simulations. Simulation results are presented graphically to the user with an option of extraction data points in the command separated values (csv) format.

1.10.2 Analytical research

Circuit analysis simulations are flawed particularly because they idealize studied cases and they have limitations in calculations. As much as discretization parameters are adjusted, they can never fully compensate for an analog signal. Additionally, simulations can never account for the losses that are not predefined. They have advantage that they are fast and that change in variable parameters can be quickly accounted for and processed. Nevertheless, to identify all parameters that play the role at any moment of circuit analysis, it is necessary to conduct analytical research.

Analytical research for this study is composed of derivation of relevant parameters from established circuit equations based on Kirchhoff's laws and laws of conservation of charge. To secure accuracy in derivation process, Wolfram Mathematica is used. It is a mathematical computation software used in many fields. Its capability to handle symbolic manipulations is used to derive multi-variable expressions.

1.10.3 Experimental research

Once the simulations and analytical studies converge, it is left to test hypothesis experimentally. The experiments are done in a closed environment of a laboratory room with a dedicated test bench with fabrication, actuation and measurement equipment are contained withing one room. Results acquired by experimental means are processed using tailored scripts in Python and through OriginPro software.

1.11 Conclusion

This first chapter of the thesis manuscript presented the classification of kinetic energy harvesters (e-KEHs), particularly their division based on the direction of the force applied or in other words their movement principles. By focusing on triboelectric nanogenerators (TENGs) a process of triboelectrification has been explained. In addition to that, an electrical equivalent of the mechanical model of the TENG has been presented in detail defining it as a combination of a variable capacitor and a constant voltage source which is the model best suited for the gap-closing topology that has been selected to be a focus of the study.

To be able to benefit from the energy that transducers generated while operating, a selection of rectifying circuits, notably stable charge pumps like half and full wave rectifiers in section 1.8.2.1 and an unstable charge pump in section 1.8.2.2.1, Bennet's doubler has been introduced from the electrical point of view. To simplify visualization and analysis of measured parameters, a QV cycle is introduced.

The hypothesis of the thesis has been defined on two levels, the first one being the idea of the modification of the mechanical aspect of the TENG creating two trasnducing capacitors, with the goal of increasing the effective area of the capacitor to convert more energy. Secondly, as a consequence of the mechanical modifications, electrical parameters defining a TENG have been changed resulting in questioning the operation of the previously mentioned charge pumps traditionally used with such transducers. Finally, research methods for simulations, and analytical and experimental research aspects of the study have been presented introducing the chapters that follow.

2 Theory and Simulations of the Bennet doubler with a double TENG

2.1 Introduction

The previous chapter gave a comprehensive introduction to the theoretical concepts that are used in the study allowing us to focus on theoretical and simulation aspects in this chapter. As the title itself states, this chapter is divided into two sections with their subsections: firstly the theoretical analysis of Bennet's doubler with a double TENG, and secondly, simulations using LTspice are elaborated in detail, concluding this chapter with a comparison of the results obtained by the two analysis.

The proposed circuit's initial conditions for a startup are defined in subsection 2.2.3. As defined in subsection 1.8.3, a QV cycle is used to represent all the relevant parameters such as charge, voltage, and capacitance levels of each of the phases of the mechanical cycle. The theoretical analysis includes expressions of all three physical quantities at the start of the QV cycle continuing with four transient infliction points before reaching the final stage of the cycle. The second half of the second chapter focuses on the simulation aspect of the study in which initial conditions considered in simulation, as well as capacitance and circuit modeling,

are defined in great detail with results obtained for some of the constructed simulations.

Finally, the comparison of the quantification of the results obtained by derived equations from theoretical analysis of Bennet's doubler with double TENG and notable simulation results are compared with the goal of concluding the congruence and continuity of the considered concepts and assumed initial conditions.

2.2 Theoretical analysis

This analytical analysis consists of the circuit analysis of a Bennet doubler with a double TENG device having 2 antiphasic variable capacitors. Voltage levels and charge flow throughout branches of the circuit are the crucial parameters on which the analysis is based on, which results in the application of Kirchhoff's voltage law and the law of conservation of charge. The results are summarized on a QV cycle graph whose principle has been explained in section 1.8.3. As the evolution of charge and voltage are followed over two TENG's capacitors simultaneously, it is expected for the expressions to be complex. The following subsections go step by step through each moment in one mechanical iteration of this "double TENG" - "double Bennet" system with the goal of complete analysis of the such system.

In the introductory section, three different TENG's architectures are presented. Each of them can be converted into a double TENG. For this analysis, a gap-closing system is chosen. Taking in account that the analysis is done on a circuit level, the difference from one TENG model to another is only present through the shape of the capacitance variation. The schematic of the double TENG" - "double Bennet" is the one shown in Figure 18. Accordingly, it is to be concluded that the analysis conducted and presented in this thesis is applicable to any TENG topology. For the theoretical analysis of double Bennet to be conducted, a set of initial constraints is set.

- Before the start of the circuit operation, all capacitors in the circuit are fully discharged. Essentially, no residual charge should be left circling the nodes of the circuit. This is the necessary condition that is kept throughout all research steps that are taken in this thesis.

- Each triboelectric layer implemented in the system is fully saturated with electrical charges located at the surface of the triboelectric layer. In other words, $V_{\mathrm{te}\mp}$ have constant values. This constraint reflects directly on the electrical model of the TENG, as DC voltage source that represents the surface voltage of the triboelectric layer would

be an incorrect representation. Once the triboelectric layer is saturated, it keeps its constant voltage levels for long periods of time and for that reason it is possible to consider them as constant voltage sources.

- The capacitance ratio η is sufficiently large to start the circuit. Equivalent to other unstable charge pumps, double Bennet has a minimum requirement for $C_{\max}/C_{\min}$ that has to be satisfied for the circuit to behave accordingly in its steady state.

- Double Bennet is operating in a steady state. As any other circuit, double Bennet has its transient and steady state. The scope of this thesis acknowledges the existence of both states, however, the objective is the analysis of the steady state of double Bennet.

The theoretical analysis that is shown in the following subsections can be applied at any point of operation of a "double TENG" - "double Bennet" system. Hence, an i^{th} cycle of the operation is taken for the study.

2.2.1 Capacitance shape

As discussed in the introductory section and shown in Figure 42, TENG is constructed in such a way that a mobile plate is placed between two fixed plates. The mobile plate then oscillates due to external mechanical stimulus. As explained in earlier subsections, TENG's electrical equivalent that is used in this study is composed of a DC voltage source, which is equivalent to the surface voltage of the triboelectric layer, and a variable capacitor which corresponds to the capacitance change caused by mechanical movement. It is natural to conclude that the shape of the capacitance variation is influenced by the shape of the mechanical movement and TENG design. In our case of a gap-closing TENG, we have chosen the cosine function for demonstration. One mechanical cycle of operation of TENG with this topology is defined by one $C_{\max}$ - $C_{\min}$ - $C_{\max}$ iteration for $C_{\mathrm{t}+}$, and $C_{\min}$ - $C_{\max}$ - $C_{\min}$ iteration for $C_{\mathrm{t}-}$ (see Figure 18). Consequently, the cycle of one of the capacitors lags after the other by half of the cycle. For example, while $C_{\mathrm{t}+}$ is at $C_{\max}$ at the beginning of its cycle, $C_{\mathrm{t}-}$ reaches that value exactly in the middle of its cycle. Regarding the expressions that define the capacitors, while $C_{\mathrm{t}+}$ is defined by a classic cosine function, the $C_{\mathrm{t}-}$ is shifted by a $T/2$ portion of the cycle, or half a period. Equations 10 and 11 contain the expressions of the two capacitors.

$$C_{\mathrm{t}+}(t) = \frac{\varepsilon_0 s}{\frac{d_{\mathrm{die}}}{\varepsilon_r} + \frac{X_{\max}}{2} - \frac{X_{\max}}{2}\cos(2\pi f t)} \tag{10}$$

$$C_{\mathrm{t}-}(t) = \frac{\varepsilon_0 s}{\frac{d_{\mathrm{die}}}{\varepsilon_r} + \frac{X_{\max}}{2} - \frac{X_{\max}}{2}\cos\left(2\pi f t + \frac{T}{2}\right)} \tag{11}$$

In furtherance of uniformity and simplified maneuvering with the variables, the two expressions of the capacitances are normalized (equations 12 and 13).

$$C_{\mathrm{t}+}(t) = \frac{C_0}{1 - \alpha\cos(2\pi f t)} \tag{12}$$

$$C_{\mathrm{t}-}(t) = \frac{C_0}{1 + \alpha\cos(2\pi f t)} \tag{13}$$

Original capacitance C_0 is substituted with

$$C_0 = \frac{2\varepsilon_0\varepsilon_r s}{2d_{\mathrm{die}} + \varepsilon_r X_{\max}}$$

and a numeric parameter α with

$$\alpha = \frac{X_{\max}}{2(2d_{\mathrm{die}} + \varepsilon_r X_{\max})}$$

The difference in motion and phase of the two capacitors is present in normalized form with a negative sign that the numerical parameter α takes. Even though physical parameters constructing a TENG's capacitor are now contained within C_0 and α, the shape of the external force applied to the system is present through the cosine.

2.2.2 Circuit analysis of double Bennet

2.2.2.1 From A^i to B^i

It is considered that the mechanical cycle starts with $C_{\mathrm{t}+} = C_{\max}$ and $C_{\mathrm{t}-} = C_{\min}$. The initial moment is defined as point A^i. In that instance, the two capacitors are equipotential, as shown in Figure 19. The same potential of the capacitors can be consequence of:

- If the first mechanical cycle is considered, all capacitors are discharged and no movement has been initiated yet which results in no voltage present on the nodes of the TENG's capacitors.
- If any other mechanical cycle is taken for the analysis, equal voltages at the nodes of the capacitors are a result of the previous, $i - 1^{st}$, cycle during which the capacitors

were connected in parallel just before the end of it, resulting in equal potential levels at their nodes.

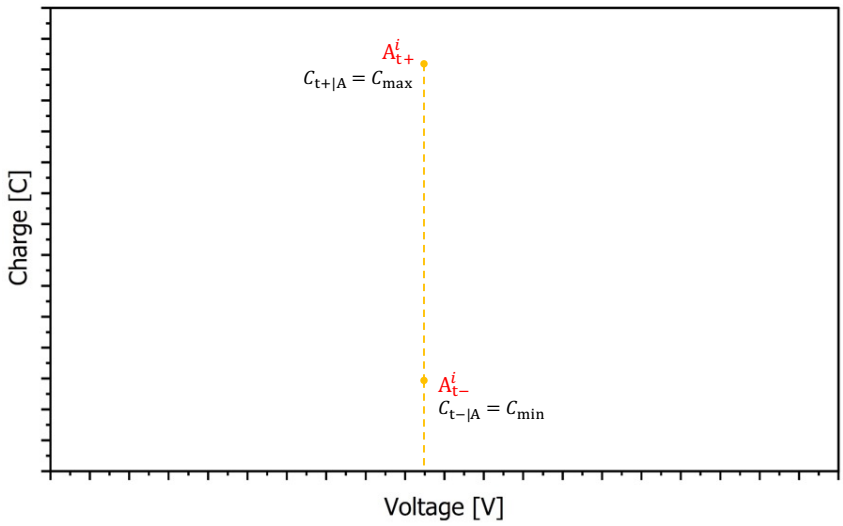

Figure 19: *Initialization of the QV cycle with point* A^i*, at which* $C_{\mathrm{t}+} = C_{\max}$ *and* $C_{\mathrm{t}-} = C_{\min}$ *set at the same potential.*

Once the initial point of the QV and mechanical cycles is established, the progression in the evolution of both can be investigated. The circuit topology that TENG form with the rest of the Bennet's doubler is defined by the conduction or insulation of diodes. Initially, none of the diodes are active, ergo transducer is disconnected from the rest of the circuit (Figure 20). At moment in time at which point A^i is defined, mechanical excitation of the system starts. This sets the mobile plate in motion resulting in a change of capacitance. Since the transducer is electrically disconnected, all changes that occur in the system are contained within it. It can be inferred that charge levels remain unchanged for this instance, as there are no other components in the loop to which they can be transferred to or from. Led by the expression $Q = CV$, it is concluded that a change in capacitance results in change of voltage.

$C_{\mathrm{t}+}$ starts with maximum capacitance, which means that from point A^i it will decrease. The decrease in capacitance naturally results in an increase in voltage over the nodes of the $C_{\mathrm{t}+}$ (voltage $V_{\mathrm{t}+|\mathrm{B}}$). On the other hand, $C_{\mathrm{t}-}$ starts the cycle with minimum capacitance which can only increase, resulting in decreasing voltage (voltage $V_{\mathrm{t}-|\mathrm{B}}$). With the progression of mechanical movement, transducer's nodes that once had equal potential, create an increasing potential difference between each other. Deviation in potential over the nodes induces for one of the diodes to start conducting. This moment is labeled as point B^i, which is the first point of change in the QV cycle.

Applying the law of conservation of charge at the instance from point A^i to point B^i (as

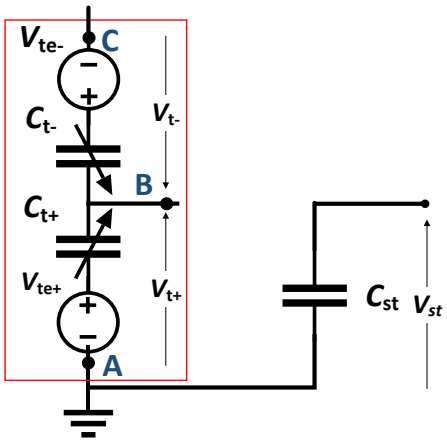

Figure 20: *Topology of double Bennet that is formed in this time instance with no active diodes and TENG being electrically disconnected from the rest of the circuit.*

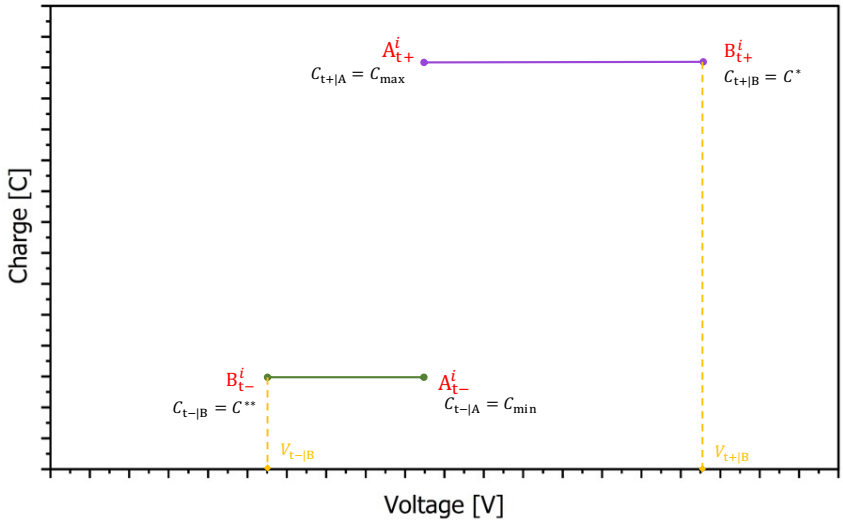

Figure 21: *The evolution of the QV cycle for the time interval* A^i *to* B^i*. Constant charge and variation in voltages are present for both* $C_{\mathrm{t}+}$ *and* $C_{\mathrm{t}-}$*.*

in equations 14 and 15) expressions for the capacitance levels at point B^i are derived.

$$Q^i_{\mathrm{t}+|\mathrm{A}} = Q^i_{\mathrm{t}+|\mathrm{B}} \tag{14}$$

$$Q^i_{\mathrm{t}-|\mathrm{A}} = Q^i_{\mathrm{t}-|\mathrm{B}} \tag{15}$$

$$(14) \rightarrow C^i_{\mathrm{t}+|\mathrm{B}} = C^i_{\mathrm{t}+|\mathrm{A}} \frac{V^i_{\mathrm{t}+|\mathrm{A}} - V_{\mathrm{te}+}}{V^i_{\mathrm{t}+|\mathrm{B}} - V_{\mathrm{te}+}} = \frac{C_{\max}(V^i_{\mathrm{t}+|\mathrm{A}} - V_{\mathrm{te}+})}{V^i_{\mathrm{t}+|\mathrm{B}} - V_{\mathrm{te}+}} = C^* \tag{16}$$

$$(15) \rightarrow C^i_{\mathrm{t}-|\mathrm{B}} = C^i_{\mathrm{t}-|\mathrm{A}} \frac{V^i_{\mathrm{t}-|\mathrm{A}} - V_{\mathrm{te}-}}{V^i_{\mathrm{t}-|\mathrm{B}} - V_{\mathrm{te}-}} = \frac{C_{\min}(V^i_{\mathrm{t}+|\mathrm{A}} - V_{\mathrm{te}-})}{V^i_{\mathrm{t}-|\mathrm{B}} - V_{\mathrm{te}-}} = C^{**} \tag{17}$$

Starting from the same equations 14 and 15 it is possible to express the potentials at point B^i.

$$(14) \rightarrow V^i_{\mathrm{t}+|\mathrm{B}} = (V^i_{\mathrm{t}+|\mathrm{A}} - V_{\mathrm{te}+})\frac{C_{\max}}{C_{\mathrm{t}+|\mathrm{B}}} + V_{\mathrm{te}+} \tag{18}$$

$$(15) \rightarrow V^i_{\mathrm{t}-|\mathrm{B}} = (V^i_{\mathrm{t}-|\mathrm{A}} - V_{\mathrm{te}-})\frac{C_{\min}}{C_{\mathrm{t}-|\mathrm{B}}} + V_{\mathrm{te}-} \tag{19}$$

With derived expressions for capacitance and voltage at point B^i, this instance, at which the first change in the circuit is about to occur, is now well defined.

2.2.2.2 From B^i to D^i

At the point of change B^i, D_2 starts conducting. That is because the voltage difference between the output node and one of the fixed plates (the fixed plate that is not connected to the ground) has surpassed the value necessary for D_2 to conduct. This diode being turned ON, the three capacitors ($C_{\mathrm{t}+}$, $C_{\mathrm{t}-}$ and C_{st}) are connected in series, as shown in Figure 22.

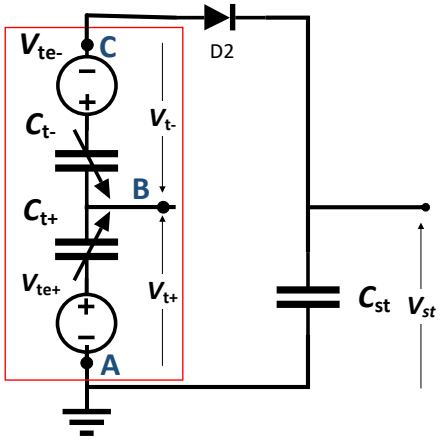

Figure 22: *Topology of double Bennet formed for the instance from B^i to D^i. The diode D_2 conducts, resulting in two TENG's capacitors and a storage capacitor being connected in series.*

The advancement in applied mechanical energy which displaces the mobile electrode continues to decrease $C_{\mathrm{t}+}$ until it reaches its minimum $C_{\mathrm{t}+|\mathrm{D}} = C_{\min}$ and $C_{\mathrm{t}-}$ to increase to its maximum $C_{\mathrm{t}-|\mathrm{D}} = C_{\max}$. This is a critical point in capacitance evolution that invokes a change in the cycle, labeled as point D^i.

Formed series configuration between the capacitors creates the conditions for the flow of charges to start. As seen in Figure 23, accumulated charges are released from $C_{\mathrm{t}+}$ while $C_{\mathrm{t}-}$ accepts the charges. During the instance, from point A^i to point B^i, charge conservation law is applied. This means that the charge distribution on the capacitors did not change; hence the total amount of charge over the transducer at points A^i and B^i is equal. This fact is used to simplify the derivation of the charge exchange equation for this portion of the QV cycle.

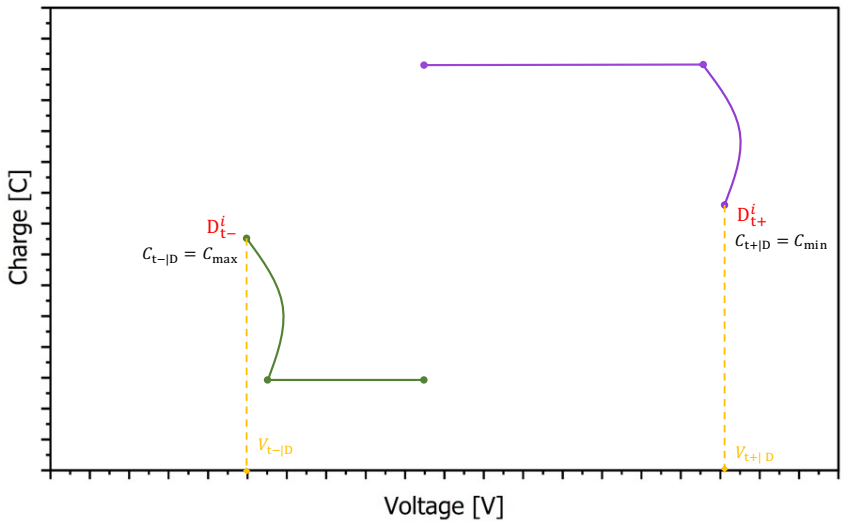

Figure 23: *The evolution of the QV cycle for the instance from* B^i *to* D^i*. The Series configuration of the capacitors causes the charges to flow.*

By the law of conservation of charge over the TENG between points A^i to D^i:

$$C_{\min}(V - V_{\mathrm{te}-}) + C_{\max}(V - V_{\mathrm{te}+}) = C_{\min}(V^i_{\mathrm{t}+|\mathrm{D}} - V_{\mathrm{te}+}) + C_{\max}(V^i_{\mathrm{t}-|\mathrm{D}} - V_{\mathrm{te}-}) \tag{20}$$

Where voltages at the initiation of the QV cycle (point A^i) over TENG's capacitors are equal and denoted by a common variable V where $V = V^i_{\mathrm{t}+|\mathrm{A}} = V^i_{\mathrm{t}-|\mathrm{A}}$. Now that C_{st} is connected too, it provides additional information about the charge distribution in the closed loop:

$$C_{\mathrm{st}}V - C_{\min}(V - V_{\mathrm{te}-}) = V^i_{\mathrm{st}|\mathrm{D}}C_{\mathrm{st}} - C_{\max}(V^i_{\mathrm{t}-|\mathrm{D}} - V_{\mathrm{te}-}) \tag{21}$$

The moment at which the charge exchange outlined by the above two expressions stops is set by the evolution of the capacitance. Once $C_{\mathrm{t}+} = C_{\min}$ and $C_{\mathrm{t}-} = C_{\max}$, the slope of the capacitance variation changes, resulting in a shift in the circuit's behaviour and discontinuation of charge flow in it.

Looking at the circuit formed when D_2 is ON, Kirchhoff's voltage law is deduced as follows:

$$V^i_{\mathrm{t}+|\mathrm{D}} = V^i_{\mathrm{t}-|\mathrm{D}} + V^i_{\mathrm{st}|\mathrm{D}} + \Delta V \tag{22}$$

Where $\Delta V = V_{\mathrm{te}+} - V_{\mathrm{te}-}$.

Equations 20, 21 and 22 provide all necessary information to define TENG's voltages at

point D^i. Resolving this set of equations defines the three circuit capacitors' voltages as:

$$V_{t+|D} = \frac{C_{\max}C_{\min}V_{\mathsf{te}+} + {C_{\max}}^2\alpha + C_{\min}C_{\mathsf{st}}(V_{\mathsf{te}+} + \beta) + C_{\max}C_{\mathsf{st}}(V^i_{\mathrm{t}+|\mathrm{A}} + V_{\mathsf{te}-} + \alpha - \Delta\mathsf{V})}{C_{\min}C_{\mathsf{st}} + C_{\max}(C_{\min} + C_{\mathsf{st}})} \tag{23}$$

$$V_{t-|D} = \frac{C_{\max}C_{\min}V_{\mathsf{te}-} + C_{\max}C_{\mathsf{st}}(V_{\mathsf{te}-} + \alpha) + {C_{\min}}^2\beta + C_{\min}C_{\mathsf{st}}(-V^i_{\mathrm{t}+|\mathrm{A}} + V_{\mathsf{te}+} + \beta + \delta\mathsf{V})}{C_{\min}C_{\mathsf{st}} + C_{\max}(C_{\min} + C_{\mathsf{st}})} \tag{24}$$

$$V_{\mathsf{st}|D} = \frac{C_{\max}C_{\mathsf{st}}V + {C_{\max}}^2\alpha + C_{\min}(C_{\mathsf{st}}V^i_{\mathrm{t}+|\mathrm{A}} - C_{\min}\beta) + C_{\max}C_{\min}(V_{\mathsf{te}+} - V_{\mathsf{te}-} + \delta\mathsf{V})}{C_{\min}C_{\mathsf{st}} + C_{\max}(C_{\min} + C_{\mathsf{st}})} \tag{25}$$

To complete the evaluation of the point D^i, the charges that are released from $C_{\mathrm{t}+}$ into the rest of the circuit have to be quantified with an expression. The released charge can be defined as a difference between the initial charge level at the beginning of the QV cycle, at point A^i, and the newly established charge level of $C_{\mathrm{t}+}$ at D^i.

$$Q^i_{AD+} = -\frac{C_{\mathsf{st}}(C_{\max}C_{\min}(V^i_{\mathrm{t}+|\mathrm{A}} - 2V_{\mathsf{te}+} + 2V_{\mathsf{te}\text{-}}) + C^2_{\max}(V_{\mathsf{te}+} - V^i_{t+|A}) + C^2_{\min}(-V_{\mathsf{te}\text{-}} + V^i_{t+|A}))}{C_{\min}C_{\mathsf{st}} + C_{\max}(C_{\min} + C_{\mathsf{st}})} \tag{26}$$

The charge $Q^i_{\mathrm{AD}+}$ is distributed across the other two capacitors in the circuit $C_{\mathrm{t}-}$ and C_{st} in consequence of series connection. As established earlier, $C_{\mathrm{t}-}$ and $C_{\mathrm{t}+}$ are nonsimultaneous equal in their amplitude as capacitors that move in opposite phases creating a phase shift between the functions of two capacitances, leading to the conclusion that $C_{\mathrm{t}-}$ is passing through its own charge exchange phase, the same as its opposing transducer capacitor. Therefore, these TENG's capacitors variations cause additional charge transfer to C_{st}. In addition to $\frac{Q^i_{\mathrm{AD}+}}{2}$ transferred to C_{st}, an additional $\frac{Q^i_{\mathrm{AD}-}}{2}$ is added to the charge of C_{st}. Keeping in mind that $Q^i_{\mathrm{AD}-} = Q^i_{\mathrm{AD}+}$ the charge of C_{st} is increased by $Q^i_{\mathrm{AD}+}$.

2.2.2.3 Parametric expressions for the instance B^i to D^i

TENG as a physical device has two variable capacitors which can not be separated from each other, therefore the equations for the segment from B^i to D^i can not be separately evaluated. From Figure 23, it is concluded that the relationship between charge and voltage is nonlinear for the instance in question.

To calculate and plot QV trajectory in this segment, it is necessary to use time-dependent parametric equations for the capacitance and voltage. It is executed by equations 23, 24 and 25 being modified so that each variable defined and calculated at this instance becomes time-dependent. This includes capacitance and voltages at this time period. Because we have already defined the terminating voltages at relevant points, from these equations we can derive and shape of the charge exchange in each capacitor which can be observed through TENG's voltage equations.

$$V_{t+}(t|_{B\to D}) = \frac{C_{\max}(V^i_{t|A} - V_{\text{te}+}) + C_{\min}(V^i_{t|A} - V_{\text{te}-}) + C_{t-}(t|_{B\to D}) + C_{t+}(t|_{B\to D})}{C_{t-}(t|_{B\to D}) + C_{t+}(t|_{B\to D})} \quad (27)$$

$$\begin{aligned} V_{t-}(t|_{B\to D}) = {} & \frac{1}{(C_{\text{st}} + C_{t-}(t|_{B\to D}))(C_{t-}(t|_{B\to D}) + C_{t+}t)}[C_{\max}C_{\text{st}}(V^i_{t|A} - V_{\text{te}+}) \\ & + C_{\text{st}}V_{\text{te}+}C_{t-}(t|_{B\to D}) + 2C_{\text{st}}V_{\text{te}-}C_{t-}(t|_{B\to D}) - C_{\text{st}}V^i_{t+|A}C_{t-}(t|_{B\to D}) + V_{\text{te}-}{C_{t-}}^2(t|_{B\to D}) \\ & + 2C_{\text{st}}V_{\text{te}+}C_{t+}t + C_{\text{st}}V_{\text{te}-}C_{t+}t - C_{\text{st}}V^i_{t+|A}C_{t+}t+) \\ & (V_{\text{te}-}C_{t-}(t|_{B\to D})C_{t+}t + C_{\min}(V^i_{t+|A} - V_{\text{te}-}C_{\text{st}} + C_{t+}t + C_{t-}(t|_{B\to D}))] \end{aligned} \quad (28)$$

Based on the relation $Q = VC$, the expressions for the $Q_{t+}(t|_{B\to D})$ and $Q_{t-}(t|_{B\to D})$ can be easily derived and are:

$$\begin{aligned} Q_{t+}(t|_{B\to D}) = {} & C_{t+}(t|_{B\to D})\frac{C_{\max}(V^i_{t|A} - V_{\text{te}+}) + C_{\min}(V^i_{t|A} - V_{\text{te}-}))}{C_{t-}(t|_{B\to D}) + C_{t+}(t|_{B\to D})} \\ & + \frac{+V_{\text{te}-}C_{t-}(t|_{B\to D}) + V_{\text{te}+}C_{t+}(t|_{B\to D}}{C_{t-}(t|_{B\to D}) + C_{t+}(t|_{B\to D})} \end{aligned} \quad (29)$$

$$\begin{aligned} Q_{t-}(t|_{B\to D}) = {} & \frac{C_{t-}(t|_{B\to D})}{(C_{\text{st}} + C_{t-}(t|_{B\to D}))(C_{t-}(t|_{B\to D}) + C_{t+}t)}[C_{\max}C_{\text{st}}(V^i_{t|A} - V_{\text{te}+}) \\ & + C_{\text{st}}V_{\text{te}+}C_{t-}(t|_{B\to D}) + 2C_{\text{st}}V_{\text{te}-}C_{t-}(t|_{B\to D}) - C_{\text{st}}V^i_{t+|A}C_{t-}(t|_{B\to D}) + V_{\text{te}-}{C_{t-}}^2(t|_{B\to D}) \\ & + 2C_{\text{st}}V_{\text{te}+}C_{t+}t + C_{\text{st}}V_{\text{te}-}C_{t+}t - C_{\text{st}}V^i_{t+|A}C_{t+}t + V_{\text{te}-}C_{t-}(t|_{B\to D})C_{t+} \\ & + C_{\min}(V^i_{t+|A} - V_{\text{te}-})(C_{\text{st}} + C_{t+}t + C_{t-}(t|_{B\to D}))] \end{aligned} \quad (30)$$

Despite point D^i being only the second point of change in the QV cycle, expressions defin-

ing the transition are rather complex. Their complexity equivalently represents the intricacies in behavior of double Bennet caused by movement of charge throughout the circuit. The shape that double Bennet forms at this instance is the significant difference in the shape of the QV cycle when compared to classic Bennet that is shown in Figure 13.

2.2.2.4 From D^i to E^i

With charge accumulation in capacitor C_{st}, its voltage V_{st} surges and potential difference between output and TENG's point diminishes until diode D_2 turns OFF at moment D^i. At that stage, TENG disconnects from the rectifying circuit as no diode conducts at the instance (Figure 24).

Nevertheless, external excitation perseveres to be applied to the system as the QV cycle continues to evolve too. Continuous movement of mobile electrode prompts $C_{\mathrm{t}+}$ and $C_{\mathrm{t}-}$ to pass through two transitional events before finally reverting to $C_{\max}$ and $C_{\min}$, respectively.

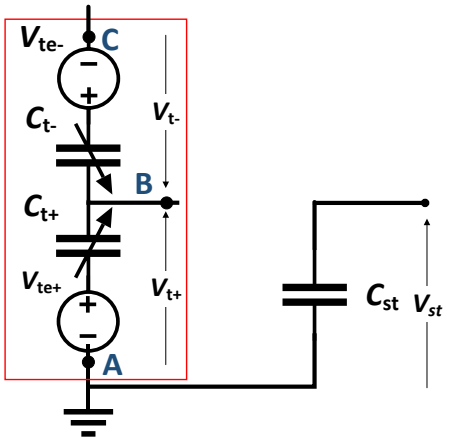

Figure 24: *Topology of double Bennet formed for the instance from D^i to E^i. TENG is being electrically disconnected from the rest of the circuit as no diodes conduct.*

From moment D^i to E^i, TENG is electrically separated from the rest, leading to stagnation in quantities of charge that are accumulated in the transducer's capacitors. Proportionally, with mechanically caused variation in capacitance, V_{t+} increases and V_{t-} decreases. Since TENG is electrically segregated from other capacitors in the circuit, the law of conservation of charge is applicable as their levels are not to be changed at this stage.

Capacitance variations which are inverted for A^i to B^i instance, result in voltage decrease over C_{t+} and voltage increase over C_{t-}. Between moments D^i and E^i, based on the charge conservation law, the states of C_{t+} and C_{t-} can be expressed as:

$$Q^i_{\mathrm{t+|D}} = Q^i_{\mathrm{t+|E}} \tag{31}$$

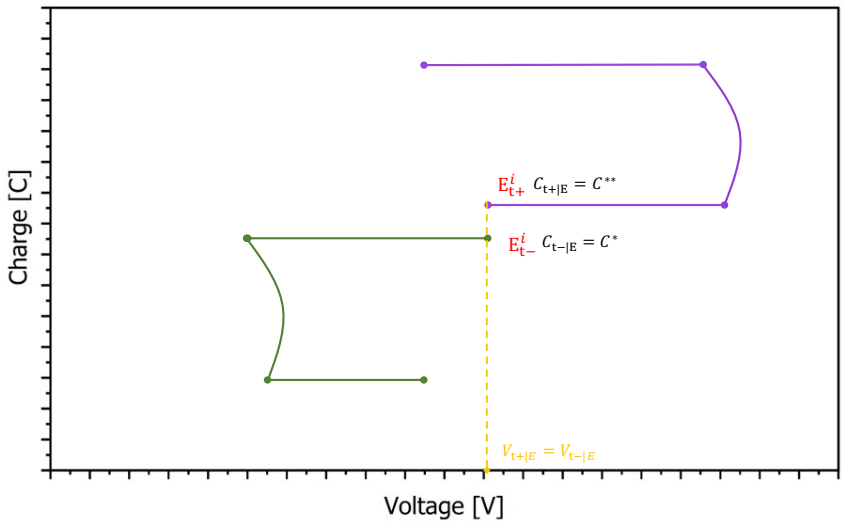

Figure 25: *The evolution of the QV cycle for the instance from* D^i *to* E^i *defined by the equal voltages of transducer's capacitors at the final point of the instance.*

$$Q^i_{t-|D} = Q^i_{t-|E} \tag{32}$$

The charge conservation equations are sourcing the expressions for a point E^i, where either capacitance (equations 33 and 35) or voltages (equations 34 and 36) characterising point E^i are derived.

$$(31) \rightarrow C_{t+|E} = C_{t+|D}\frac{V^i_{t+|D} - V_{\mathrm{te}+}}{V^i_{t+|E} - V_{te+}} = C_{\min}\frac{V^i_{t+|D} - V_{te+}}{V^i_{t+|E} - V_{te+}} = C^{**} \tag{33}$$

$$(31) \rightarrow V^i_{t+|E} = \left({V_{t+|D}}^i - V_{\mathrm{te}+}\right)\frac{C_{\min}}{C_{t+|E}} + V_{\mathrm{te}+} \tag{34}$$

$$(32) \rightarrow C_{t-|E} = C_{t-|D}\frac{{V_{t-|D}}^i - V_{\mathrm{te}-}}{V^i_{t-|E} - V_{\mathrm{te}-}} = C_{\max}\frac{V^i_{t-|D} - V_{\mathrm{te}-}}{V^i_{t-|E} - V_{\mathrm{te}-}} = C^* \tag{35}$$

$$(32) \rightarrow V^i_{t-|E} = \left({V_{t-|D}}^i - V_{\mathrm{te}-}\right)\frac{C_{\max}}{C_{t-|E}} + V_{\mathrm{te}-} \tag{36}$$

If V_{te+} and V_{te-} are equal, both TENG's voltages are equal too $V^i_{(t+|E)} = V^i_{(t-|E)}$. This statement is only correct if it can be ensured that V_{te+} and V_{te-} are equal. In the interest of constraining the least number of parameters, this thesis does not take into consideration the assumption that V_{te+} and V_{te-} are equal, which is hardly the case in practice.

2.2.2.5 From E^i to F^i

As stated earlier, at point E^i the potential over the two TENG capacitors equalizes ($V_{\mathrm{t}+} + V_{\mathrm{te}+} = V_{\mathrm{t}-} + V_{\mathrm{te}-}$). Once they both approach to V_{st}'s, the diode D_1 conducts. The two

capacitors are connected in parallel, closing the loop and causing for the recurrence of charge exchange, nevertheless in the opposite direction. An inversion of occurrences at point B^i at which $V_{\mathrm{t}+}$ released charges to the rest of the circuit and $V_{\mathrm{t}-}$ accumulated part of them takes place at point E^i. At instance from E^i to F^i, $V_{\mathrm{t}+}$ now absorbs and accumulates charges from other capacitors in the circuit and $V_{\mathrm{t}-}$ releases them.

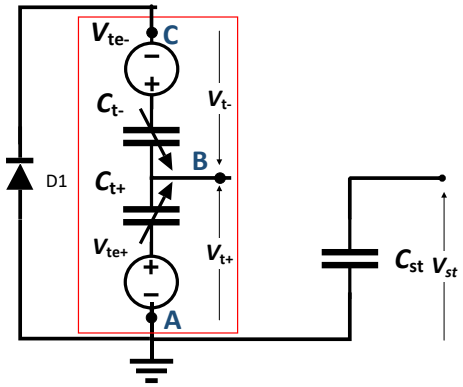

Figure 26: *Topology of double Bennet formed for the instance from* E^i *to* F^i. *Conduction of diode* D_1 *creates a parallel connection of TENG's capacitors.*

The charge is fed from $C_{\mathrm{t}-}$ into $C_{\mathrm{t}+}$. As those are only two capacitors in the circuit, charge conservation law defines the total charge in the circuit to be equal to:

$$Q_{tot|E} = Q_{tot|F} \tag{37}$$

As two TENG's capacitors close the circuit loop containing two voltage sources and two variable capacitors with specific potential differences over their nodes, Kirchhoff's law is deduced as:

$$-V_{te+} + V_{t+|F} - V_{t-|F} + V_{te-} = 0 \tag{38}$$

Equations 37 and 38 are the base for derivations of $V_{t+|F}$.

$$V_{t+|F} = \frac{C_{t-|F}V_{te+} - C_{t+|E}V_{te+} + C_{t+|F}V_{te+} - C_{t-|E}V_{te-} + C_{t-|E}V_{t-|E} + C_{t+|E}V_{t+|E}}{C_{t-|F} + C_{t+|F}} \tag{39}$$

As a consequence of the parallel connection of the capacitor at this considered instance, they are continuously at the same potentials. This shows that equation 39 is valid for both capacitors ($V_{t+|F} = V_{t-|F}$).

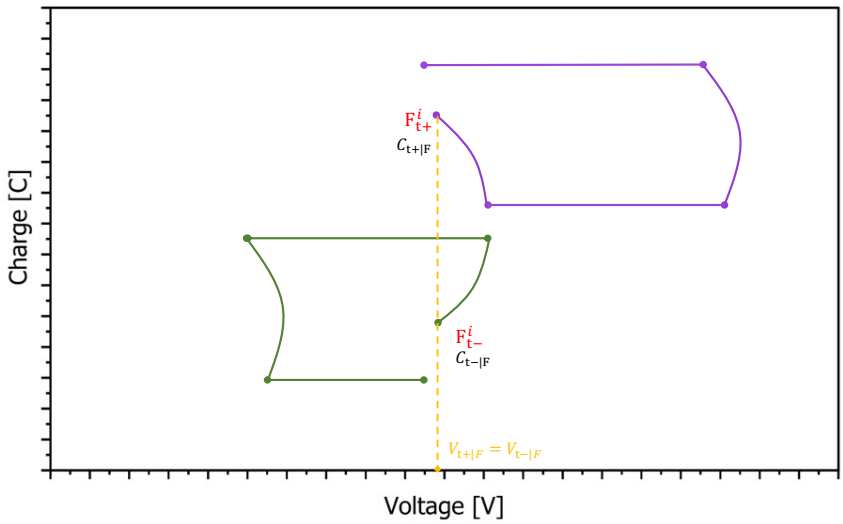

Figure 27: *The evolution of the QV cycle for the instance from* E^i *to* F^i*. The parallel connection of TENG's capacitors starts the charge accumulation process in* C_{t+}*.*

2.2.2.6 Parametric equation for the interval E^i to F^i

The nonlinear relationship of charge and voltage in this instance requires parametric analysis of voltage in time. The QV cycle evolution of $C\mathrm{t}+$ between E^i and F^i moments is defined by the $C_{\mathrm{t}-}$ capacitance. Since they are in parallel, the slope of the QV curve is directly proportional to $-C_{t-}|_{F_i}^{E_i}$, which is equivalent to the $C_{\mathrm{t}+}$ capacitance values within this time interval.

$$V_{\mathrm{t}\mp}(t|_{\mathrm{E}\to\mathrm{F}}) = \frac{C_{\mathrm{t}-|\mathrm{F}}V_{te+} - C_{\mathrm{t}+|\mathrm{E}}V_{\mathrm{te}+} + C_{\mathrm{t}+|\mathrm{F}}V_{\mathrm{te}+} - C_{\mathrm{t}-|\mathrm{E}}V_{\mathrm{te}-}}{C_{\mathrm{t}-|\mathrm{F}} + C_{\mathrm{t}+|\mathrm{F}}} + \frac{C_{\mathrm{t}-|\mathrm{E}}V_{\mathrm{t}-}(t|_{\mathrm{E}\to\mathrm{F}}) + C_{\mathrm{t}+|\mathrm{E}}V_{\mathrm{t}+}(t|_{\mathrm{E}\to\mathrm{F}})}{C_{\mathrm{t}-|\mathrm{F}} + C_{\mathrm{t}+|\mathrm{F}}} \quad (40)$$

2.2.2.7 From F^i to A^{i+1}

As mentioned in the subsection above, while D_1 conducts both TENG's voltages transcend to V_{st} and at the moment at which all three voltages levels equalize, diode D_3 starts conducting too. Now with two diodes ON, as shown in Figure 28, C_{st} is added in parallel to $C_{\mathrm{t}+}$ and $C_{\mathrm{t}-}$ ($C_{\mathrm{t}+}||C_{\mathrm{t}+}||C_{\mathrm{st}}$). The same configuration is kept until the end of the energy conversion cycle.

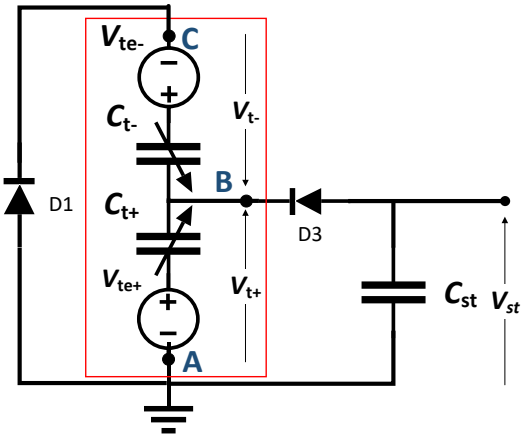

Figure 28: *Topology of double Bennet formed for the instance from* F^i *to* A^{i+1}. *Conduction of diodes* D_1 *and* D_3 *creates a parallel connection of three capacitors.*

At the interval B^i to D^i, storage capacitor C_{st} receives charges from $C_{\mathrm{t}+}$ and $C_{\mathrm{t}-}$ which it keeps until critical point F^i when it releases an amount of it back to the circuit and keeps the rest until the end of the mechanical cycle. Due to its fixed capacitance value and stable charge levels, the potential that V_{st} possesses is the one to which other capacitors gravitate towards.

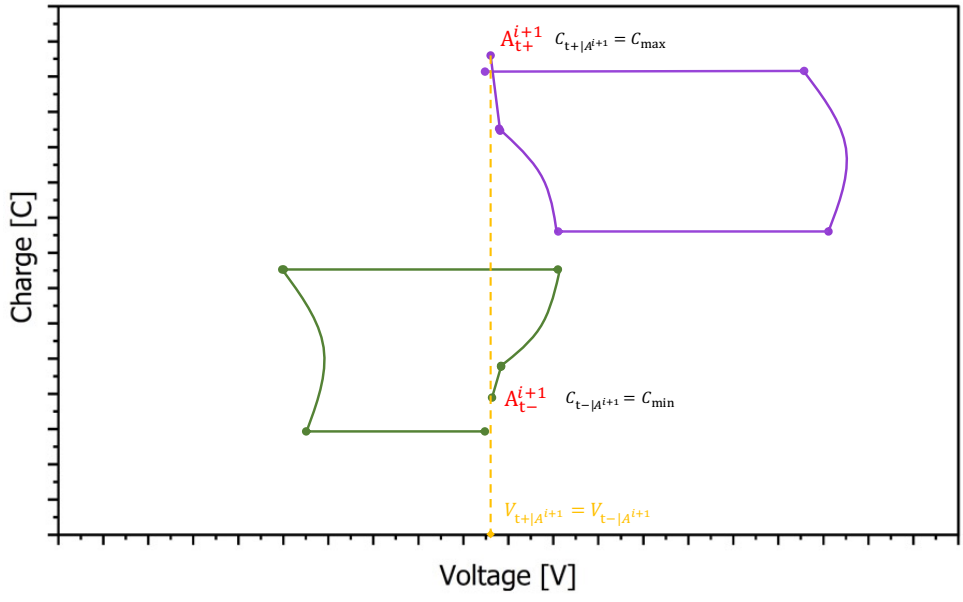

Figure 29: *The evolution of the QV cycle for the instance from* F^i *to* A^{i+1} *completing full mechanical cycle.*

At the interval F^{i} to A^{i+1}, $C_{\mathrm{t}+}$ and $C_{\mathrm{t}-}$ complete their variations towards $C_{\max}$ and $C_{\min}$, respectively. $C_{\mathrm{t}-}$ continues to give away the charges that are now shared between $C_{\mathrm{t}+}$ and C_{st}, and the trend at which it occurs differs from the previous period as the circuit changed. Charge conservation law defines the total number of charges that have passed through newly formed loop sets as $Q_{\mathrm{tot|F}} = Q_{\mathrm{tot|A^{i+1}}}$. Factoring in the parallel connection of three capacitors, it can conclude that they are at the equipotential point.

$$V_{\mathrm{t}+|\mathrm{A^{i+1}}} = V_{\mathrm{t}-|\mathrm{A^{i+1}}} = V_{\mathrm{st}|\mathrm{A^{i+1}}} = V_{\mathrm{A^{i+1}}} \tag{41}$$

Finally, the expression of the terminal voltage of the i^{th} QV cycle and the initial voltage of the $i+1^{st}$ cycle, that characterises all the capacitors can be developed as:

$$V_{\mathrm{A^{i+1}}} = \frac{C_{\mathrm{t}+|\mathrm{F}}(V_{\mathrm{t}+|\mathrm{F}} - V_{\mathrm{te}+}) + C_{\mathrm{t}-|\mathrm{F}}(V_{\mathrm{t}-|\mathrm{F}} - V_{\mathrm{te}-}) + C_{\mathrm{st}}V_{\mathrm{st}|\mathrm{F}} + C_{\max}V_{\mathrm{te}+} + C_{\min}V_{\mathrm{te}-}}{C_{\max} + C_{\min} + C_{\mathrm{st}}} \tag{42}$$

The total amount of charge at the moment A^{i+1} is equal to the sum of the individual charges in each capacitor. $Q_{\mathrm{tot|A^{i+1}}}$ is defined by the equation 43.

$$Q_{\mathrm{tot|A^{i+1}}} = \frac{C_{\mathrm{t}+|\mathrm{F}}(V_{\mathrm{t}+|\mathrm{F}} - V_{\mathrm{te}+}) + C_{\mathrm{t}-|\mathrm{F}}(V_{\mathrm{t}-|\mathrm{F}} - V_{\mathrm{te}-}) + C_{\mathrm{st}}V_{\mathrm{st}|\mathrm{F}} + C_{\max}V_{\mathrm{te}+} + C_{\min}V_{\mathrm{te}-}}{C_{\max} + C_{\min} + C_{\mathrm{st}}}$$
$$(C_{\max} + C_{\min} + C_{\mathrm{st}}) - C_{\min}V_{\mathrm{te}-} - C_{\max}V_{\mathrm{te}+} \tag{43}$$

The moment A^{i+1} is at the same time the terminal point of the i^{th} cycle and the starting point of the $i+1^{st}$ cycle. Each cycle starts at predefined voltage and charge levels, based on the previous cycle and at its end, sets values for the next cycle. The increase from the start to the end of the mechanical and QV cycles provides proof of the fundamental principle of Bennet's charge doubler, that is continuous charge and voltage increase from one cycle to another. By examining derived equations and principles of Bennet's charge doubler, there is no saturation point by which cycle-to-cycle energy conversion increase would be restricted.

2.2.3 Startup condition of double Bennet

The behavior of double Bennet is heavily dependent on the physical parameters of the TENG. Thus there are constraints that are set by the rest of the circuit, which provide the minimum conditions that need to be satisfied for the circuit correctly start and run. To set those conditions, we can observe the point B^i which corresponds to the first point on the QV cycle at which a circuit element is activated and formed a closed loop. Since it is the first point of change from the start of the QV cycle at which a change in the circuit occurs, if the conditions for its repetitive occurrence from one mechanical cycle to the next one are met, that indicates that the initial conditions are met. It is expected that it is dependent on the TENG's physical parameter, to be more specific to the ratio of minimum and maximum capacitance. The necessary ratio can be derived from the voltage law equation at point B^i.

$$V^i_{\mathrm{t+|B}} = V^i_{\mathrm{t-|B}} + V^i_{\mathrm{st|B}} \tag{44}$$

Substituting $V^i_{\mathrm{t+|B}}$ and $V^i_{\mathrm{t-|B}}$ with the expressions derived previously at subsection 2.1.

$$\frac{C_{\max}}{C^i_{\mathrm{t+|B}}}(V^i_{\mathrm{t+|A}} - V_{\mathrm{te+}}) - V_{\mathrm{te+}} = \frac{C_{\min}}{C^i_{\mathrm{t-|B}}}(V^i_{\mathrm{t+|A}} - V_{\mathrm{te+}}) - V_{\mathrm{te-}} + V^i_{\mathrm{t+|A}}$$

If we consider that $V_{\mathrm{te+}} = V_{\mathrm{te-}} = V_{\mathrm{te}}$ the above equation can be simplified.

$$\frac{1-\alpha\cos(\omega t_{\mathrm{B}})}{1-\alpha} - \frac{1+\alpha\cos(\omega t_{\mathrm{B}})}{1+\alpha} = \frac{V^i_{\mathrm{t+|A}}}{V^i_{\mathrm{t+|A}} - V_{\mathrm{te}}} \tag{45}$$

Where α is defined as:

$$\alpha = \frac{X_{\max}}{2(2d_{\mathrm{die}} + \varepsilon_r X_{\max})}$$

Continuing from equation 45:

$$\frac{2\alpha - 2\alpha\cos(\omega t_{\mathrm{B}})}{1-\alpha^2} = \frac{V^i_{\mathrm{t+|A}}}{V^i_{\mathrm{t+|A}} - V_{\mathrm{te}}} \tag{46}$$

$$cos(\omega t_{\mathrm{B}}) = 1 + \frac{V^i_{\mathrm{t+|A}}}{V^i_{\mathrm{t+|A}} - V_{\mathrm{te}}}\frac{1-\alpha^2}{2\alpha} \tag{47}$$

To ensure the integrity of the QV cycle, it is necessary to set conditions on α and therefore $cos(\omega t_{\mathrm{B}})$ which has to be greater than -1.

The marginal case is the one when $cos(\omega t_{\mathrm{B}})) = -1$ leading to $\alpha_{\min}$ expression.

$$\cos(\omega t_{\mathrm{B}}) = 1 + \frac{V^{i}_{\mathrm{t+|A}}}{V^{i}_{\mathrm{t+|A}} - V_{\mathrm{te}}} \frac{1 - {\alpha_{\min}}^{2}}{2\alpha_{\min}} = -1 \tag{48}$$

$$\frac{1 - {\alpha_{\min}}^{2}}{2\alpha_{\min}} = -\frac{2}{\frac{V^{i}_{\mathrm{t+|A}}}{V^{i}_{\mathrm{t+|A}} - V_{\mathrm{te}}}} \tag{49}$$

From equation 49 the expression for $\alpha_{\min}$ is derived:

$$\alpha_{\min} = -\frac{2}{\delta} + \sqrt{\frac{4}{\delta^2} + 1} \tag{50}$$

where δ is defined by:

$$\delta = \frac{V^{i}_{\mathrm{t+|A}}}{V^{i}_{\mathrm{t+|A}} - V_{\mathrm{te}}} \tag{51}$$

2.2.4 Energy per cycle

To calculate the energy generated at each mechanical cycle, it is necessary to consider the points A^{i}, D^{i} and A^{i+1}. At the point A^{i}, the energy is defined by capacitors' energy as:

$$W_{\mathrm{A}^{i}} = \frac{1}{2} V^{2}_{\mathrm{t+|A^{i}}} \left(C_{max} + C_{min} + C_{st}\right) \tag{52}$$

By the time cycle reaches point D^{i}, charge generation process is complete and its distribution over the three capacitors starts. This process is completed at the point A^{i}. This moment is defined by Q^{i+1} for which all capacitors have the same voltage $V_{A^{i+1}}$ over them. The energy at point A^{i+1} is expressed by the following equation.

$$W_{\mathrm{A}^{i+1}} = \frac{1}{2} {V_{\mathrm{tot|A^{i+1}}}}^{2} (C_{\mathrm{max}} + C_{\mathrm{min}} + C_{\mathrm{st}}) = \frac{Q^{2}_{\mathrm{tot|A^{i+1}}}}{2(C_{\mathrm{max}} + C_{\mathrm{min}} + C_{\mathrm{st}})} \tag{53}$$

2.2.5 Highest voltage

After critical points of the QV cycle are defined with their voltage, capacitance and charge expressions, it is crucial to define the highest voltage that occurs during one mechanical cycle. This parameter helps assess the maximum capabilities for energy conversion and limitations to which the equipment that is used in practical applications can be stressed. Based on above-

derived equations it is concluded that the highest voltage occurs at the peak of the transition between points B^i and D^i at the $C_{\mathrm{t}+}$ side of the TENG.

To define $V_{\max}$ point, it is necessary to find a (y-axis) derivative of the charge of function shaping the QV cycle at that interval. Furthermore, the voltage is defined by a zero derivative of such function. As indicated before, charge and voltage equations at this time instance are parametric, time-dependent, equations. The derivative of the two parametric equations is calculated as the time derivative of one, divided by the time derivative of the other.

$$\frac{V'(t)}{Q'(t)} = \frac{\left(-x\cos(2\pi ft)C_{\max}\left(V^i_{t+|A} - V_{\mathsf{te}+}\right) - x\cos(2\pi ft)C_{\min}\left(V^i_{t+|A} - V_{\mathsf{te}-}\right)\right)}{\epsilon\mathsf{s}\left(\epsilon\mathsf{s}V_{\mathsf{te}+}\epsilon_r 2d + x\epsilon_r + C_{\max}\left(V^i_{t+|A} - V_{\mathsf{te}+}\right)\left(d + x\epsilon_r\sin^2(\pi ft)\right)^2\right)} \\ \frac{+\epsilon\mathsf{s}\left(V_{\mathsf{te}+} - V_{\mathsf{te}-}\right)\left(d + x\epsilon_r\sin^2(\pi ft)\right)^2}{+C_{\min}\left(V^i_{t+|A} - V_{te-}\right)\epsilon s\left(d + x\epsilon_r\sin^2(\pi ft)\right)^2} \tag{54}$$

When this parametric derivative is equal to zero, meaning the slope of this function is equal to 0, it corresponds to the highest voltage or $V_{\max}$ point. From zero derivative we can extract the expression of the time corresponding to that point. This expression can be injected back to the voltage equation for $\mathrm{B}^i \rightarrow \mathrm{D}^i$ period and maximum voltage can be defined.

$$t(V_{\max}) = \frac{1}{2\pi f}\tan^{-1}\left(\frac{2d_{\mathsf{die}}}{X_{\max}\epsilon_r} + 1, -\frac{2\sqrt{-d_{\mathsf{die}}\left(d_{\mathsf{die}} + X_{\max}\epsilon_r\right)}}{X_{\max}\epsilon_r}\right) \tag{55}$$

From the expression that defines the moment at which the maximum voltage is reached, it can be concluded that this parameter is purely based on the characteristics of the TENG, i.e. distance between the plates, their maximum displacement and dielectric properties of the triboelectric material used in device fabrication, and the frequency of its operation. Finally, the maximum voltage can be analytically expressed as:

$$V_{max} = -\frac{-2V^i_{\mathrm{t}+|A}C_{\max} + 2C_{\max}V_{\mathsf{te}} - C_{\min}V_{\mathsf{te}+} - V_{\mathsf{te}+}\frac{s\epsilon_0}{\frac{d_{\mathsf{die}}}{\epsilon_r} + \frac{X_{\max}}{2} - \frac{1}{2}X_{\max}\cos(2\pi f(V_{\max}))}}{C_{\min} + \frac{s\epsilon}{\frac{d_{\mathsf{die}}}{\epsilon_r} + \frac{X_{\max}}{2} - \frac{1}{2}X_{\max}\cos(2\pi ft(V_{\max}))}} \tag{56}$$

2.3 Simulations of double Bennet

2.3.1 Simulation setup

Theoretical analysis of double Bennet gives extensive insight into the complexity of behaviour of this circuit. To understand the limitations of the circuit and verify the accuracy of the conducted analysis, simulations of the electrical circuit are conducted. The speed of calculations done by simulation software is unprecedented to calculations done by utilizing derived equations.

Electrical simulations are done using LTspice software. Each netlist contains three segments: TENG initialization (description of the physical parameters of the TENG), circuit elements connections and simulation parameters defining the type and scope of simulation that is done. As LTspice is a circuit solver program, TENG's characteristics need to be presented as electrical parameters, or in other words through its electrical equivalent model defined in section 1.7.4 with a DC source and capacitance that is varied through movable plate parameter of maximum displacement.

Equation 57 contains all variables that need to be defined by set values in the first segment of the simulation setup.

$$C_t = \frac{\varepsilon_0 s}{\frac{d_{die}}{\varepsilon_r} + \frac{X_{max}}{2} - \frac{X_{max}}{2} cos(2\pi f t)} \tag{57}$$

The transducer has two capacitors that are equal, yet in opposite phases. Using the property of cosines being an even function, the change of one capacitor is defined by cosines (cos) and the other one with negative cosines (-cos) to compensate for the phase shift between the two. Moreover, surface voltage defined by surface charge density (σ_0) of the triboelectric layer is presented with a DC voltage source. Surface voltage is a parameter that is not measured precisely. It is estimated based on the saturation properties of 100 μm thick PTFE layer. The constant voltage of the voltage source is calculated by the following equation.

$$V_{te} = \frac{\sigma_0 d_{die}}{\varepsilon_0 \varepsilon_r} \tag{58}$$

The polarity of the material used is manifested through the sign of σ_0. Whether it is positive or negative material on the triboelectric scale, σ_0 defines the polarity of the voltage source in the circuit. Parameters used for TENG initialization are listed in Table 1.

PHYSICAL PARAMETER	NOTATION	VALUE
Permittivity of free space	e0	8,854pF
Dielectric permittivity of PTFE	er	2,1
Dielectric thickness of PTFE	ddie	100 μm
Surface charge density	ro	-10 $\frac{\mu C}{m^2}$
Maximum displacement between electrodes	Xmax	50 μm
Surface Area of the Device	S	$0,0025\mathrm{m}^2$

Table 1: *TENG parameters used for simulation setup*

After the TENG is described with its electrical equivalent, the connections in the circuit are left to be determined. The default setup of LTspice is that lumped elements are ideal. Equivalently, the model of a basic diode has instant conduction and no reverse current thus has a threshold voltage making it not fully ideal. In the first iteration of simulations, the diode model is left to be ideal. It simplifies circuit analysis as losses and effects of other circuit components are neglected. The output capacitor is a fixed capacitor of 10 nF (this value propagates through simulation and experimental sections of the thesis). For correct circuit operation, it is considered that all capacitors are completely discharged as per the necessary initial condition demonstrated in section 2.2. To fulfill this condition, the initial charge in a capacitor *ic* is set to zero.

Another iteration of simulations is performed to match the realistic conditions. A non-ideal diode model is declared in the netlist. The most relevant parameters are breakdown voltage (Bv), peak-to-peak voltage (Vpk) and leakage current (Ibv). Information provided in table 2 is taken from a datasheet of a diode that is stipulated to be used in the experimental research section.

PHYSICAL PARAMETER	VALUE
Breakdown voltage (Bv)	200 V
Peak-to-peak voltage (Vpk)	200 V
Leakage current (Ibv)	1 nA
Parasitic capacitance (Cjo)	4 pF
Forward voltage (Vj)	0,62 V

Table 2: *Non-ideal diode parameters used in simulations*

Another initial condition that is considered in simulation is the saturation of the triboelectric layer carrying a certain amount of charge. To account for the initial charge of the triboelectric layer, q_0, it has to be calculated and added so that the simulation software can calculate based on the correct data. A product of surface charge density and surface area on which the charge is accumulated equals the accumulated quantity of charge,

$$q_0 = \sigma_0 S. \tag{59}$$

Fulfilled initial conditions have completed the setup of the electrical simulation of the system in a steady state.

2.3.2 Capacitance profile

As the first block in the energy management system is the energy harvesting element - the TENG, intuitively it is the first component to be observed after the simulation is complete. Figure 30 shows the shape of the capacitance. The red and black curves show that the signal is periodic. Comparing the two curves of $C_{\mathrm{t}+}$ and $C_{\mathrm{t}-}$, it is clear that they take the same shape. Nevertheless, observing their phases, it can be concluded that one of them lags after the other one, or in other words, that a 180-degree phase shift between the two curves is present. This is due to the mechanical nature of double TENG for which the middle plate dictates the capacitance. When it is at the maximum displacement in one of the directions, it forms a $C_{\max}$ with the plate it is closest to and a C_{min} with the other plate. In that manner, it is ensured that when one capacitor has its maximum capacitance, the other one is at its minimum creating a phase shift that is equal to half of the mechanical cycle of the TENG.

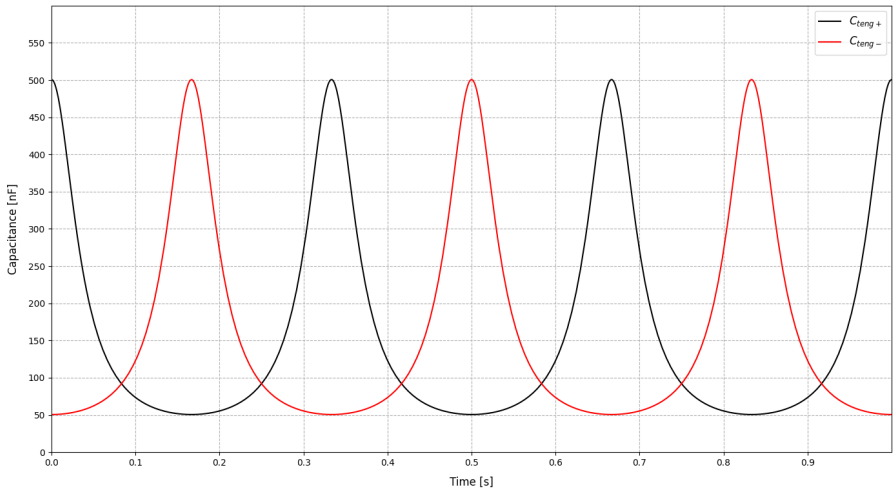

Figure 30: *Simulated capacitance shapes of $C_{\mathrm{teng}+}$ and $C_{\mathrm{teng}-}$.*

The values of the capacitances are at 500 pF for $C_{\max}$ and 50 pF for C_{min}. This corresponds to $\eta = C_{max}/C_{min}$ equal to 10. By using such a high ratio, it is made sure that the device can provide results that can be compared without compromising the transducer or the circuit's start-up.

2.3.3 Simulations results

After capacitance shape and values have been established, it is necessary to observe the behavior of the complete "double TENG" - "double Bennet" system. Variables that are necessary to be investigated are the charge and voltage over TENG's capacitors. Considering that simulations are done for the system in a steady state (transient phases are not observed in conducted electrical simulations) any time instance of the simulated period can be taken for observation. A selected time frame is 1 second which contains 3 simulated mechanical cycles. Firstly, charge curves over C_{t+} and C_{t-} are observed for selected period. As a consequence of the mechanical movement, the symmetric antiphasic behaviour of the system transposes to the shape of the charge curve too. In Figure 31, one period of operation has been highlighted for observations.

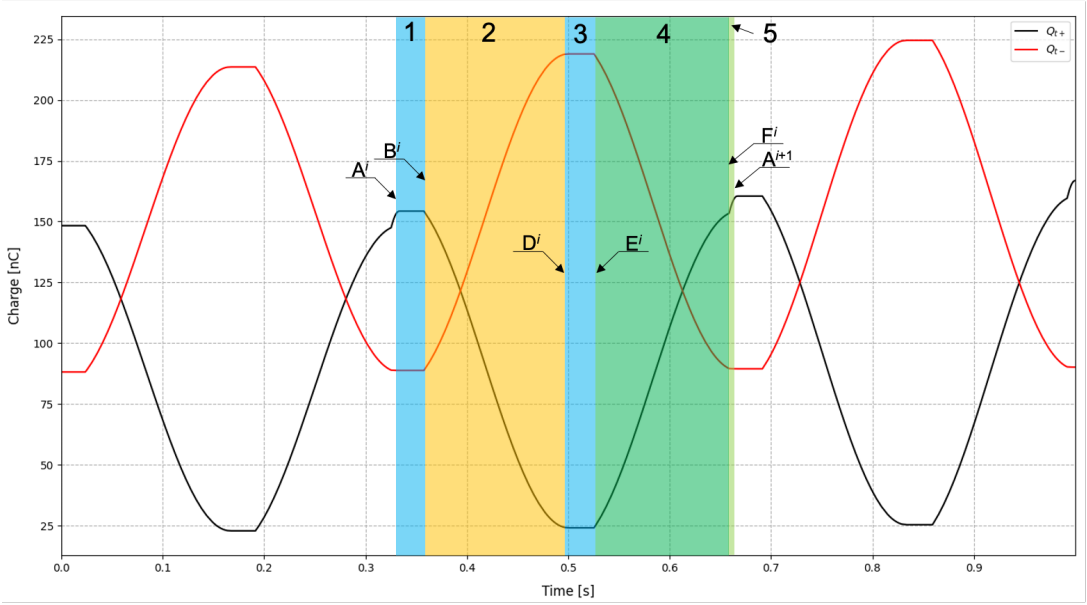

Figure 31: *Simulation results for the charge levels of the C_{t+} and C_{t-} for the cycles 48-51.*

The mechanical cycles start with a constant charge of both capacitors (zone 1 in Figure 31). While the circuit progresses, capacitor C_{t+} releases charges to the circuit, and the other capacitor C_{t-} accepts the charges from the circuit (zone 2). By zone 3, a stagnation in charge exchange is reached after which C_{t-} releases charges and C_{t+} absorbs them (zone 4). The cycle is closed by a narrow interval (zone 5) during which charge exchange (accumulation and release) is finalized. Identified phases in charge circulation during one cycle align with the phases identified by the theoretical research. Figure 31 leads to the conclusion that there is a symbiotic relationship between two TENG's capacitors. This relationship improves the performance of the system as there is a continuity of charge in the circuit that is now doubled so that, while one part of the system is building up to accumulating charge, the other half of

the system is benefiting from that process by generating the charge in that time.

Voltage and charge curves of C_{t+} are placed on the same graph in Figure 32. The red curve represents the charge and the black curve is the voltage over the capacitor. Simultaneously observing the two and using the above-established charge variation periods, it is possible to track the voltage behaviour over a set time period. The voltage first increases until it peaks to its maximum for the cycle, V^i_{max}, which is a local maximum on a general voltage curve. After V^i_{max}, it decreases. The moment at which the second constant charge period is complete indicates the moment at which voltage invigorates an increase and yet another decrease. From a short interval shown in Figure 32, voltage increase from one cycle to another is noted.

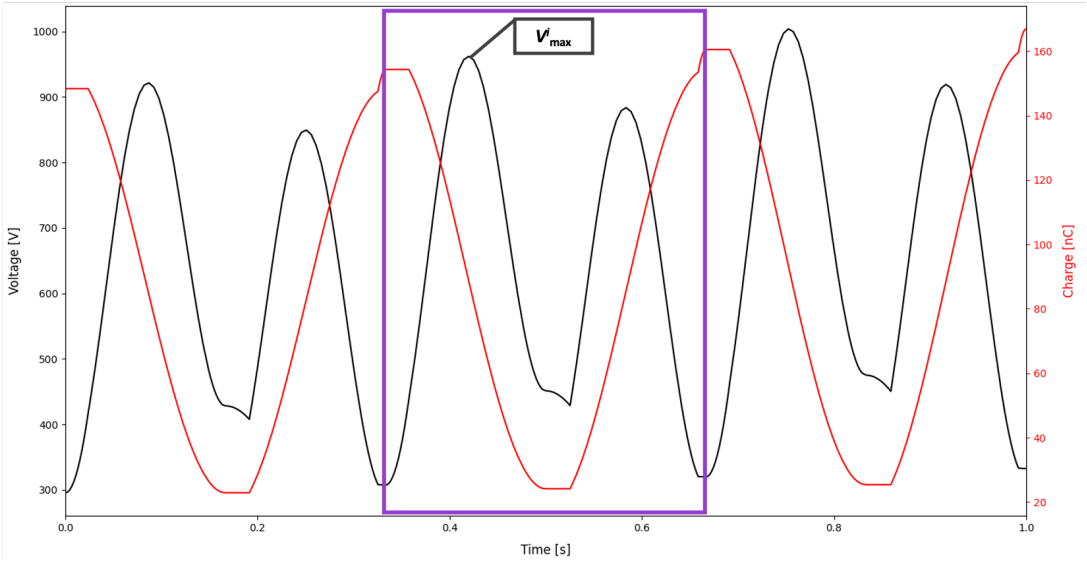

Figure 32: *Simulation results of the evolution of charge and voltage over C_{t+} with identification of local maximum voltage for the cycles 48-51.*

The simulation is run for a period of 40 seconds and a charge over C_{t+} has been derived as one of the simulation results. In Figure 33a) an exponentially increasing accumulated charge in the TENG's capacitor is prominent. The general inference about the progression of the charge in time has now been corroborated through simulations too. Double Bennet maintains its primary characteristic of exponentially increasing the quantity of charges moreover it has been proven that the "double TENG" - "double Bennet" system indeed has predicted characteristics.

Let us take a look at the output voltage of the current system, that is, the voltage of the output capacitor of double Bennet, C_{st}. From Figure 33b it is clear that there is a distinct and significant exponential increase in voltage over time. The output voltage has a slow start reaching a voltage of approximately 100 V in the first 15 seconds of operation. Thus within the next 15 seconds, the exponential behaviour reflects on voltage levels reaching 450 V.

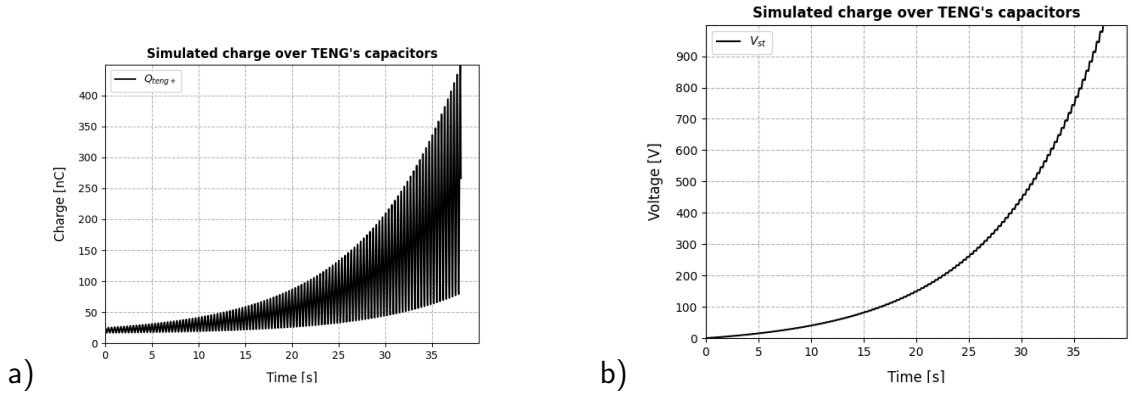

Figure 33: *a) Observation of simulated charge over $C_{\mathrm{t}+}$ for an elongated period. b) Simulated output voltage of double Bennet over the capacitor C_{st}.*

Within 37 seconds it has reached 1000 volts showing that at higher voltages cycle-to-cycle starting voltages increase abruptly.

Through these simulations, the capabilities of double Bennet when applied with a double TENG are visible. After some time, voltages have risen drastically and the quantity of charge in a TENG is considerable.

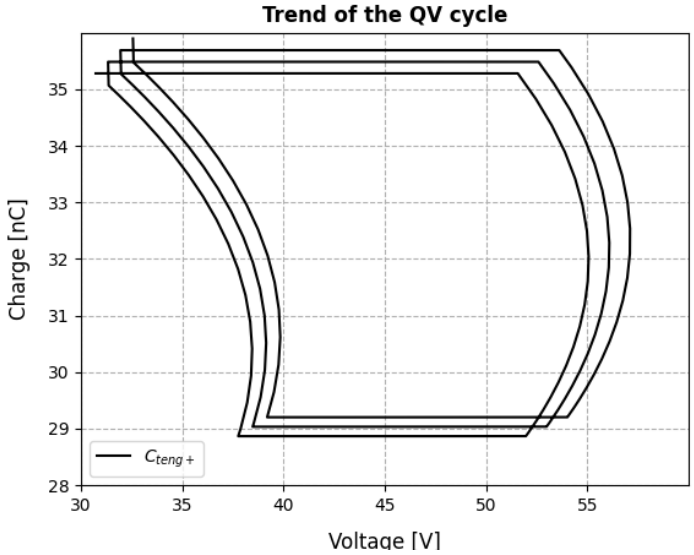

Figure 34: *QV cycle simulation of $C_{\mathrm{t}+}$.*

Finally, characterized charge and voltage of the TENG are simulated one against the other to form a QV cycle. Three instances of $C_{\mathrm{t}+}$'s cycle are depicted in Figure 34. The simulated shape corresponds well to the shape of the QV cycle generated by the theoretical derivations. The five phases in the cycle are identified which correspond to zones 1,..,5 of charge versus time in Figure 31 Each cycle contains a constant charge and varying voltage phase. Once charge levels change, their nonlinear relationship with voltage reflects on the shape of the second, fourth and fifth phases of the cycle.

As the simulation is run on a short interval, even though the trend of increase is not clear, the presence of one is established: three simulated QV cycles in Figure 34 are defined by each starting at a new and higher voltage.

2.4 Simulation and analytical results comparison

To effectively determine QV cycle's merit, it is put against simulations of the QV cycle generated by the calculations of derived equations for a system with the same characteristics. A Matlab script is contracted which calculates the results of derived equations and imports data from LTspice simulations. The result of the script is shown in Figure 35. Simulation results are in red and the calculated QV cycle is in blue color.

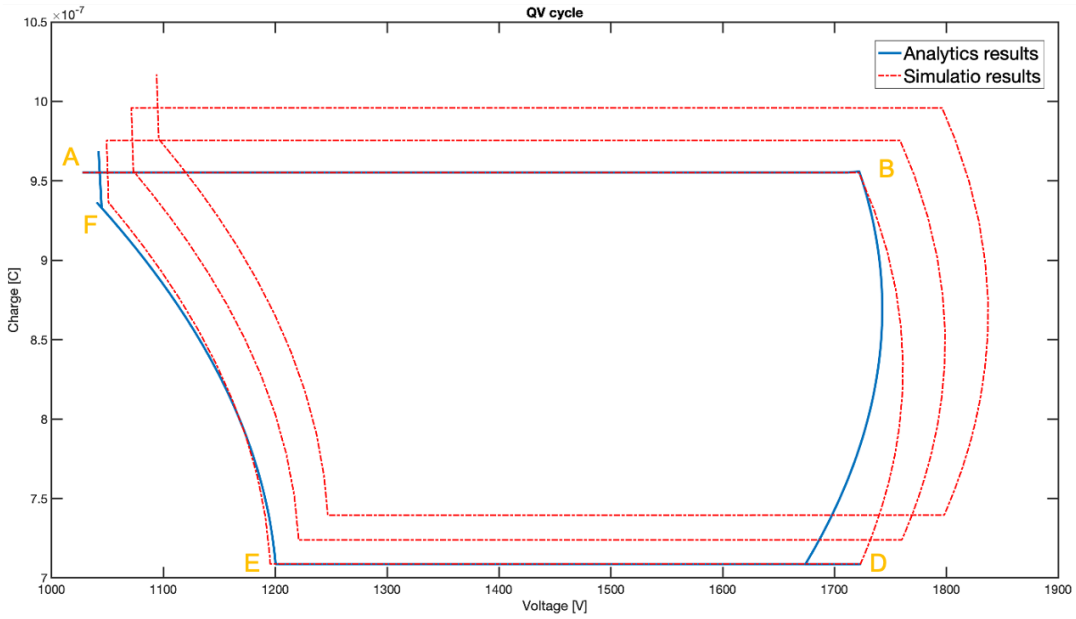

Figure 35: *Comparison of QV cycles obtained by analytic calculations and simulations.*

From simulations, it has been initially concluded that the QV cycle does indeed have the expected shape. The Blue (derived) line largely follows the red (simulated) line with small deviations. For the instances of constant charge, the match is perfect. However, a mismatch occurs in nonlinear segments. The largest discrepancy is at point D^i of the QV cycle at which calculations predict a steeper voltage decrease. As per Figure 35, in cycle fragment E^i - F^i -A^{i+1} of the cycle, two curves do follow the same trends with slight deviations that can be neglected due to order of magnitude in question (the charge being in nano coulomb range). After assessing the capabilities of software employed for simulations the possibility

of its deficiencies have been considered. The program has limited possibilities for adjusting simulation parameters. After establishing test simulations using another electrical circuit simulation software (Xyce and Ngspice) and comparing the results, it has been concluded that those are more suitable for simulations of this type. Total migration of simulations to software that suits better is one of the goals set for the continuation of this research.

It is to be concluded that simulation and theoretical results match at a high rate which gives the motivation to proceed with experimental research as the last step to the completion of analysis of the "double TENG" - "double Bennet" system.

2.5 Conclusion

Chapter two of the study has shown in great detail the complexity of the operation of Bennet's doubler with double TENG through extensive analytical analysis. The deduced expressions are obtained based on the evolution of the circuit itself as in different internals, different diodes are conducting, resulting in different configurations. Charge conservation and Kirchoff's laws allow for the derivation of rather complex voltage expressions starting from point A^i to A^{i+1}. The QV cycle covers two intervals with constant charge and two additional intervals with dynamic change of Q and V parameters. The dynamic Q and V are analytically defined by detailed parametric analysis of the two with respect to capacitance varying in time.

In section 2.3 a motive and methods used to set up Spice simulations are mentioned. Observing collected simulation results, five stages that are identified in the analytical stage of the study are clearly identified on the charge curves of the two TENG's capacitors.

Concurrence in the predicted and simulated circuit operation led to a direct comparison of the results generated by the two methods. It is to be concluded that, based on the generated QV cycle of the C_{teng+}, simulation and theoretical results match at a high rate which gives the motivation to proceed with experimental research as the last step to the completion of analysis of the system.

3 Experiments on double Bennet

3.1 Introduction

Chapter three of the study focuses on the work in the experimental domain. Concluding from chapter two of the manuscript, the theoretical and simulation work has shown a small margin of error between the two, leading to this experimental aspect of the research. The chapter starts by defining the methods used in the fabrication of the TENG used to conduct experiments in further subsections. Given that the TENG has been fabricated, the rest of the experimental setup is introduced as a complete system of control, actuation, and measurement of electrical parameters of the TENG and circuits applied to it. The following subsections continue to explain the methodology that is used to characterize the electrical parameters of the TENG, such as capacitance values and their shape. Furthermore, it is defined in detail how it is possible to estimate the value of the surface voltage of the triboelectric layer avoiding direct interaction with the triboelectric layer in question. Once the transducer is characterized, later subsections present and elaborate in great detail results obtained by measurements of half and full-wave rectifiers, a classic and hypothesized Bennet's doubler. The measurements focus on elaborating the output voltage of the mentioned circuits. Shown curves lead to the comparison of the charge pumps and obtained experimental results to simulation ones.

3.2 Experimental bench

3.2.1 Device fabrication

Based on the assessment of the availability of materials, operation and measurement equipment of the laboratory facility where experimental analysis is conducted, we have to lead to the conclusion that it is best to fabricate and run the experiments of double Bennet with a gap-closing TENG. The initial goal of the experimental analysis is to validate the behavior of double Bennet that has been established through analytical and simulation analysis. To accomplish that, a gap-closing TENG of significant size is designed with the intent of it being a proof of concept device. By increasing the size of the device, the scale of converted energy and other parameters including parasitic variables proportionally increases which gives a wider window for the detection, elaboration and elimination of necessary components.

Two materials are used as base plates for the conductive electrodes. Those are the FR4 and Polyethylene terephthalate (PET). FR4 is used as the base material for the support of the mobile capacitor's plate. The composite of the FR and copper is commonly used for printed circuit boards. The characteristics of it along with copper thickness are dictated by the manufacturer of the used plates. The utilization of this material ensures good surface conductivity of the copper and low parasitic variables through an insulating layer. The material used for the two outer plates is PET plastic sheets. The molecular structure of it can be either an amorphous or a semi-crystalline thermoplastic. Amorphous PET has lower mechanical strength, while semi-crystalline one can endure significantly higher mechanical stress due to its rigidity and strength. For the experiments, more durable, 3 mm thick, semi-crystalline PET sheets are used. Relative permittivity varies between 3 at minimum and 4 at maximum. Both support materials have similar dielectric properties. The thicker and more rigid material is used on the sides so that the effects of the mechanical impact of the plastic collision between the mobile and the fixed plate is best absorbed and its effects diminished. On top of the PET sheet, a 9 cm by 9 cm conductive adhesive supported by a tin-coated copper foil carrier is adhered. The thickness of the copper foil is 35 μm. Adhesive thickness is 25 μm.

To complete the construction of the TENG, it is necessary to add triboelectric material. To achieve that, sheets of polytetrafluoroethylene (PTFE) are adhered over a double-sided tape. It is popularized by and is known today under the name Teflon. This electret material is chemically resistant and not susceptible to mechanical wear with one of the lowest coefficients of friction of any solids. On the scale of the triboelectric series, it is on the extreme end of

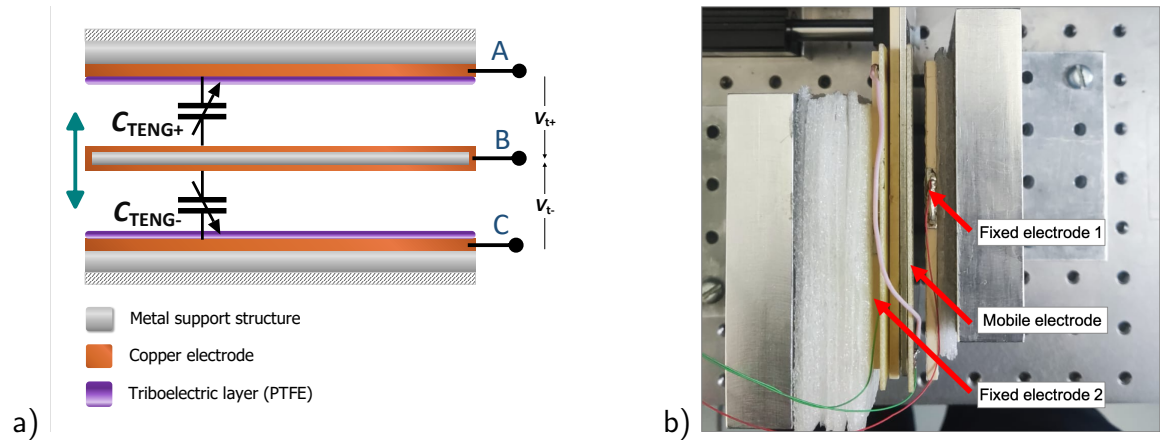

Figure 36: *a) A schematic representation of plate distribution and materials on them constructing a double TENG. b) A photograph of constructed TENG with one fixed plate on the right, a mobile plate in the middle and another fixed plate on the left side*

negatively polarized materials. Its relative permittivity is 2,1. Because of that property is it widely used and is therefore chosen for this TENG. PTFE comes in different forms, thus sheets of it in various thicknesses were available. A 100 μm layer of PTFE is deposited to two copper plates of the TENG.

The plates are squares with 10 cm long sides. The size of the conductive part of the plates which are effectively the capacitor's plates is selected to be 9 cm by 9 cm, giving plates a total area of 81 cm^2. The triboelectric layer is deposited on the entire area of the supports. This method of layering is used to prevent any possible short circuit that might occur when two plates are at a close distance. To be able to derive electrical connections from the capacitors and finally have a device with three nodes, a small copper extension is added to the square area on each plate. PTFE is deposited on top of the two fixed electrodes. The other two are attached to each other to form the middle plate. The middle plate is the common plate for the two capacitors which requires it to be conductive on both sides and for those sides to be connected. Due to the availability of materials during the fabrication stage, this was achieved by attaching two single-coated FR4 plates. All materials and their dimensions used in the fabrication of the TENG are listed in Table 3.

PHYSICAL PARAMETER	VALUE
PET and FR4 plates area	100 x 100 mm
Conductive layer area	90 x 90 mm
Thickness of conductive layers	35 μm
Double-sided tape thickness	$\sim$100 μm
Thickness of PTFE	100 μm

Table 3: *Dimensions of materials used for fabrication of TENG*

3.2.2 Motor setup with device

TENGs are actuated by kinetic energy and thus can be considered motion-driven transducers. To emulate the movement of TENG's mobile plate, a linear motor is used. To closely observe TENG's behaviour, the system is subjected to controlled movement rather than random one that would be present in the environment with real applications. TENG and its control system are placed on an optical table that absorbs mechanical vibrations from the test bench. Metallic "L" shaped stand structures attached to the table are used to position the plates that are fixed. Thanks to the screw holes on the optical table, the distance between two fixed plates is controlled and constantly fixed. Mobile plates are attached to a larger plastic plate that is used as a mounting latch that is attached to the motor.

To ensure contact between plates, the movable plate hits the fixed plate with a significant force. Initially, the contact was elastic with a little dumping, and bouncing effects present. This resulted in short contact time between the plates and not enough charge transfer. To resolve the issue, TENG's outer (fixed) plates are positioned on stands that are covered with foam to absorb shock. They added damping losses to the system thus ensuring long enough contact. Chosen foam is 2 mm thick. It is of medium stiffness which allows it to act as a dumper without compromising the stability of fixed electrodes. Within a few actuation of TENG with a motor, it was concluded that 2 layers of said foam are sufficient to completely eliminate unwanted mechanical effects.

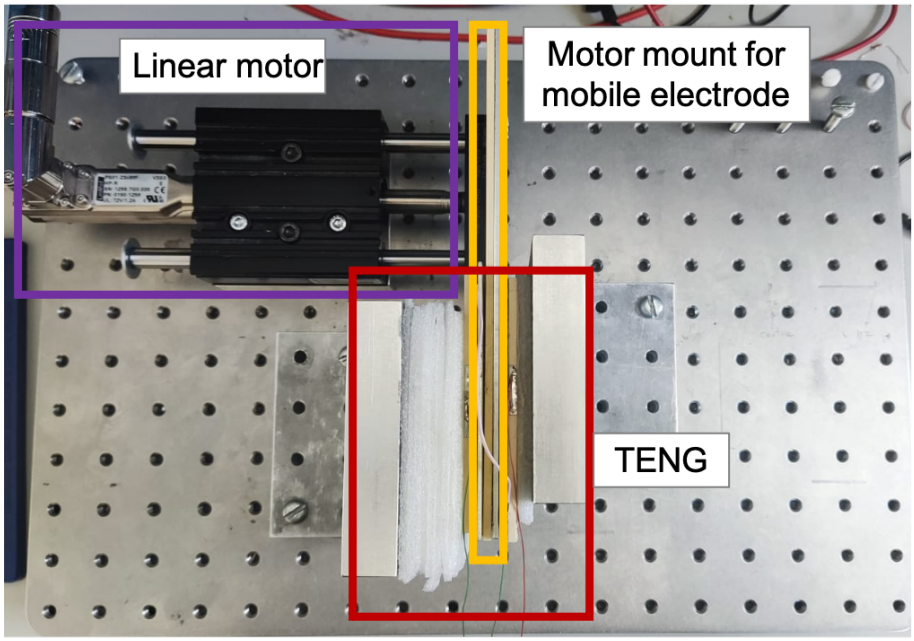

Figure 37: *Complete system of TENG and its actuation mechanism - a linear motor*

The motor used as controlled movement input is a linear motor (PL01-12x200/160-HP).

The setup of the motor's initial position, furthest and nearest point and shape of the trajectory is controlled through its computer software. The initial position of the motor refers to the initial position of the slider to which the mobile plate is attached. It is so that the mobile plate is in contact with the left fixed plate. It is operating at the frequency of 3 Hz with sinusoidal excitation. The effective displacement is 3 mm in each direction.

3.3 TENG characterisation

3.3.1 Capacitance measurement

To characterize the device that is fabricated, it is necessary to obtain data on its capacitive properties, as well as the triboelectric layer properties. Capacitance is characterized by the determination of its minimum and maximum values and the shape that capacitance takes. The boundary values are substantial to ascertain the capacitance ratio η which has a major role as its value determines whether the initial condition for circuits startup is satisfied or not (valid for Bennet's doubler). Quantification of the surface voltage of triboelectric layer represents the electrical characterisation.

For capacitance characterisation, firstly, it is measured with an LCR meter in C (capacitance) mode. Read values are used to get a notion of the order of magnitude for maximum and minimum capacitance. Utilized LCR meter measures fixed values. For that reason, TENG is kept stationary. The mobile plate is moved to the extreme of full contact between two plates which gives the maximum capacitance, $C_{\max}$. The value of $C_{\min}$ is obtained by moving the mobile plate to the furthest possible distance from the fixed plate.

Once the order of magnitude of $C_{\max}$ and $C_{\min}$ is obtained, the exact behavior of two capacitors is recorded using the dynamic capacitance method or otherwise called the phase shift method. This method generates a curve of capacitance shape and gives capacitance values in a specified time interval. This method provides information about the capacitance value based on the phase shift that is obtained between a carrier signal and a measured signal. To obtain the shift, a resistor-capacitor (RC) circuit is used where the fixed capacitor is substituted by one of the TENG's capacitors. When an alternating signal of specific frequency and amplitude is fed to the filtering RC circuit, the capacitor creates a phase shift of the fed signal which is then recorded. The shift is measured as the difference of x-intercepts of the two signals.

From the transfer function of the RC circuit in equation 60, it is derived that its argument

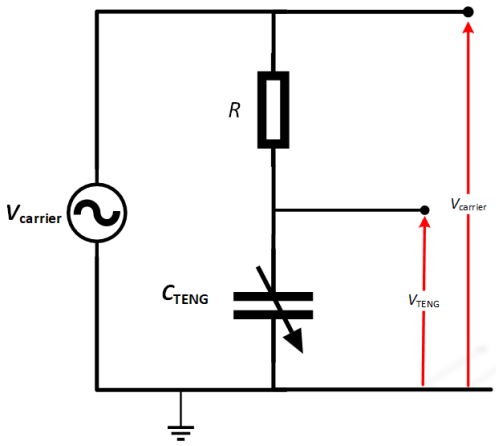

Figure 38: *RC circuit used for the dynamic capacitance measurement method*

is directly related to the value of the capacitor, as per equation 64.

$$H(j\omega) = \frac{V_{out}}{V_{in}}; V_{out} = V_{in}\frac{Z_c}{(Z_c + R)} \tag{60}$$

$$H(j\omega) = \frac{\frac{1}{j\omega C}}{\frac{1}{J\omega C} + R} \tag{61}$$

$$\mathbb{I}m[H(j\omega)] = -\frac{\omega RC}{(\omega^2 R^2 C^2 + 1)}; \mathbb{R}e[H(j\omega)] = \frac{1}{(\omega^2 R^2 C^2 + 1)} \tag{62}$$

$$Arg[H(j\omega)] = tan^{-1}\frac{\mathbb{I}m[H(j\omega)]}{\mathbb{R}e[H(j\omega)]} \tag{63}$$

$$Arg[H(j\omega)] = tan^{-1}(-\omega RC) \tag{64}$$

As per equation 65, when capacitance expression is extracted from the above equation, the expression shows the direct relationship between the angle of displacement θ, or phase shift of the carrier signal in the time domain, and the capacitance value.

$$\theta = tan^{-1}(-\omega RC) \rightarrow -tan(\theta) = \omega RC \rightarrow C = \frac{tan(-\theta)}{\omega R} \tag{65}$$

If the capacitor used in the circuit is fixed, a single value of the phase shift would be obtained corresponding to a constant capacitance value. Nevertheless, when a variable capacitor like TENG's capacitor is implemented, the variation in capacitance creates a variation in phase shift. As the dynamic capacitance measurement method allows for continuous recording of phase shift, a continuous measurement of capacitance is derived. In this way, each recorded

phase shift corresponds to a specific capacitance that is calculated. In other words, if the value of θ is known in any given moment, it is possible to extract the capacitance in that time period.

For chosen circuit to operate in its predicted range, resistance and capacitance values have to be in accordance. As the circuit is determining the exact value of capacitance, it is necessary to select a resistor that is compliant with the expected capacitance range. The following equation calculates the estimated necessary resistor value.

$$R = \frac{1}{C_{approx}\omega} \tag{66}$$

Where C_{approx} is the approximated capacitance, ω is the angular frequency and is equal $\omega = 2\pi f$. f is the frequency of the sinusoidal wave that is supplied at the input of the circuit. The amplitude of the supplied signal is 10 V peat-to-peak set at the frequency f = 9,5 kHz. For this calculation, capacitance values measured by an LCR meter are used. The approximated capacitance is around 550 pF for the $C_{\max}$. Calculating the resistor from the equation 66, the selected value is 56 $\mathrm{k}\Omega$. The output of the circuit is connected to the oscilloscope with 10 $\mathrm{M}\Omega$ probe to which the carrier input signal is connected too. Once at least three $C_{\max}$ - $C_{\min}$ - $C_{\max}$ revolutions are present on the screen of the oscilloscope, the data is acquired. It is imperative to visualize and process more than one capacitance revolution to avoid utilizing the signal that contains an anomaly or a faulty operation of the TENG. The stability of obtained signal is crucial. Post-processing of data is done using a Python script where two signals are fed and the script processes the data as per equations 60 - 65. At the end of the process, it provides a plot of the capacitance and a file containing plotted data. For fabricated TENG, the measurement results are as follows $C_{\max} = 500pF$ and $C_{\min} = 55pF$ for the left capacitor (referred to as C_{TENG+}), and $C_{\max} = 560pF$ and $C_{\min} = 55pF$ for the right capacitor (referred to as C_{TENG-}). The discrepancies between the two capacitors probably are due to human error as the transducer is fabricated and placed in the system by hand.

Figure 39 shows two curves of the capacitors. The two capacitors are symmetric and reach almost similar maximum and minimum values as expected.

The capacitance ratio for two capacitors are calculated in equations 67 and 68.

$$\eta_{\mathrm{TENG+}} = \frac{C_{\mathrm{TENG+_{max}}}}{C_{\mathrm{TENG+_{min}}}} = \frac{500pF}{55pF} = 9 \tag{67}$$

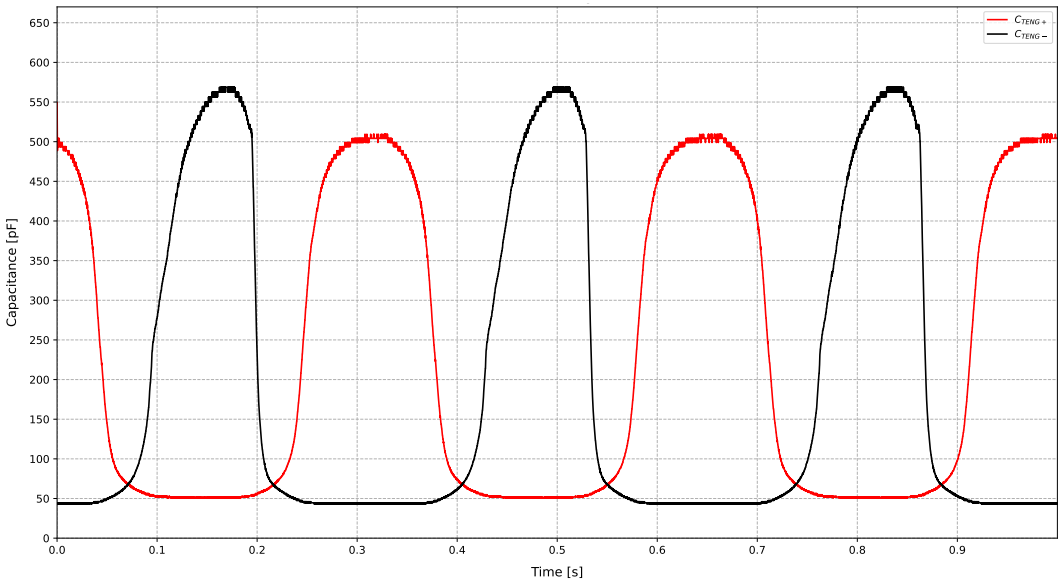

Figure 39: *Results of the dynamic capacitance measurement of* $C_{\mathrm{TENG}+}$ *and* $C_{\mathrm{TENG}-}$

$$\eta_{\mathrm{TENG}-} = \frac{C_{\mathrm{TENG}-\mathrm{max}}}{C_{\mathrm{TENG}-\mathrm{min}}} = \frac{550pF}{55pF} = 10 \tag{68}$$

The calculated minimum capacitance for the dimension of a single TENG capacitor is 50 pF, while the measured value is 55 pF. This shows that at the low capacitance values when the capacitor is most susceptible to accumulating the parasitics from the environment and the system itself, TENG's capacitors are rather stable and true to their minimum value. The calculated maximum capacitance is 1 nF and the measured capacitances are 500 pF and 550 pF which shows larger discrepancies. Even though the difference is rather large, it is not unexpected as the device is constructed by hand and imperfections in layering may have altered the estimated smallest distance between two plates. As it is known, to calculate maximum capacitance, the minimum distance between two plates is considered. In this case, it is the sum of thicknesses of double-sided tape and the triboelectric layer which in this case, ideally, would be 200 $\mu\mathrm{m}$. There are uncertainties that can be present in the physical model. There is a risk of the presence of air between layers and the exact thickness and electrical properties of the double-sided tape (its relative permittivity) are unknown. Taking this dimension as minimum distance brings the C_{max} value to 1 nF. On the other hand, if imperfections are considered and the minimum distance is increased from 200 $\mu\mathrm{m}$ to 250 $\mu\mathrm{m}$, maximum capacitance would be calculated to be 600 pF which is significantly closer to measured values. The difference in thickness of 100 $\mu\mathrm{m}$ is not clearly visible to the eye and could easily be overseen. It is concluded that both C_{max} and C_{min} are coherent with expected values.

Capacitance ratios of 9 and 10 are not typical η values for a TENG. In this case it is a consequence of the effective area and distance between the capacitor's plates. Such large capacitance ratios give a level of comfort when TENG is applied with different circuits. Different circuits have a different value of η set as a necessary initial condition for a start-up of one. In this case, η values are well above the necessary range for each of the circuits that are considered, then for better control over voltage, current and charge levels in circuits, the capacitance ratios are reduced by adding a fixed capacitor with a known value. The capacitor is added in parallel to the TENG's capacitor so that its value contributes to both $C_{\max}$ and $C_{\min}$ with a significant impact of the $C_{\min}$ as it is a smaller value. As it is considered that the operation of the circuit with fabricated TENG is guaranteed, the aspect ratio of set output capacitance and speed by which the output voltages are reached is brought into question. To be able to set the system to an equilibrium of ratios between multiple circuits, it is necessary to control the trend of the increase of the V_{out}. The speed at which the output capacitor is charged and the voltage over it increased, is defined by its capacity and capacitance ratio. Therefore, for a fixed output capacitance value, it has been decided to reduce the η to slow down and better control the output voltage. The selected capacitor's value that is added to each side of the TENG (to both capacitors so that their symmetry is kept through the experiments) is $C_{\text{para}} = 33\text{pF}$. This brings the capacitance ratios to $\eta_{\text{TENG+}} = 6$ and $\eta_{\text{TENG−}} = 6,6$.

3.3.2 The estimate of V_{te} and η

Once the shape and amplitude of the capacitance have been characterized, the estimate of V_{te} is the second step in the electrical characterization of TENG. The initial condition in regards to the stability of the triboelectric later for the circuit operation is defined by its full saturation, a constant value of voltage, at the moment at which measurement took place. It is possible to measure surface charge density by a non-contacting voltmeter (like the one available at the laboratory facilities - TREK 347) nevertheless, it requires close proximity of the sensing probe to the material whose charge density is measured, in this case to a triboelectric layer. Due to the structure of the TENG and the proximity of the transducer's plates, it is impossible to conduct measurements when TENG is active and its plates are positioned parallel to one another without disrupting the system's mechanical integrity. Assuming that the triboelectric layer is fully saturated and stabilized, it would be necessary to remove the plate with the layer physically, after that perform the measurement with a non-contact electrometer and finally return the plate to its initial position. It is hardly possible to perform the measurements without tempering the layers. For that reason, measurements of the output voltage of a full-wave rectifier are used. More specifically, the saturation voltage of the output capacitor of the full-wave circuit elaborates the voltage of the triboelectric layer, as shown in equation 69. Figure 40 depicts the connection between TENG and the full-wave circuit.

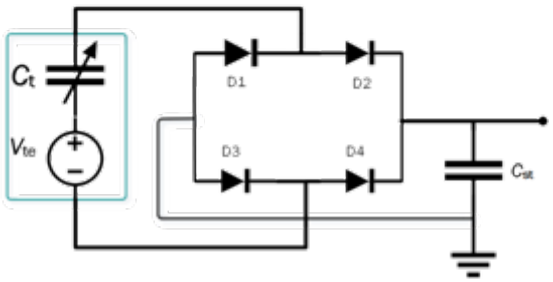

Figure 40: *Full-wave circuit in combination with one of the TENG's capacitors*

In the previous section, η has been measured. In addition to the η measurements, once the saturation voltage of the full-wave circuit is recorded and known, it is possible to calculate the value of the surface voltage of the triboelectric layer, V_{te}. The calculation is done by deriving an expression for V_{te} from the equation initially reported in [37].

$$V_{\mathrm{sat}} = -V_{\mathrm{te}}\left(\frac{\eta-1}{\eta+1}\right) \rightarrow V_{\mathrm{te}} = -\frac{V_{\mathrm{sat}}}{\frac{\eta-1}{\eta+1}} \tag{69}$$

The procedure to measure the output voltage of the full-wave rectifier involves performing

the experiment with one of the TENG's capacitors, after which it is disconnected and the remaining capacitor is connected for the measurements. Chosen output capacitor has a fixed known value of 10 nF. To measure the voltage over it, a charge through its branch is measured. As the capacitor value is known and constant, based on the relation $V = Q/C$, the voltage of the output capacitor can be obtained. The apparatus that has the capability to measure the amount of charge flowing between the terminal of the TENG is Keithley 6514 system electrometer in *Q - charge* mode is used to measure the charge.

In Figure 41, the red and magenta colored curves represent the trend of the output voltages of the full-wave circuit run with both capacitors. Due to the time limitations of the oscilloscope used in this case, the final saturation voltages are not presented on the graph. Nevertheless, the actual measurement apparatus (the electrometer) has continuously recorded constant saturation values equal to 92 V for $C_{\mathrm{TENG}+}$ and 123 V for $C_{\mathrm{TENG}-}$.

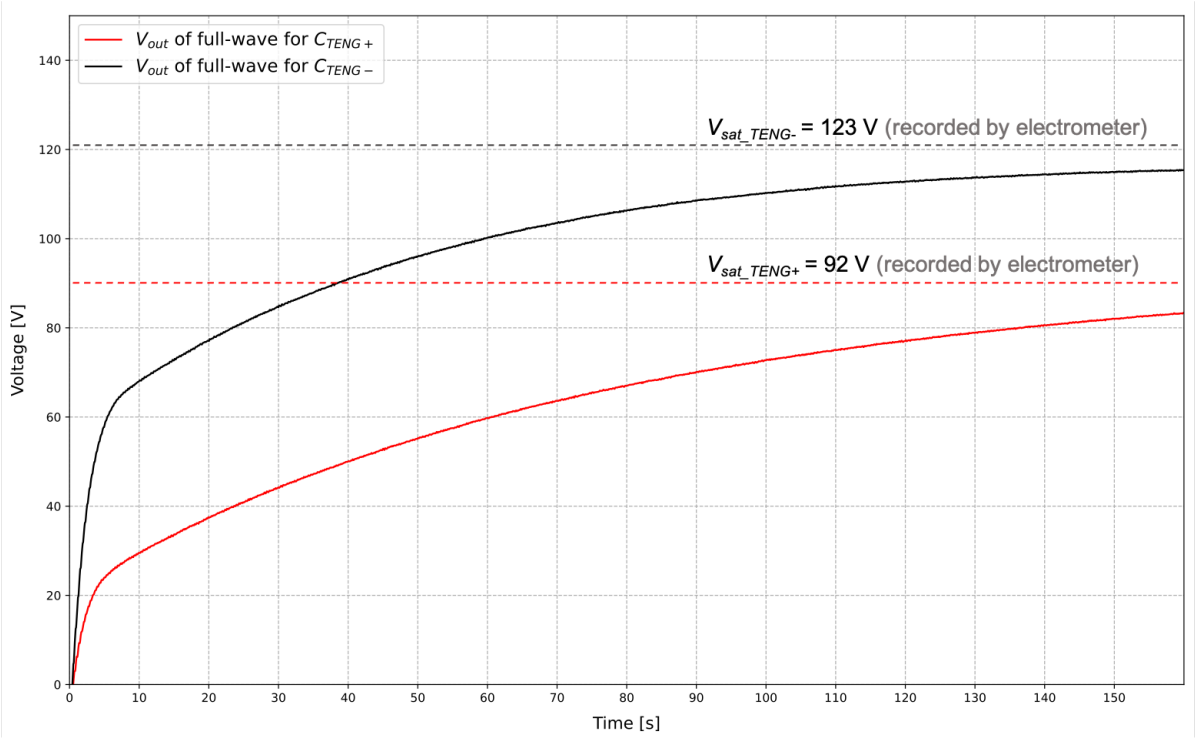

Figure 41: *Output voltages of the full-wave rectifier circuit for two TENG's capacitors*

$$V_{\mathrm{te}+} = -\frac{V_{\mathrm{sat}_{\mathrm{TENG}+}}}{\frac{\eta-1}{\eta+1}} = -\frac{92V}{\frac{6-1}{6+1}} = -128,8V \tag{70}$$

$$V_{\mathrm{te}-} = -\frac{V_{\mathrm{sat}_{\mathrm{TENG}-}}}{\frac{\eta-1}{\eta+1}} = -\frac{123V}{\frac{6,6-1}{6,6+1}} = -166,9V \tag{71}$$

The values calculated in equations 70 and 71 confirm the assumption that the two triboelectric layers contribute similarly to the operation of the TENG. It is clear that the envelope

of the difference between the two derived values is 13 %. Nevertheless, it has to be taken into account that the TENG has been manufactured by hand in a non-controlled environment resulting in a larger margin of error permissible for such TENG. On the other hand, in further sections it is proven that TENG with such a level of disbalance of V_{te} values operates well and does not compromise the operation of the electronic circuit it is attached to.

Yet another way to estimate the η is by comparing the output voltages of a half-wave rectifier. The process used to perform output voltage measurement for the full-wave rectifier is kept the same for the half-wave rectifier, keeping the same output capacitor.

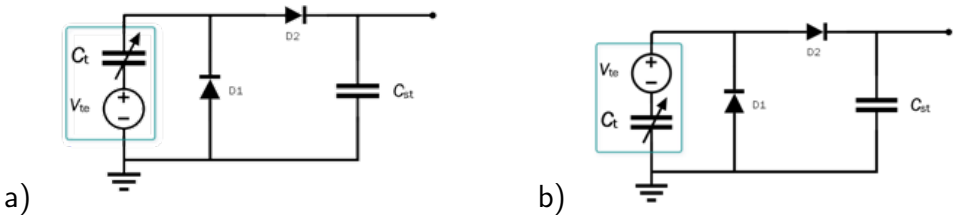

Figure 42: *Half-wave circuit with a) TENG capacitor's plate with triboelectric layer is grounded (circuit labeled as half-wave 1). and b) Another plate of the capacitor is grounded and plate with triboelectric layer is connected towards the rest of the circuit (half-wave 2).*

In addition to the already presented reliable and accurate capacitance measurement process, it has been proven useful to use a method of η determination by half-wave measurements. This method is used to verify the mechanical integrity of the TENG (which would in any case of discontinuity modify values of maximum and minimum capacitance) as it is attached to an external excitation-inducing mechanism for which there is no control and verification system provided. In this way, it is possible to assess an important electrical parameter of the TENG without repeating the extensive procedure and post-processing required by the dynamic capacitance measurement method, cutting down on time between the tests. By performing a simple measurement of the output saturation voltage of the two configurations of the half-wave rectifier, it is possible to deduce the capacitance ratio of the TENG's capacitor under test. Considering that the TENG's capacitors are in fact capacitors with plates covered in different materials (an addition of the triboelectric layer to one of its plates) creating an electrical equivalent of the variable capacitor and a constant voltage source, it is possible to connect one of the TENG's capacitor to the half-wave rectifiers in two ways. Each of the cases is numbered as 1 or 2 to avoid possible confusion between the circuit topologies.

The two possible TENG and half-wave configurations are the following:

1. The terminal of the plate that is covered with a triboelectric layer is connected to the ground. An electrical model in which a constant voltage source is connected to the ground (later called half-wave 1) as shown in Figure 42a).

2. The free electrode (bare electrode with just the copper on it) can be connected to the ground. An electrical model in which a variable capacitor is connected to the ground (later called half-wave 2) as shown in Figure 42b).

When the plate with triboelectric layer is connected towards the ground, a case of half-wave 1, V_{sat} is calculated as per equation 72 derived by A. Ghaggarinejad et al. in [37]. On the other hand, if the variable capacitor is the component of the TENG that is connected towards to ground plane, an expression defining the relationship between the V_{sat}, V_{te}, and η is first derived in [14]. In the case of half-wave 2, the saturation voltage is calculated as in equation 73, starting with the left-hand side of the equation and isolating the V_{te} parameter to obtain the value of the surface voltage of the triboelectric later implemented in the transducer.

$$V_{te_{HW_1}} = -\frac{V_{sat}}{\eta - 1} \tag{72}$$

$$V_{sat} = -V_{te_{HW_2}} \frac{\eta - 1}{\eta} \rightarrow V_{te_{HW_2}} = -\frac{V_{sat}}{\frac{\eta - 1}{\eta}} \tag{73}$$

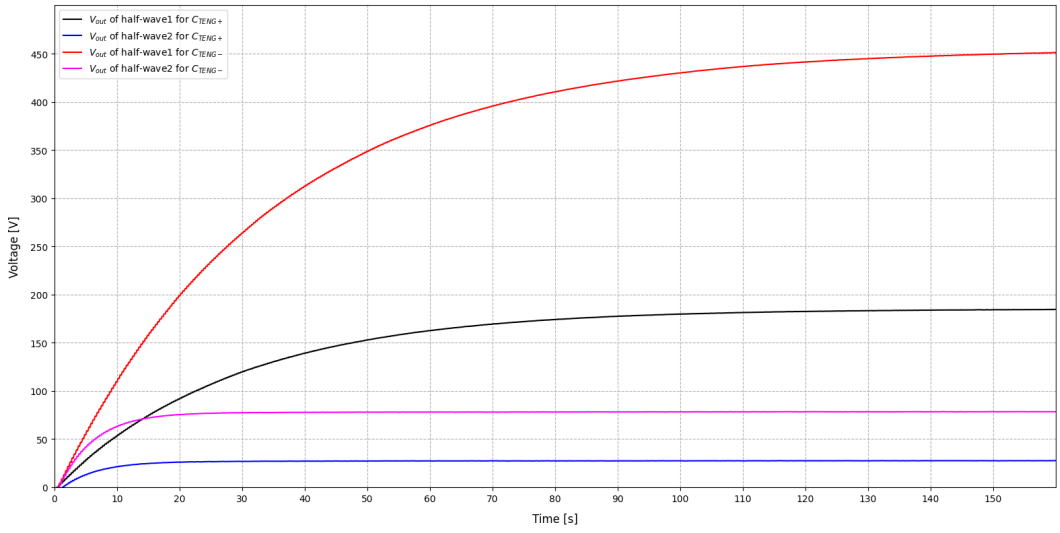

Figure 43: *Output voltages of the two half-wave rectifier circuits for TENG's capacitors*

Data used to complete the calculations of η is extracted from Figure 43. In red and magenta colors are output voltages of half-wave 1 and half-wave 2 rectifiers, respectively, combined with the C_{TENG-}. The saturation voltage of the first half-wave circuit is 450 V and of the second one is 85 V. The curves in black and blue correspond to the two circuits with the C_{TENG+}. The saturation voltage of half-wave 1 is 193 V and 33 V of half-wave 2. It

is not unexpected that saturation voltages of the two TENG's capacitors with these circuits are not equal. To find the ratio of the V_{te} parameters from two half-wave configurations, equations 72 and 73 are used. As derivation in equation 74 shows, once the expressions are divided, they simplify and only a η parameter remains, allowing us to conclude that the ratio of the voltages obtained by half-wave measurements gives a numerical value equivalent to η parameter.

$$\frac{V_{te_{HW_1}}}{V_{te_{HW_2}}} = \frac{-\frac{V_{sat}}{\eta-1}}{-\frac{V_{sat}}{\frac{\eta-1}{\eta}}} \rightarrow \frac{V_{te_{HW_1}}}{V_{te_{HW_2}}} = \frac{V_{sat}(\frac{\eta-1}{\eta})}{V_{sat}(\eta-1)} = \eta \tag{74}$$

Essentially, the most relevant parameter is the ratio of the saturation voltages. As calculated in equations 75 and 76, the ratio of the even though the saturation voltages are not the same, obtained ratios are.

$$\eta_+ = \frac{V_{te+_{HW_1}}}{V_{te+_{HW_2}}} = 5,8 \tag{75}$$

$$\eta_- = \frac{V_{te-_{HW_1}}}{V_{te-_{HW_2}}} = 6 \tag{76}$$

If the precision of η calculation is required, it is clear that this method does not provide a precise $C_{\max}$ - to - $C_{\min}$ ratio however, it gives a good approximation of it. For the capacitor labeled as $TENG+$, η obtained from dynamic capacitance measurement is equal to 6, while approximated value is 5,8. On the other hand, $TENG-$'s η obtained from dynamic capacitance measurement is equal to 6,6, while approximated value is 6.

3.4 Output voltage measurements

3.4.1 Construction of the experimental circuit

When characterisation of the TENG is complete, it can finally be subjected to operation with Bennet's doubler. Firstly, each of the two capacitors are operated with a classic Bennet configuration. After which, TENG is operated with double Bennet. Each experiment is initiated so that curves of the output voltages can be extracted and later compared.

The circuit that is implemented is soldered on a prototyping board. As per schematics of double Bennet, it requires 3 diodes and a reference and a storage capacitor. To construct a circuit, MMBD1503AD87Z general purpose diodes are used. The advantage of these diodes

is their low reverse current of just 1 nA. The disadvantage of using them for this type of circuits is their relatively low breakdown voltage of 200V. One surface mount component of such diodes contains two diodes connected in series. To increase the supported voltage that can pass through the circuit, 8 diodes are connected in series, increasing the breakdown voltage to 1600 V. The actuation voltage per diode is 0,68 V therefore because there are 8 of them connected, the actuation voltage is increased to more than 5 V. This does not represent a problem for our Bennet circuit with high capacitance ratio η, as this voltage is overcome immediately within one mechanical cycle of operation of TENG.

3.4.2 Output voltage measurements with a classic Bennet's doubler

Construction of the classic Bennet's doubler is completed with a selection of the reference capacitor. As it is previously reported, the ratio between storage, reference and transduction capacitors' values defines the proper start of the circuit. ($C_{\mathrm{TENG}} \succ C_{\mathrm{ref}}$) The storage capacitor is kept the same as in measurements of the rectifying circuit ($C_{\mathrm{st}} = 10\mathrm{nF}$). The value that is selected for the reference capacitor is $C_{\mathrm{ref}} = 500\mathrm{pF}$. This value is specifically chosen with the vision of comparing of performance of classic Bennet to double one. Knowing that the maximum value of TENG's capacitor substituting C_{ref} is in the range of 500 pF that value is chosen as a value of the fixed capacitor. Consequently, the effects of the second TENG's capacitor will be depicted at the output of double Bennet that is comparable to the output of classic Bennet.

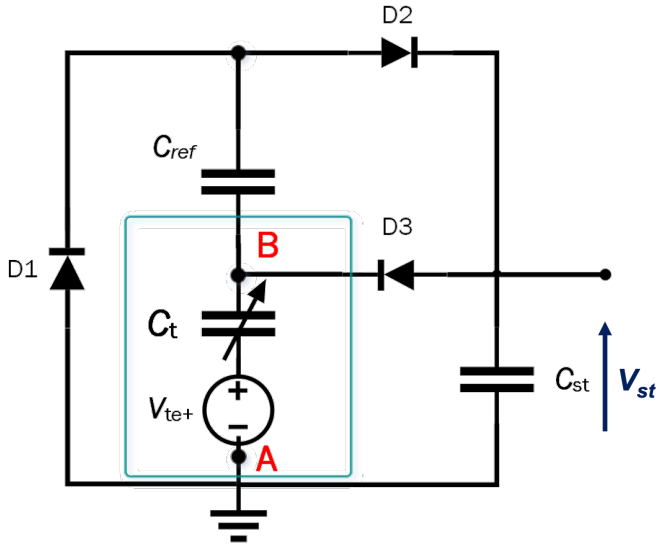

Figure 44: *The schematic of classic Bennet's doubler circuit.*

The system of one TENG capacitor connected to the classic Bennet's doubler circuit (the schematic of it is shown in Figure 44) is run and the output voltage is recorded. The results of the experiments for both capacitors are shown in Figure 45. The expected exponential increase that characterises Bennet is present for both capacitors. With all necessary initial conditions satisfied, the system behaves just as expected. To reach 400 V at the output it only took 16-17 seconds, which corresponds to 48-51 mechanical cycles of the TENG. Small differences in the performance of the two capacitors are expected as they are not a perfect image of one another. This is seen through 1 second difference in their performance.

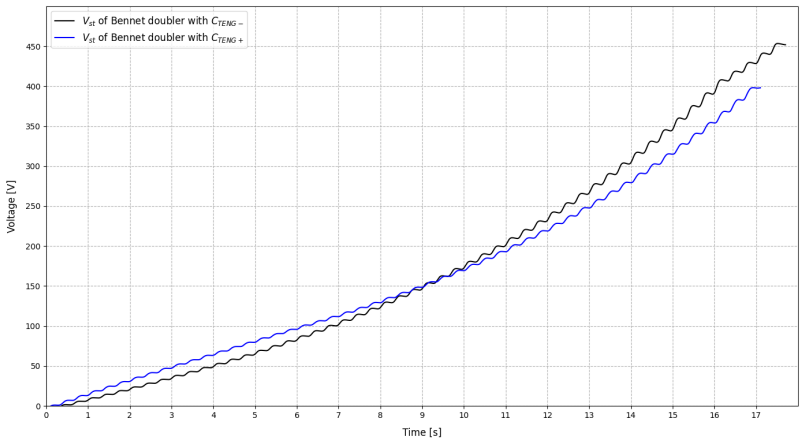

Figure 45: *A graph of output voltages recorded for two TENG's capacitors implemented with classic Bennet's doubler.*

3.4.3 Output voltage measurement of a double Bennet

The circuit of classic Bennet is easily adjusted to accommodate the second variable capacitor by substituting C_{ref} by it. The same set of experiments is run and the output voltage of the double Bennet is recorded shaping the curve shown in Figure 46. From the figure, it is clear that double Bennet first passes through a very short transient phase before it starts to have the organic exponential increase of the voltage across the storage capacitor. It includes transient processes of two parts of the system. Firstly, it is the transient process of the TENG. To be exact, its initial charging and saturation of triboelectric layer. Secondly, the transient phase of the circuit before all nodes in the circuit exceeds diode voltages. The combination of both transient phases lasts about 2 mechanical cycles or 0,66 seconds. Once all transient phases are complete, reaching 400 V double Bennet takes exactly 13 seconds or 36 mechanical cycles.

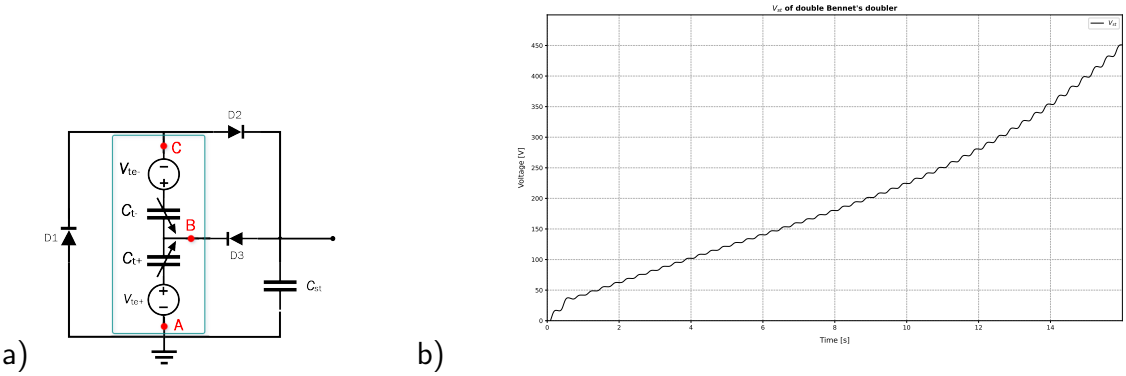

Figure 46: *a) A schematic of the double Bennet circuit implemented with a double TENG. b) A graph of the output voltage curve of a double Bennet with a voltage limited at 450 volts.*

The true potential of double Bennet is observed at high voltage (Figure 47). The shape of the curve gives us more information about the nature of the operation of double Bennet in practice. The circuit passes through a couple of phases. Firstly, there is a transient phase at the start-up of the circuit that stops at 200 volts. At that voltage, the phase of exponential increase starts. It is significant to remark that voltage increase at higher voltages is so high that it takes only 4 mechanical cycles for the voltage to increase 100 V. To reach voltages as high as 950 V it took 25 seconds or 75 mechanical cycles at 3 Hz frequency. The third phase that is expected is the linear phase at which the exponential increase becomes linear due to the diode and capacitors leakages and approaching their maximum supported voltages. This phase is not recorded as it is seen at even higher voltages.

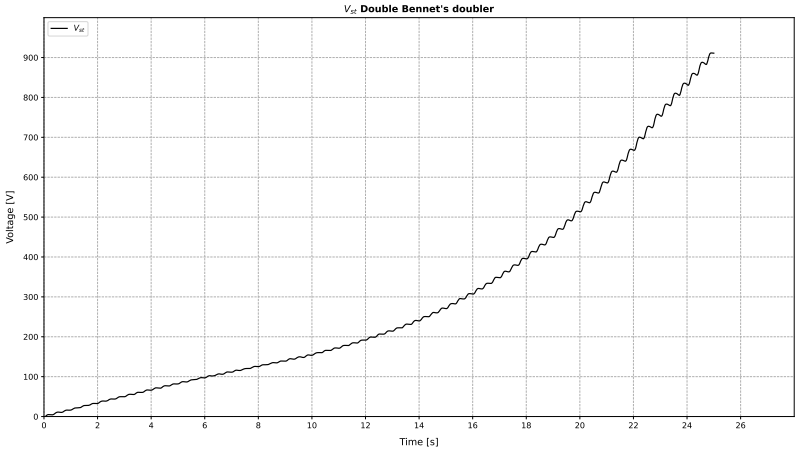

Figure 47: *Measurement of the output voltage of a double Bennet over a longer period of time*

Transient phases of the double Bennet in combination with a TENG are explored further however, are not in the scope of this thesis.

3.5 Comparison of double Bennet and other charge pumps

In this section performance of double Bennet is compared to the performance of other charge pumps, both stable and unstable ones. That encompasses a classic Bennet's doubler as well as two configurations of the half-wave rectifier and full-wave rectifier circuits. There are many ways the performance of two charge pumps can be compared. It can be done, for example, by looking at their output voltages, stored energy per cycle, shape and size of respective QV cycle, etc. The designed experimental setup provides data about the voltages over the output capacitor of the circuits based on which they are compared in this study. Each of the circuits uses the same TENG and has the same output storage capacitor of 10 nF which provides the ground for equal comparison between them.

Firstly, the output voltage of double Bennet is compared to one from classic Bennet's doubler. As traditional Bennet's doubler is used as a base for the double one, observations of their behaviour in practice are the most interesting to investigate. Figure 48 portrays the curves of two classic Bennet's in black and a double Bennet's output voltage in red.

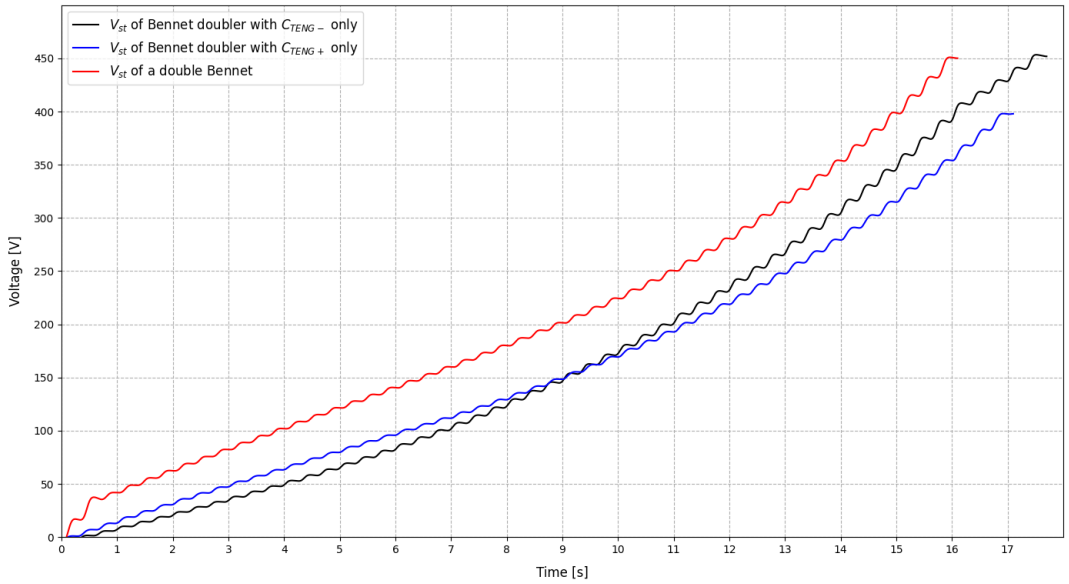

Figure 48: *A comparison of output voltages of two TENG's capacitors with classic Bennet and output voltage of a double Bennet.*

In accordance with theoretical analysis and simulation results, it is expected for both circuits to have equal capabilities of reaching high voltages and for both to have an exponential increase. Based on the information provided in subsections 3.4.2 and 3.4.3 the difference between the two circuits used in the experimental test is the substitution of the fixed reference capacitor by a variable TENG capacitor that has values in the range of the first variable one.

It is to be concluded that the presence of TENG's second triboelectric layer that is located between the nodes of the previous reference capacitor (in an electrical sense) benefits the circuit's output.

From Figure 48 it is clear that even in the early stages of its operation, double Bennet outperforms the classic Bennet. Considering the time that it takes for each to reach 400 V, it is clear that it takes less time for double Bennet to reach the same voltage. That is because of a higher increase in voltage at each mechanical cycle, resulting in a higher slope formation from the moment circuit starts operating. 16,5 seconds is the time that is necessary for classic Bennet's doubler to reach 400 V, thus it takes double Bennet 15 seconds to reach the same voltage. When the red curve is closely observed, it is observed that the first two mechanical cycles do not exert the same behaviour that is homogeneously kept for the remaining period of the circuit's operation. This is due to the initial transient phase that double Bennet goes through. As mentioned, it takes 2 mechanical cycles that equate to 660 ms for the circuit to start operating in a steady state. This reduces the effective steady state operation time of double Bennet to 14,33 seconds.

In conclusion, due to a higher voltage increase from one mechanical cycle to another, double Bennet takes 6 mechanical cycles less to reach the same voltage when compared to classic Bennet. As both circuits have exponential increase, it is expected that the difference in speed is more prominent as the voltage range increases. The addition of a second TENG's capacitor did speed up the performance of the circuit resulting in a faster increase. Therefore, for applications when time is a factor that may influence the throughput of the whole system, double Bennet is a speedy circuit.

The second finding of this study compares the output voltage of double Bennet to the output voltages of other charge pumps which are shown in Figure 49. There is a clear separation between stable and unstable charge pumps. Stable charge pumps saturate, whereas unstable charge pumps do not saturate. An indication of this can be seen in the given figure. Red, green and violet curves correspond to the stable charge pumps, while orange and blue curves are the two Bennet doublers. This figure illustrates the advantages of the double Bennet circuit. In addition to its non-saturating state, it can achieve higher voltages in a short time interval. The electronic circuits in the system that follow after the rectification state have a higher amount of energy at their disposal to be used. The fact that stable charge pumps reach saturation voltage at their output directly reflects on the shape of the formed QV cycle and maximum converted energy per cycle which is a finite value for circuits in question (from a theoretical point of view as well as in practice). On the other hand, Bennet doubler's

unique exponential increase provides an increased amount of converted energy per cycle for any time interval that the system is subjected to operation. The findings about the behaviour of double Bennet have been already reported. Thus conducted experimental tests confirm that the constructed system of the gap-closing TENG and double Bennet indeed has a steep sloped exponential increase at its output that accommodates for high rates of converted stored energy at its output capacitor.

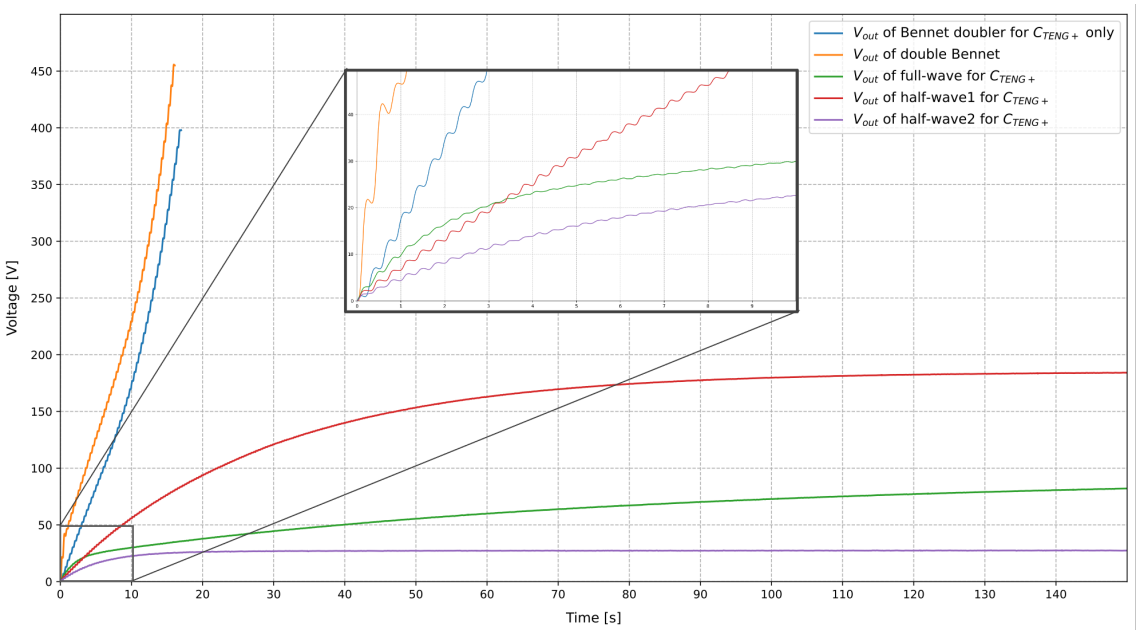

Figure 49: *Output voltages of studied stable and unstable charge pumps.*

Output voltage is just one of the aspects that characterise the performance of a circuit like Bennet's doubler. It is necessary to focus on the observations of the charge levels which complement the voltage and in this case directly reflect on the amount of energy that is effectively converted from its mechanical form to electrical. The experiments that simultaneously track the voltage and charge distribution in the circuit are under construction and results are planned for the near future.

3.6 Simulation and experimental results comparison

After it has been established that double Bennet operates in practice within the states that are determined theoretically, it is possible to further explore the compliance of experimental and simulation data.

Electrical simulations of two circuits are conducted and put against experimental data that

is obtained, as shown in Figure 50. Red and black curves correspond to obtained experimental results for the two Bennets. Yellow and blue curves are the simulation results simulated for the two circuits.

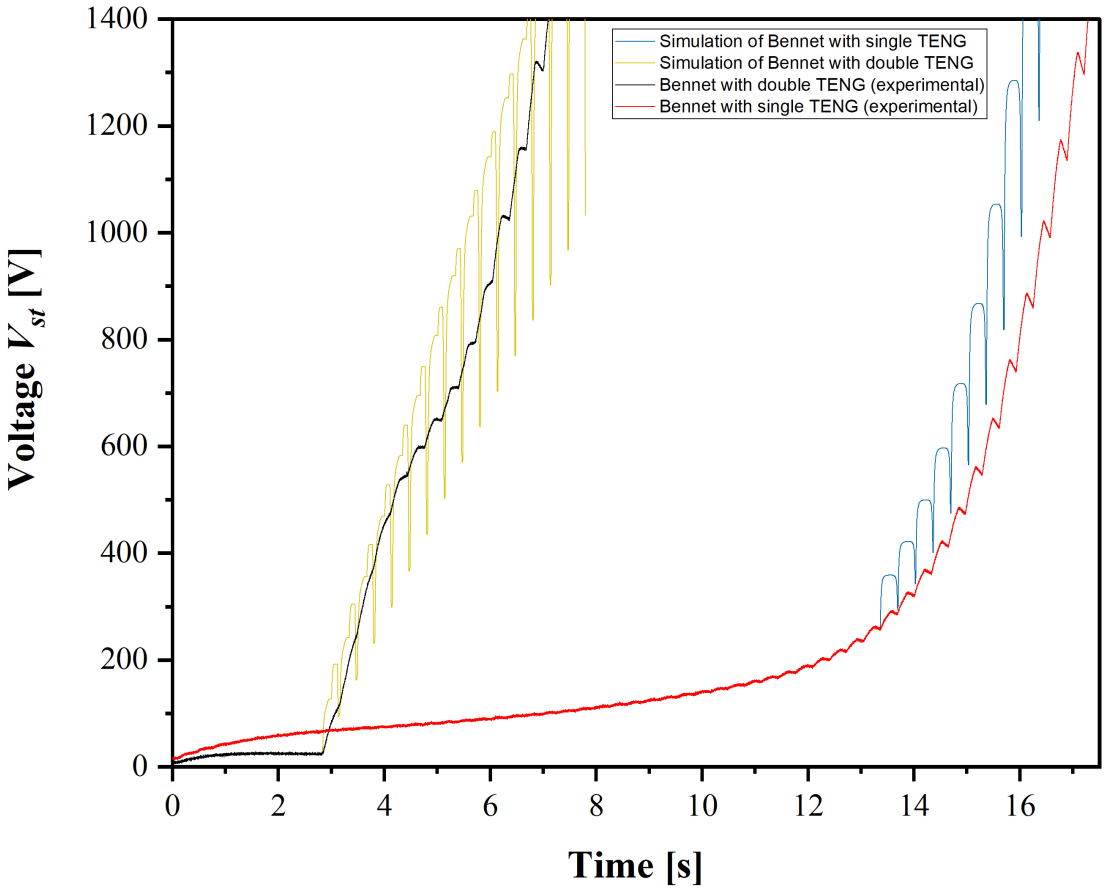

Figure 50: *Experimental and simulation results obtained for classic and double Bennet.*

The experimental section of this research is done over an extended period of time of a couple of years. It resulted in damage to the TENG that is due to environmental conditions (fluctuations in temperature and humidity in the space where the experiments were conducted) and wear and tear of the triboelectric layer due to mechanical stress continuously applied to it. The maintenance of the transducer is done by redepositing the triboelectric layer. The effects of the change of the layer can be seen in the given figure where both classic and double Bennet go through a transient phase that is attributed to the stability of the saturation level of triboelectric surface voltage. Once the layer's saturation voltage is reached, both show an already discussed exponential increase.

By observing the curve pairs (black-yellow for double Bennet and red-blue for classic Bennet), it is concluded that the envelope formed by the simulation curve follows the trend of the results that are experimentally obtained. Simulations consider just the steady state operation of the circuits, therefore the data is comparable for the time interval after the

transient phase. Simulation curves do not perfectly align with experimental curves that is due to the limitations in the adjustment of simulation parameters provided by the used software tool. Simulation results are generated in LTspice, the software that performs circuit analysis. The congruence of results signifies that on an experimental level, studied circuits do behave in accordance with circuit analysis and electrostatic principles. Even though simulations are not precisely depicting the experimental setup their envelopes do follow the same shape and predict the same behaviour of each circuit.

It is possible to validate experimentally obtained results about output voltages of two unstable charge pump circuits through simulations, thus leading to the confirmed congruence of theoretical, simulations and experimental results studying double Bennet.

3.7 Conclusion

In chapter three of the thesis manuscript, an experimental aspect of the study of Bennet's doubler circuit implemented with double TENG. Firstly, previously theoretically covered architecture of double TENG is now translated into a real physcial system. A classic PCB plates as well as hand-made copper conductive layers covered with PTFE are used. The complete system with its externally controlled excitation mechanism (linear motor) is introduced as the base of the system that is used for testing combinations of the TENG with various rectifying circuit. Before performing the test, the transducer is characterized by dynamic capacitance measurement method as a tool to obtain the shape and values of the capacitance. It has been concluded that obtained capacitance shape is the that is expected from theoretical and simulation parts of the study. Obtained capacitance give a high ratio η which is reduces to better control the speed of the obtained output voltage over the storage capacitor. A method of evaluation of surface voltage of the triboelectric layer using measurement of output saturation voltage of full-wave rectifier has been presented as non-invasive method of characterizing the device.

Further sections present output voltages obtained for classic Bennet's doubler as well as for the double Bennet, clearly showing that the trend of the exponent presented in both cases is significantly higher in case of double Bennet resulting in an output that reaches high voltages faster. Finally, stable and unstable charge pumps are graphically compared showing the superiority of double Bennet in terms of the speed of increase starting from a steep initialization of the circuit.

The third chapter is completed with the comparison of simulation and practical results of

the output voltage where it is concluded that, observing the steady state of the system, the envelope of the simulated output voltage takes the same shape as the experimentally recorded output voltage. These results complete the initial stage of the full analysis of double Bennet opening questions for the future work defined in later chapters.

4 High voltage plasma MEMS switch

4.1 Introduction

In chapters 2 and 3 of the thesis first and second blocks of energy conversion and management system are elaborated. The energy for the environment has been converted to an electrical signal that has been conditioned. Bennet's doubler produces high voltages at its output. It is an imperative to construct a circuit that regulates and decreases the voltages to lower levels (3,3 V or 5 V) that allows for the system to be paired with the commercially available electronic components. The proposed solution is to use Buck DC-DC step-down converted. To handle the transfer of accumulated charges from the output storage capacitor of double Bennet to the input nodes of the Buck converter, a control element is implemented as a bridge between the two. This chapter of the thesis presents the use of a high-voltage micro-plasma MEMS switch as a control element for the energy conversion and management system.

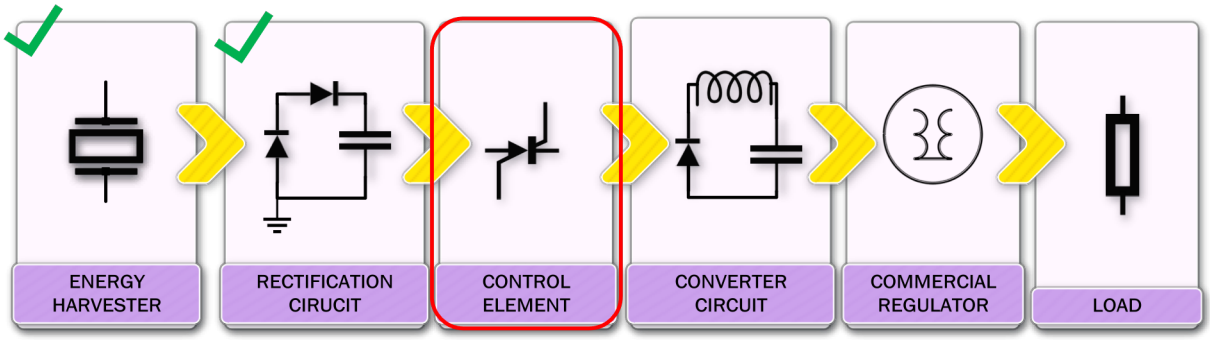

Figure 51: *Proposed 5-stage system for energy harvesting and management adapted for use with commercial components. Progression to stage 3.*

4.2 Theoretical principle of micro-plasma MEMS switch

A switch, by definition, is a component that makes a connection or a break in a circuit. They can be bulky as ones used as light switches in homes or as small as couple millimetres. Both and all other types of switches in the range work on the same principle. The two conductors are placed in proximity to one another. This is considered as open or off-state. Once the connection between two conductors is established, conductors start to conduct and transfer power from one node (anode) to another (cathode). Various methods can be used to form a contact. It can be by mechanically placing a conductive material to connect (mechanical switches like push buttons and relays) or by utilizing semiconductor properties of constitutional materials (electronic contactless switches like transistors). Another type of switches that is proposed by this thesis are the spark-gap switches. Their conduction principle is based on the formation of a plasma conduction channel between two conductors. For plasma to form a conduction channel, or in other words for a discharge to take place, a strong electric field formed by high voltages at the ends of conductors is necessary. At a high voltage, a current pass through two conductive electrodes due to the electrical breakdown in a specific gas at a specific pressure. The environment in which the anode and cathode are placed plays an important role in the level of control and characteristics of the switch. Initially, micro-plasma sources were developed however, there was little control of supported voltages and general operation of the switch. Taking the quality and accuracy of MEMS fabrication processes it has been made possible to accurately control the gap between electrodes and therefore to control actuation voltages by utilizing the microplasma. Figure 52 shows the general principle of operation of a plasma switch that is then translated to a micro-scale.

Micro-gaps can vary in size from 100 μm to small values in the nm range. Pressures,

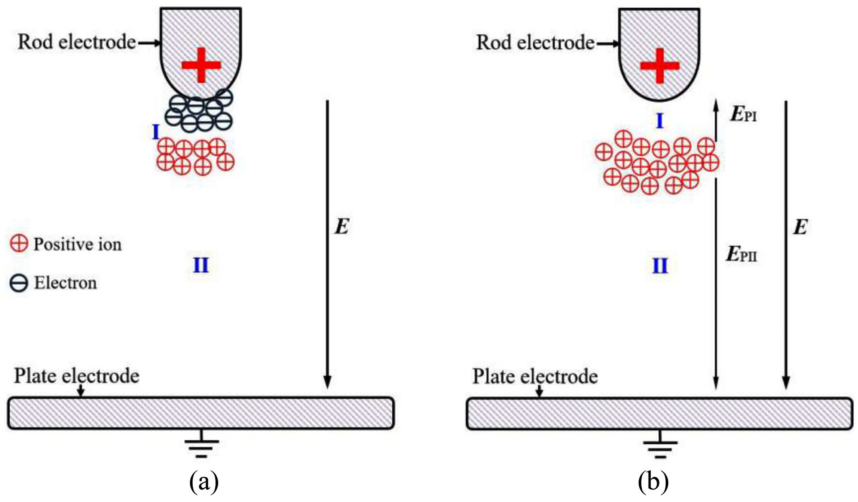

Figure 52: *Principle of formation of plasma discharge. Distribution of space charge under positive polarity.[46]*

at which a plasma discharge may form for the gap distances mentioned, range from high vacuum to atmospheric pressure. A physical principle that defines the relationship between the anode-cathode gap, pressure and voltage at which plasma forms and conducts is Paschen's law.

4.2.1 Paschen's law

Friedrich Paschen was a German scientist that first experimentally investigated the gas breakdown phenomenon in 1889. His experiments yielded a curve that explained the relationship between environmental characteristics (pressure and distance) and breakdown voltage between two conductors. Today, this curve is known as Paschen's law. It is mostly used for the determination of breakdown voltages of electronic devices and equipment.

Plasma is the fourth state of matter, in which electronics and ionized species are significant constitutive parts of the gas, to a degree that an electromagnetic field strongly affects plasma's behaviour. Paschen's law is initiated by Townsend avalanche. It is when under the influence of an electric field between an anode and a cathode, electronics mobilize and collide with molecules present in the gas (neutral particles and positive ions) bombarding the cathode. This multiplicative process avalanches which permits electrical conduction in gas. For the phenomena to occur, anode and cathode with substantial electric fields forming between them have to be placed in an environment with an abundance of electrons and particles that can be polarized. There are three regimes of plasma discharge:

1. Townsend discharge - voltage gradient is insufficient to ionize atoms

2. Glow discharge - voltage gradient is large enough to ionize atoms. Ions migrate towards the cathode (the α process)

3. Arching - thermal effects become significant and the cathode becomes a source of electrons that ionize atoms near the cathode. (formation of a high-current stream of plasma along the voltage gradient)(the γ process)

The mathematical expression that sumps up above listed phenomena constituting a plasma discharge in Paschen's law is the following:

$$V_{bd} = \frac{Bpd}{ln(Apd) - ln(ln(\frac{1}{\gamma} + 1))} \tag{77}$$

where V_{bd} is the breakdown voltage, p the operating pressure, d the gap between anode and cathode, γ the gas constant, A the saturation ionization and B is the ionization energy.*A* and *B* are constants determined by the gap type. They are calculated using the equations 78 and 79.

$$A = \frac{\sigma}{K_{BT}} \tag{78}$$

$$B = \frac{U\sigma}{eK_{BT}} \tag{79}$$

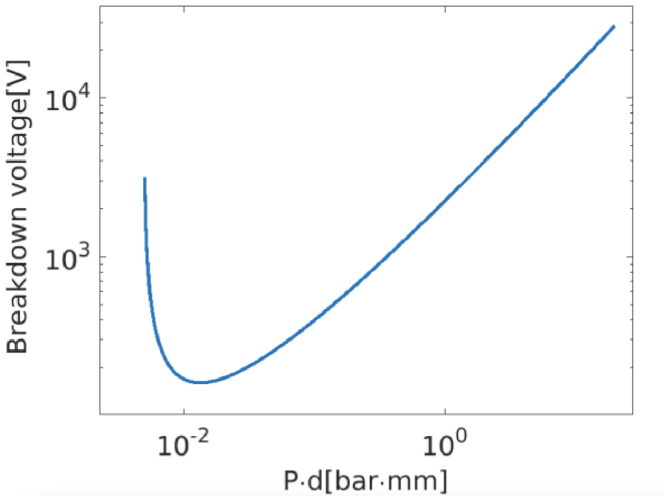

Figure 53: *Paschen curve for room temperature argon, calculated using the equation 77 [47]*

The curve that shows expression in 77 forms is depicted in Figure 53. Paschen's law explains that on its right branch, with decreasing *pd*, breakdown voltage linearly decreases to a characteristic minimum. The left branch, decreasing pd increases breakdown voltage. That is because with large gaps, stronger electric field is necessary to activate the plasma as the mean free path of electrons is longer. On the other hand, when gaps are on the opposite spectrum, it is impossible to mobilize and ionize gas particles as physically, there is no space

for their movement. Therefore, higher voltages are necessary to excite particles for forming plasma discharge.

Paschen's law defines the breakdown voltages at small gaps, however, [48] has discussed the deviations to the curve for gaps smaller than 10 μm. It has been concluded that when the mean free path of electrons is of the order of the gap, the Townsend breakdown cannot occur, however other types of breakdown are possible. This leads to modifications in the Paschen curve, which agrees with the "standard" Paschen curves at gaps larger than 10 μm and exhibits a plateau for breakdown voltage between 4 and 10 μm, and a linear drop in V_{bd} at lower. The experimental confirmation of the plateau in the curve has been confirmed, which is considered to be the transition region from Townsend avalanche to ion-enhanced field emission.

Selected values of the gap between the anode and cathode that are taken as a scope of the research in this thesis are 5, 7 and 9 μm. These gaps set predicted values of the breakdown right at the plateau region of Paschen's curve.

Selected values allow for the calculation of breakdown voltages and the formation of the Paschen curve for those. A is the saturation ionization is equal to 112,50 $(kPacm)^{-1}$, B is the ionization energy is equal to 2737,50 $V(kPacm)^{-1}$ and γ the gas constant is equal 0,02 are all constants that are defined by the environment of the switch. These values are the standard values (constants) used for the plasma discharge at atmospheric pressure in the air. Obtained breakdown voltages are 369,2 V, 273,5V and 260,2 V for gaps 5,7, and 9 μm.

4.2.2 Pull-in voltage effect

When the anode and cathode are static, Paschen's law is the ruling principle of the system. However, it is possible to construct dynamic switches. Their design difference is in the fact that their anode or cathode is no longer static and thus is mobile. Mobile yet still anchored anode has a range of movement that allows for plasma discharge formation at distances, or a full ohmic discharge once it touches the cathode conductor. Due to the fact that switches operate at high voltages, a pull-in voltage has to be considered. It is unavoidable to consider the effect for any system that has two conductors at varying distances and are biased. When two conductors are placed in close proximity to one another and voltage is applied, electrostatic force works towards the reduction of the gap between the two conductors. If the electrostatic force is stronger than the mechanical one pulling the anode away from the cathode, permanent contact between two electrodes occurs.

4.3 Spark discharge for high voltage repetitive switching

The first research on plasma has been published in 1927. With many understandings of what plasma is and its complex definitions, it has been understood as a gas with a significant presence of charged particles, both positive and negative, and other neutral particles, whose behavior is dictated by its thermal properties. Inherently, plasma is electrostatically neutral, with differently charged particles balancing each other out. It is not until a certain influence on plasma that it starts being charged leading to a discharge at critical conditions.

In 1991, S.L. Moran et al. in [49] first investigated pressurized spark-gap switches and low-pressure glow-type switches. They have found that recovery of the switch can be faster by triggering the switch well below self-break. The amount of time needed to recover half of the self-breakdown voltage is about 10 times less than the time needed to recover the full self-breakdown voltage. Recovery time can be decreased by making the operating voltage significantly less than the static DC break-down voltage, allowing voltage to be re-applied before the gas has returned to ambient temperature. Voltage as a main factor that affects the repetitive operation of spark gaps has been reported by S.J. MacGregor. et al. in [50]. Application of a suitable bias voltage to the anode can help control the residual ion population regulating the level of discharge that forms. J.M. Koutsoubis et al. in [51] addressed the effect of the type of the gas (SF_6 and air mixtures) to which the switch is subjected at charging voltages of 23 kV. Assessment of the sustainability of system operating as high voltages has been reported by S.H. Nam et al. in [52][53] who proposed the use of two similar spark gaps in the pulser system to increase the voltages and reduce pulse (spark) speed.

A different application of a spark gap has been investigated by Faisal K. Chowdhury et al. in [54] where it has been used as a field effect transistor (FET) at low voltages. A three-dimensional Micro -plasma Field Effect Transistor (MOPFET) devices that operate inside atmospheric RF helium plasma has found their applications in space exploration and nuclear research. This is the first time that spark-gap switch is used as an electronic switch combining the two principles.

Zhang H. et al. in [17] have first reported about the use of a high-voltage MEMS switch in a self-sustained system with a TENG. The system yields high-energy conversion rates without power-consuming electronics as designed switches have low losses compared to commercial ones. Effectively, this paper reports on advancements in the research that is done as a base

for the research results reported in this thesis.

The voltage breakdown can progress abruptly or progressively. Zuber and von Laue [55][56] propose a probability distribution function describing the statistical description of gas breakdown. From a statistical perspective, the V_{bd} is the maximum voltage at which an electrical system can operate without any breakdown – the probability of breakdown is zero. From the experimental perspective, V_{bd} is the smallest voltage at which breakdown has been detected. The two determinations are naturally consistent. To obtain the onset voltage corresponding to breakdown, the applied voltage is increased at a rate that initiates the electron avalanche and consequently a breakdown. It was previously confirmed that the breakdown is a function of the voltage increase rate [57]. The rate should be small enough to avoid the overshooting onset of breakdown. The onset can be estimated, for example, for voltage rise rate variation from 10 to 100 Vs^{-1} estimated static breakdown is about 415 V. This phenomenon is attributed to increased surface charge accumulation at small rates, which reduced the potential difference, requiring a higher applied voltage [58][59][60].

The roughness of electrodes in micro-systems is a significant concern as it affects the breakdown voltage. Besides that, the surface's roughness may also be introduced from handling and assembly procedures. Therefore, exploring the effects of electrode geometry on the breakdown process is of critical importance. The effects of designed surface morphologies on the electric breakdown in the sub-millimeter regimes have been numerically investigated in [61][62][63]. Led by these research reports, two topologies: flat and with protrusions, are encompassed by this thesis work.

4.4 Switch design, fabrication and packaging

Motivation for the chosen design of the MEMS switches shown in Figure 54 came from work that has been done previously on this topic [17]. Two designs of fixed anode-cathode switches are designed and fabricated. Each dice contains two spark gap switches. The first design contains a single rectangular structure (a finger) from the anode leading to the cathode. The ends of both are flat, making it a plate-to-plate geometry. The second sample design that is positioned on the same dice has a slight variation from the first one. At the strip at which the anode and cathode are the closest, an array of triangle-like intrusions has been added to both sides. The second design has multiple fingers. 3 fingers are attached to the anode and the remaining two are from the cathode. This design provides significantly more area for the discharge to occur. Analogously to the sample in Figure 54 a), the sample in 54

b) contains a modified design with extrusions. These designs have been used as a base to create variations in design. They are depicted through changes in the gap between the anode and the cathode.

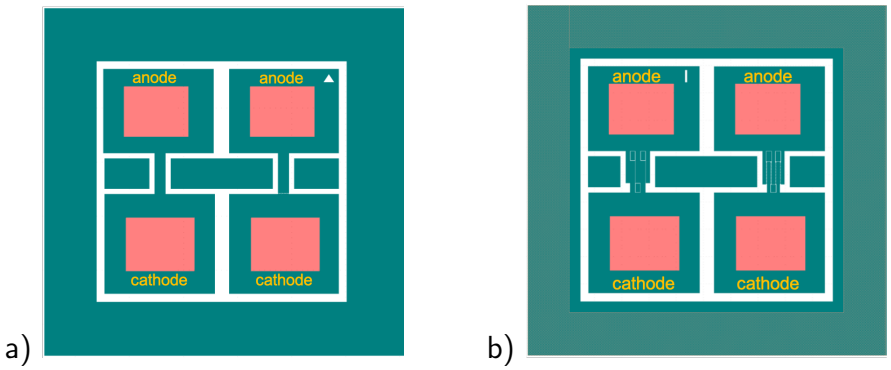

Figure 54: *An example of a dice each containing two switches per sample.*

Figure 55 shows the intricate design of the masks that are used in fabrication. To ensure that the fabrication process is done uniformly throughout the whole wafer and equally on a dice, dummy structures are used. One of the key steps of the fabrication process is chemical etching. As with chemical etching, it is harder to control the uniformity of the process, if there is a large gradient with smaller and open spaces on a design, dummy structures are added. The sample with a single finger contains three rectangular structures that are positioned at double the switch gap. Design with multiple fingers contains more dummy shapes that are positioned around the structure following the same method.

The designed masks are used in a process of fabrication of the samples in the facilities of the clean room at ESIEE Paris. For the wafer, a silicon-on-insulator (SOI) wafer is used. It is a type of wafer substrate composed of an insulating material (box layer) sandwiched between a thin layer of silicon (device layer - top layer) and a silicon substrate (handle layer - bottom layer). The specific wafer used in fabrication has 40 μm thick device layer, 2 μm box layer and 400 μm thick handle layer.

The fabrication process starts by growing 0,8 μ m oxidation layer on SOI on top of which a photoresist is deposited for photolithography. That is done so that trench between the anode and cathode and openings for pads can be created. Once the mask is formed, the wafer is etched using oxide etching and a cleaning step is done to remove any photoresist. To form connection pads, over the area of the wafer a 0,8 μ m layer of aluminum is deposited. The shape and position of the pads are determined by a mask created by photolithography. To do that, another layer of photoresists is deposited and photolithography is used to form the pattern for aluminum removal from the parts of the wafer that do not pad openings. After

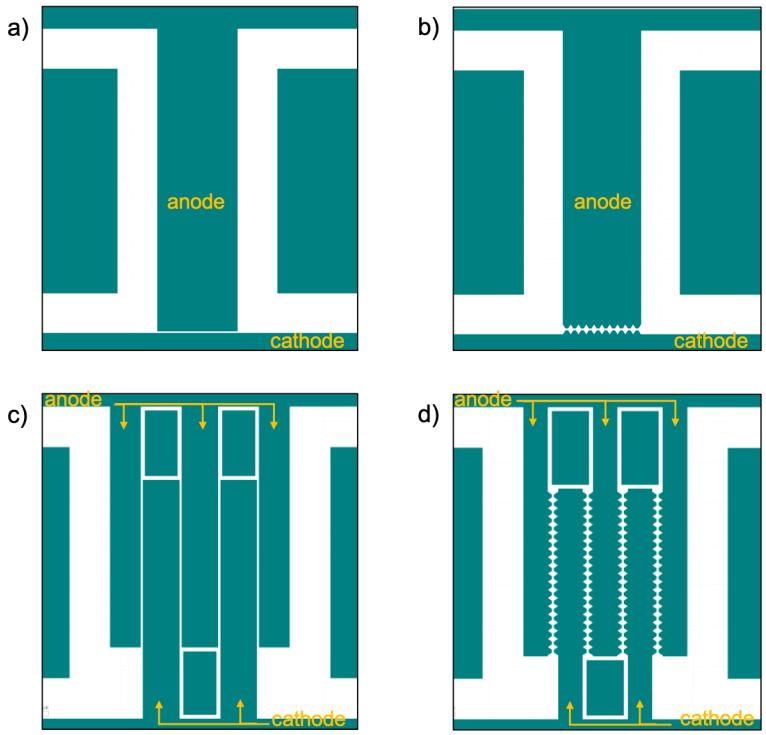

Figure 55: *Designs of fabricated switches. a) A single beam with a flat surface facing the cathode. b) A single beam with 10 triangle-like extrusions at its end facing the same extrusions on the cathode. c) Comb-like structure of five fingers with flat surfaces on both anode and cathode. d) Comb-like structure with 100 extrusions distributed over 3 anode and 2 cathode fingers.*

the aluminum is etched, the wafer is cleaned and prepared for the 40 μm silicon (device layer) etching using DRIE. The final step includes oxide etching using vapor HF. It is an isotropic process that etches the box layer in both vertical and horizontal directions. Before samples are ready to use, the Al metal is annealed and samples are diced. The process is presented on a cross-section of one of the samples in Figure 56.

Once the samples are fabricated and diced, they are of the size 10 mm by 10 mm. They are delicate compared to other components and capacitors used in the system. It is necessary to mount them on a stand that will allow them to easily be connected to a PCB or breadboard. A PCB with four connection pads corresponding to four pads at the sample (one for the anode and one for the cathode of each sample) has been designed. The protection of samples against dust and other airborne particles as well as protection from mechanical impacts like dropping or wrong handling of the samples. A frame surrounding the dice and covering part of the connection pad adheres to the supporting PCB on top of which a clear glass plate of the same size is placed. The sample is protected from the unwanted effects and the assumed environmental conditions of pressure and the type of gas that the switch is submerged in. The connection pads are designed to be large so that wire bonding from the connection pads on the dice to the pad on the PCB can be done comfortably while framing the system and

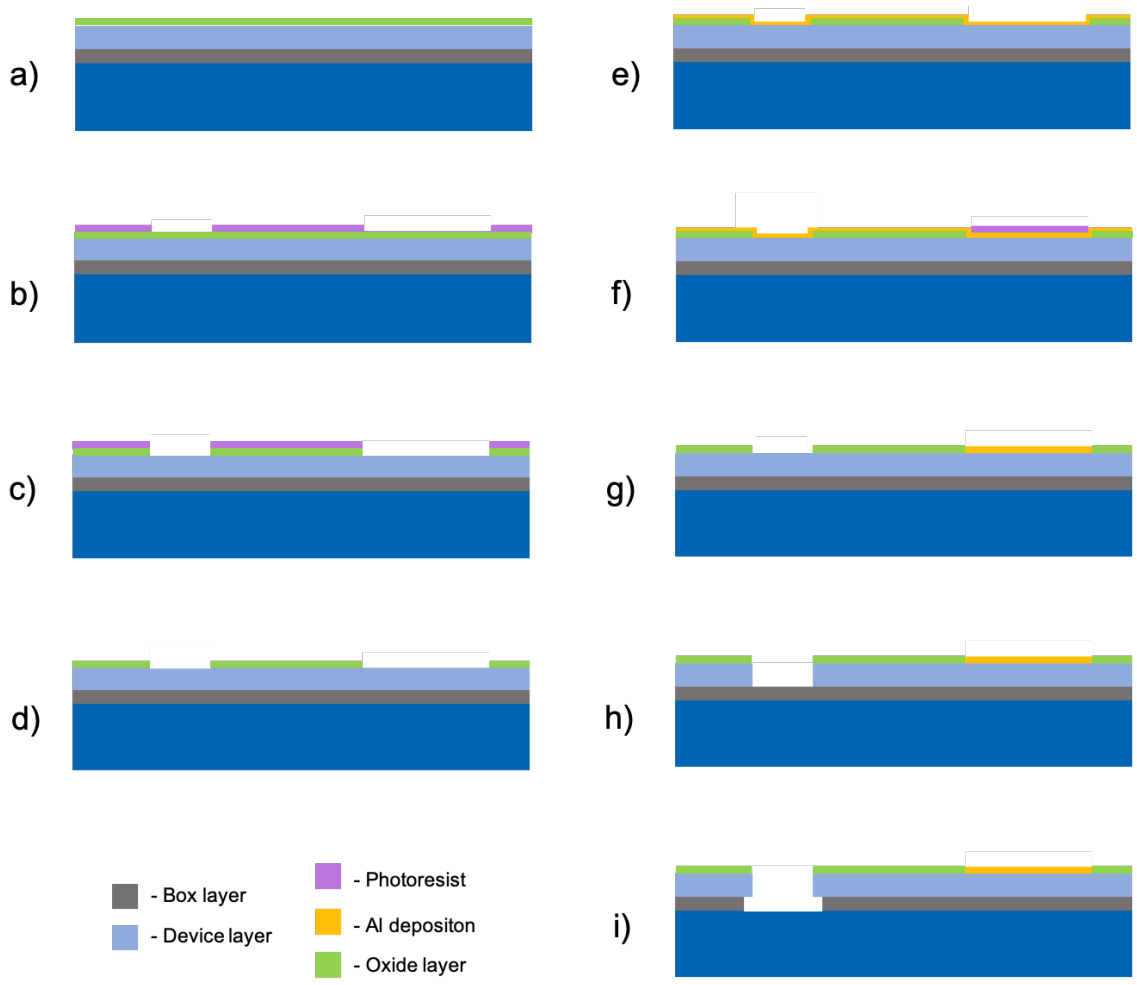

Figure 56: *The fabrication process. a) SOI wafer with oxidation. b) Photoresist added as a sacrificial layer and photolithography. (general trenches) c)Oxide etching. d) Cleaning. e) Al deposition. f) 2nd photoresist layer and photolithography. (pad area) g)Al etching and wafer cleaning. h) DRIE of the full thickness of the device layer. (anisotropic) i)Oxide etching using vapor HF. (isotopic)*

allowing for the possibility of monitoring the connections of the switch through header pins to which pads are connected to for more robust connections or directly on the pads with needle probes for more delicate observations under the microscope.

4.5 Experimental tests

The method of testing fabricated switches starts with establishing their actuation voltages. Despite Paschen's law predicting the breakdown voltages, it is known that it deviates from its original shape and reaches the plateau for gap dimensions that are studied in this thesis. The samples are sealed with a frame and protection glass in an environment with non-regulated air quality which contributes to the uncertainty in the composition of the switch's environment and interferes with actuation voltages. Determination of the realistic actuation voltages with experiments is imperative in determining the accuracy of calculations as well as the quality of

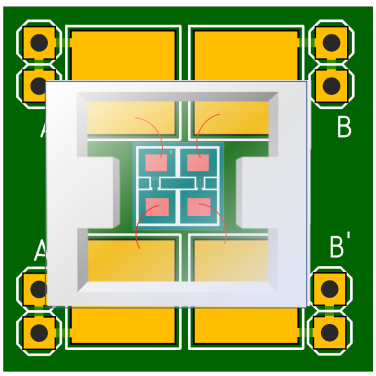

Figure 57: *Packaging used for fabricated switches for their integration on a more robust PCB. The package is composed of an adapter on which the sample is mounted and wire bonded, which is then covered by a frame and protection glass.*

the fabrication process.

The test circuit is composed of a TENG that is connected to a half-wave rectifier. The switch under test (SUT) is connected between the rectifier's output capacitor and the output capacitor (see Figure 58).To assess the performance of the SUT, voltage levels before and after it are monitored simultaneously. The voltage signal before the switch is monitored using an electrometer and the signal from the capacitor after the switch is fed through an operational amplifier (OPA) in a follower configuration so that the output signal can be observed on an oscilloscope. Instead of using a single capacitor at the output of the rectifier and switch, capacitive voltage dividers are used. The reasoning behind using this specific configuration is based on the capabilities of measurement equipment, namely, the electrometer in voltage setup and the supporting voltages of the OPA. (Figure 58) The half-wave rectifier is the initial conditioning circuit of choice because it supplies the switch with voltages that reach saturation, which allows better control of switch operation at the testing phase. In later experimental tests, Bennet's doubler is used to truly test switch capabilities and full operation of the proposed system.

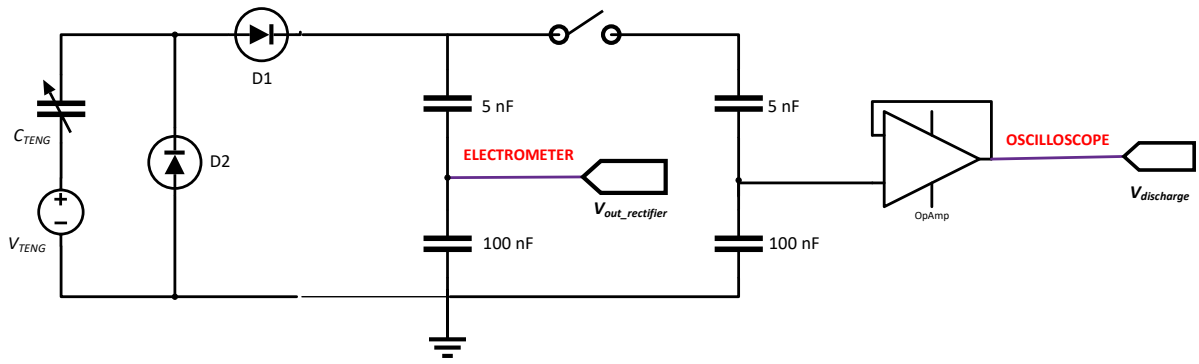

Figure 58: *The schematic of the circuit used to test the actuation voltage of fabricated switches.*

The selection criteria that is used for the switches to be tested is to perform tests design per design. It refers to selecting one design and testing it for all gaps to make conclusions about their operation and margin of error compared to the theoretically predicted curve and then moving on to another design. The first selected design to go under test is the design with comb-like structures with extrusions as in Figure 55 d) with 7 μm gap.

The initial tests are run on the first set of switches to which energy stored in a capacitive voltage divider of 5 nF and 100 nF (divider ratio of 50) is supplied. Once switches actuate it is planned for the energy to be transferred to another capacitive divider formed from the capacitors of the equal value as those at the output of the half-wave rectifier.

The results of one such experiment are presented in Figure 59. The curve in red corresponds to the output of the half-wave rectifier and the one in black represents the voltage over the capacitor after the plasma switch. The output capacitor of the half-wave rectifier charges with the trend that is expected for that circuit. Once the voltage over the capacitor that is connected to the anode of the switch had risen to 350V plasma discharge occurs and the output capacitor is discharged into the capacitor after the switch. The actuation voltage of the SUT is the voltage at which the discharge occurred. By magnifying the segment of the graph at which the SUT conducts, it has been measured that one is active for 0,6 ms. The energy that is transferred via the switch charges the capacitor at its cathode to 285 V. Once the plasma conduction channel between the anode and cathode breaks, the voltage of the HW's output capacitor does not measure 0 V. It is inferred that it is not fully discharged, thus a new cycle of charging starts at 100 V. As TENG continuously harvests energy, HW's output capacitor has been charging again (after part of the accumulated charges have been released through the switch). Once the difference in voltage between the anode and cathode reached 350 V, another discharge occurs. The actuation of the switch is repeated multiple times in a row as well as when system is restarted.

An important parameter in the fabrication and testing of the MEMS switches is not only the repeatability of results but also consistency in fabricated samples. As explained earlier, a difference in a micrometer can generate a large discrepancy between results obtained by calculations and experimentally. As a result, multiple samples with the same dimensional characteristics have been tested and their results have been shown in Figure 60. The second SUT activates at 340 V and charges the capacitor connected to the cathode to 275V. The switch is active for 0,6 ms and stops conducting once the voltage at the output of the half-wave rectifier reduces to 100 V. Its second activation is recorded when the voltage difference between the anode and cathode is equal to 325 V which equates to 590 V recorded at the

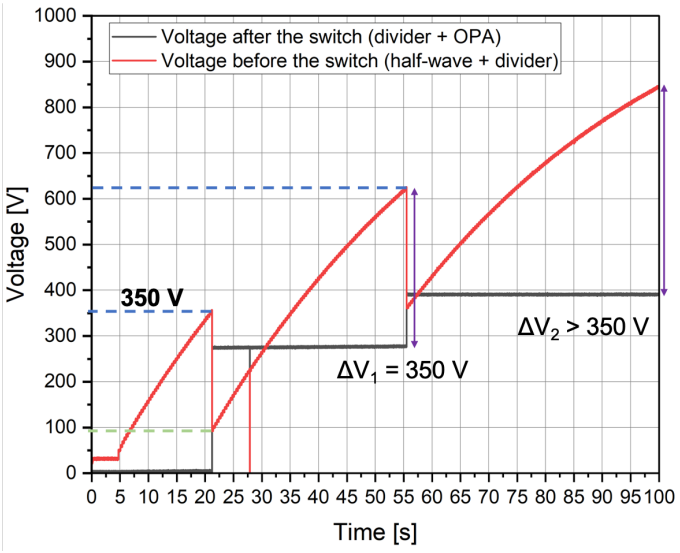

Figure 59: *Measured output voltages of half-wave rectifier (red) and voltage at the capacitor after the switch (black) with a breakdown voltage of 350V.(Sample I)*

terminal before the switch.

Looking at the activation voltages at which SUT II and III activate, it can be concluded that SUT III requires additional 10 volts (resulting in an activation voltage equal to 350 V) compared to SUT II. The presence of the higher activation voltage established at the first switch ignition of the SUT III is propagated towards further activations. The greater difference is visible at the second activation when the second sample has a reduced voltage difference between the anode and cathode that is necessary for it to start to conduct. Even though divergence between two samples is present when discrete voltages values are taken, they account for less than 5% of the difference between tested samples.

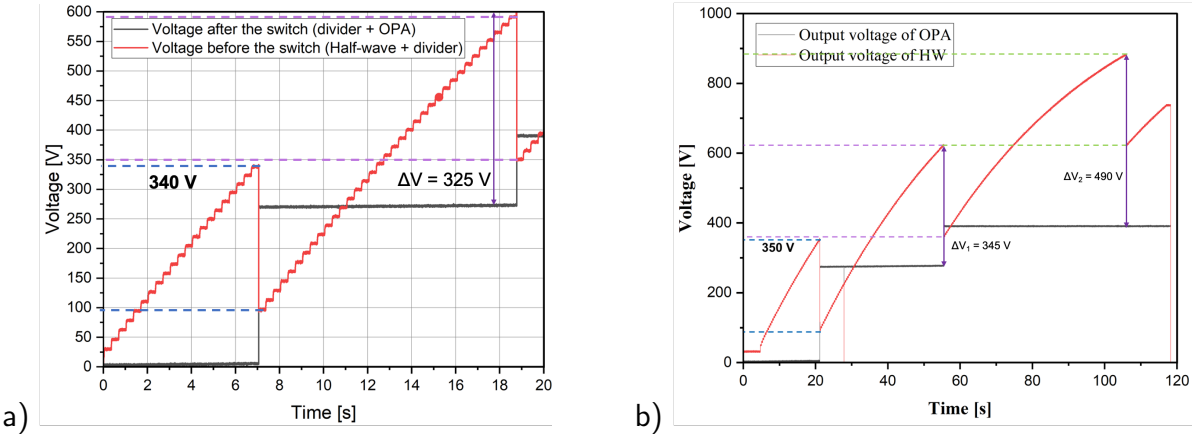

Figure 60: *Measured output voltages of half-wave rectifier (red) and voltage after a SUT II (black). a) SUT II with an activation voltage of 325V. b) SUT III with a progressive activation voltage.*

To derive a conclusion about the operation consistency of this geometry of the switches, the third sample with the same design and dimensions is tested. Figure 60b shows the output voltages that are measured for the third SUT. Once it has been established that this switch has

the same activation voltage as previously tested samples, it has been tested for a longer period of time (120 seconds) with the goal of recording the next possible activation of it. The SUT activated at an already established voltage ranging from 325 V to 350V the first two times, at 350V and 345V, with active periods of 0,88 ms and 0,72 ms respectively. Nevertheless, the third SUT activation occurred at a significantly higher voltage of 450V. The increase in the necessary voltage difference between the anode and cathode of the switch can be accredited to switch deformations which will be later discussed in detail. The three tested switches comply well with the predicted voltage breakdown. The theoretical value is 369 V and obtained values are between 340 V and 350 V which in case of the largest divergence is a maximum error of 5%.

In the following, instead of using half-wave rectifier, Bennet's doubler is connected to the system. Its output capacitor (using the same capacitive voltage divider combination as in the first test bench with HW) is connected to the anode of the switch and its cathode is connected to the input of the Buck converter. (Figure 61) Monitoring of the operation of the switch in this setup is planned at the input of the switch (output of Bennet's doubler) and at the capacitor at the output of the Buck converter. In fact, the measurements at the second point of interest are done using a standard oscilloscope probe. It means that voltage is measured over the load of 10 MΩ which is a value provided by the manufacturer.

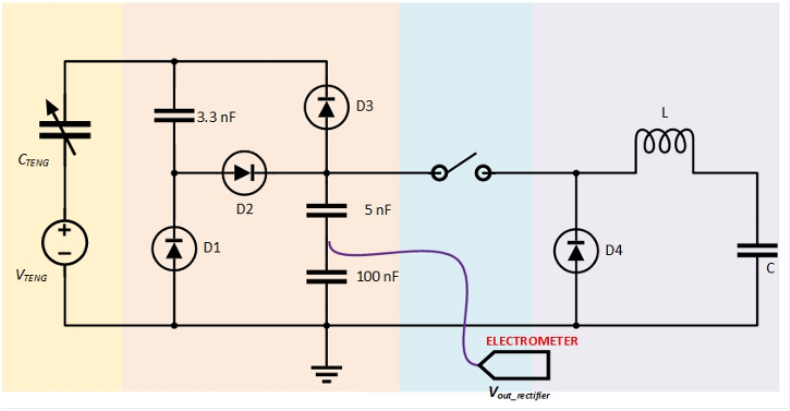

Figure 61: *The schematic of Bennet - plasma switch - Buck system used for measurement of actuation voltages of plasma switch.*

The Buck converter is a step-down voltage converter that has the purpose of reducing voltage levels generated until that point. When this circuit works in discontinuous conduction mode, the moment at which the switch starts to conduct, the current starts to flow through the inductor resulting in a linear surge of current. The voltage over its capacitor increases to a constant value of the time interval during which the switch conducts and reduces back to zero once conduction stops. The circuit is completed with a flyback diode. The voltage to

which the converter's output rises is determined by the input voltage, the frequency of the operation of the switch and L and C values. The equation defending how these parameters are related in case of this circuit has been derived and explained in detail by S. Ang et al. in [64]. The exact relationship is shown in equation 80

$$V_{outBuck} = V_{in} D \sqrt{\frac{RT}{2L}} \tag{80}$$

where D is the duty cycle, R is the value of load resistance, T is the period and L is the inductance of the inductor in the circuit. In the studied case, input and output voltages, as well as period and duty cycle, are predefined parameters, the one parameter that allows for flexibility in achieving desired voltages at the circuit's output is the value of inductance. The output that is expected from this test circuit is an exponential increase at the output of Bennet's doubler and a step signal at the output of the Buck. The presence of the voltage increase in the form of a step would indicate an activation of the plasma switch and energy transfer from Bennet's output to Buck's input.

Figure 62 shows the results obtained with this test circuit. Bennet's output voltage initially takes the correct form (black) and there is no voltage present at the output of Buck (red). At the moment t=10s, the dynamics in the system change. The trend of increase of output voltage at Bennet's output significantly decreases and the voltage starts to build at the load. This indicates an improper operation of the system due to continuous conduction.

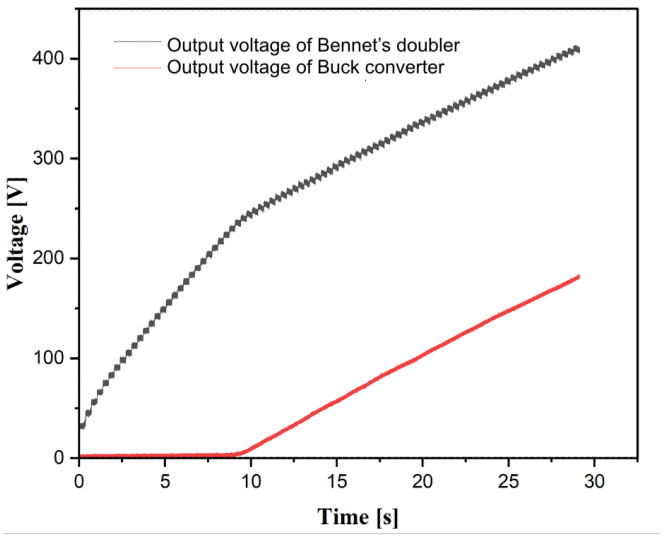

Figure 62: *Results of the tests measuring output voltages of Bennet's doubler and Buck converted connected via an SUT.*

There are two possibilities for this phenomenon to occur. Firstly, the plasma conduction channel between the anode and cathode is very strong that enables continuous conduction

over an extended period of time that exceeds its, by now recorded, operation times. In the recorded case, the conduction period is 20 seconds which is several orders of magnitude larger than established conduction periods. Even though this hypothesis is hardly likely it has been put to the test. All capacitors in the circuit are discharged and the system can start a new fresh operation. The second run of the system is unsuccessful as the voltage at the anode and at the load follow each other simultaneously. These results disproved the initial hypothesis and led to the second more likely scenario. Anode and cathode have come to a state of permanent physical contact. It is most likely due to high currents and thermal effect that the two have morphed together and are acting as a conductor without the possibility of a break.

Samples containing comb-like structures are capable of repeatedly actuating at the same voltages with partial discharge. The results of the first experiments have shown that the methodology used for the design and fabrication of plasma switches is in accordance with their predicted behaviour.

Once samples with single finger have been subjected to the same test, they have shown some vulnerability in design choices. Namely, after a couple of switch actuations, the actuation voltage would increase significantly. Considering that switches were not interfered with, a possible explanation for the unusual behaviour would be damage to the structure.

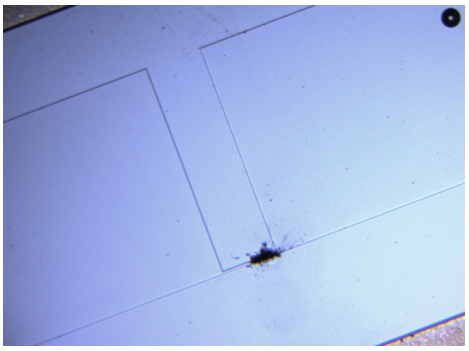

Figure 63: *Microscope image of effects of plasma discharge in a switch caused by high currents.*

The possibility of structural damage to the switch has been investigated by placing the samples under the microscope and observing the geometry. Figure 63 shows the clear damage that has been made to the structure. Once the initial hypothesis has been confirmed the severity and nature of the damage has been assessed under an electron microscope. Figure 64 shows a close-up image of the deformation of both the cathode and anode.

It has been understood that due to the arch formation process, electrons are shot into the cathode. As discharge is concentrated at one location on the gap, the stream of electrons penetrates the material at a very small area (the total area of damage is 20 microns). The secondary effects of the damage come from the thermal release during the discharge. The

combination of the effects results in samples with fused cathode and anode or enlarged gaps.

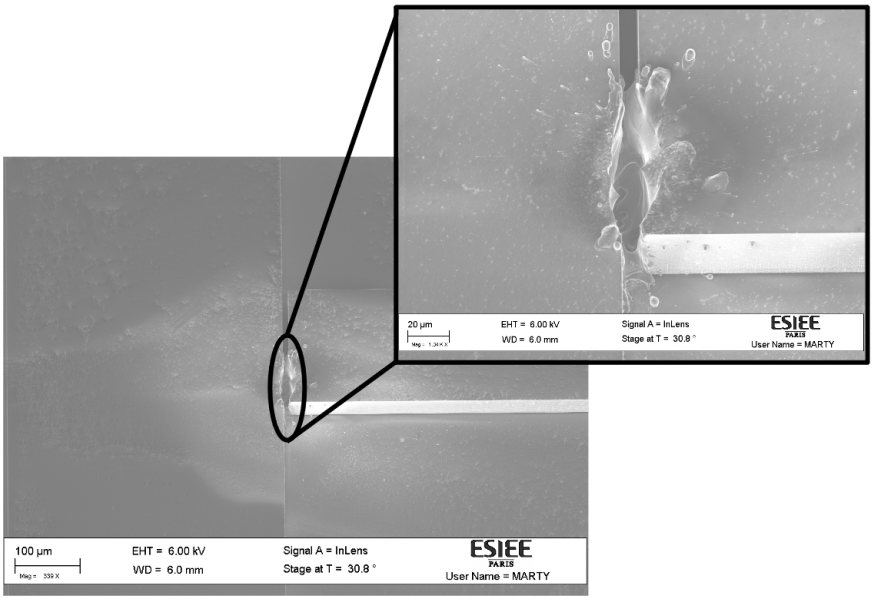

Figure 64: *A closeup image of the level of damage created on the tested switch. Destruction of materials contracting anode and cathode and fusion of the two.*

The recorded behaviour of the output voltage is a natural response to the change of gap between the anode and cathode. An increase in the gap results in increased breakdown voltage. The effects of structural damage are first seen through the exhibition of unexpected results while testing the electrical performance of the switches. Therefore the first step in determining whether it is the case or not is running a test that monitors the voltage before and after the switch (removal of additional circuits and placement of discharged capacitor at the cathode). If two voltages take the same form from the start of TENG's operation, as shown in Figure 65, there is clearly no switch or interruption element in that circuit. Based on these results it can be concluded with confidence that this sample is defected and can no longer be used as a plasma switch.

4.6 Conclusions on micro-plasma MEMS switch

Composing the results obtained by experimentally testing the high-voltage plasma switches it has been concluded that fabricated switches give control over actuation voltages through their design. For relatively small gaps, supported voltages are high which accommodates the need to control the high voltages at Bennet's output. Considering that plasma discharge is a self-initiated process centered around anode voltages, there are low losses during the process of switch activation and during transfer. Experimental results have shown that the materials used to fabricate the latest samples has to to be changed. The merit of this material does not

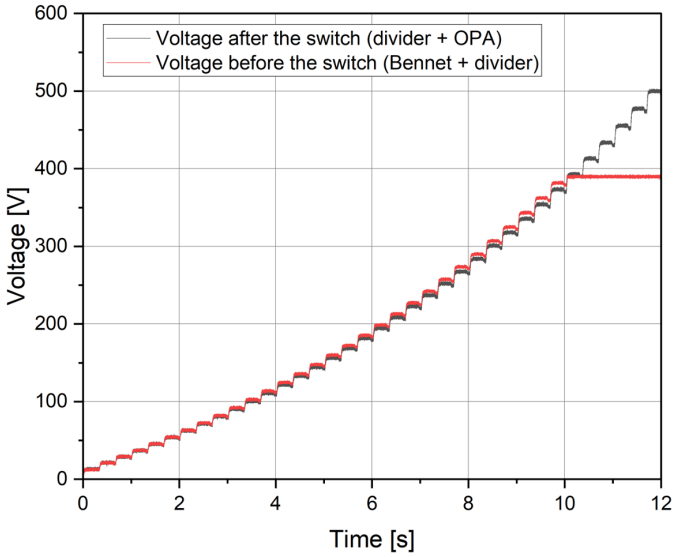

Figure 65: *Measured output voltages of half-wave rectifier (in red) and voltage after the switch (in black) with a breakdown voltage of 350V.*

lay in supporting high voltages on a small surface area. Nevertheless to material limitations at this stage of the research, switch samples have shown the capability of actuating and limiting the discharge period creating an incomplete discharge of Bennet's output capacitor which gives a frame of possible research that can be conducted in the future.

5 η and V_{te} measurement automation

Now that all steps of the energy management system have been explored, it is possible to work on its optimization. A question of best control is raised. The best control is one that enables for most efficient and fastest energy conversion. It refers to the frequency of transmission, control element's efficiency and supported voltages (like high voltage MEMS switch earlier discussed). Whether a certain control element fits the application depends on the conditioning circuit used. For example, there is a difference in the shape of the output that is generated by stable and unstable charge pumps. For stable charge pumps, power over the load is a function of η, V_{te}, α and $U(t)$ which is the function of the control element ($P_s = f(\eta, V_{te}, \alpha, U(t))$). For given values of α and η, the control element function has an output defining its behavior and efficiency ($V_{out} = (1-\alpha)f(\eta, t)$). The power over a load of an unstable charge pump is defined by η, V_{te} and γ and $U(t)$ ($P_u = f(\eta, V_{te}, \gamma, U(t))$). Where η is the capacitance ratio ($\eta = C_{max}/C_{min}$) and α and γ are the variables derived from voltage equations consisting mainly of capacitance ratios. Considering that all other values except $U(t)$ that are explored here are either fixed or given values, the straightforward way of getting its value is by taking combinations of η and γ that are possible and obtaining the function values that will help determine the best control for optimum energy conversion. Consequently, the first step is to establish the values of η and V_{te}. The circuit that is considered in this

experimental study is the half-wave rectifier. The voltage of the HW is defined by

$$V_{out} = V_{te}(\eta - 1)(1–\alpha^2) \tag{81}$$

η is a parameter that is purely related to the geometry of the transducer i.e., minimum and maximum distance between capacitors pates. α is equal to $\frac{C_{out}}{C_{out}+C_{min}}$. The α is majorly dependent on the value of C_{out} therefore it can be determined that it is a circuit parameter more than the transducer parameter. If C_{min} is significantly smaller than C_{out} (typically a couple of orders of magnitude) the V_{out} and consequently the V_{te} expressions can be significantly simplified. The above equation shows the direct relationship between output voltage, the built-in voltage of the TENG, η and α. For the analysis to be possible and derivation of V_{te} executable, some of the HW parameters have to be fixed. In this case, it is the V_{out} that is taken as a known value and η that is considered to be fixed. The quantity that is determined by the equation is V_{te}. In theory, one value is considered fixed indefinitely or by superposition. In practice, those values are previously determined so that they can be set as known values in experiments that measure quantities like V_{te}. This section discusses the experimental method used to determine η and V_{te}. General constraints that are put on the system are the following:

- $V_{te} < V_{max}$

  This means that the saturation voltage of the triboelectric layer is not supposed to be larger than the maximum supporting voltage of the component. As per the electrical model of the TENG, the triboelectric layer's analogy is the DC voltage source. As a component that continuously supplied voltage to the circuit, it is critical that components can sustain supplied voltage.

- $V_{ci} < V_{bd}$

  The breakdown voltage of the capacitor (V_{ci}) has to be less than the breakdown voltage of diodes (V_{bd}). This means that diodes can support the operation of the result of the circuit. Whatever the potential difference is between the nodes of the capacitor, the diodes have to be able to support that voltage. Especially, as we have seen, double Bennet has that V_{max} that goes beyond the range of the voltage that is created by classic Bennet.

- $V_{Lmin} < V_{L(t)} < V_{Lmax}$

  Voltage over the load ($V_{L(t)}$) is always within the range that is considered minimum and maximum. Maximization of the time during which load is supplied with voltages in

the ideal range. Combination of energy conversion rates and maximum and minimum powers and supported voltages.

- $P_0 << P >$

  P_0 is the minimum power that is necessary for the system to operate and $< P >$ is the average consumed power. That refers to the fact that it is necessary to take in consideration the power consumption of the components that are used to construct the measurement circuits. The estimate of the power consumption is an approximation of the minimum power that has to be transformed for the system so that it can start its operation.

An assumption that is made about the system is that $C_{TENG}(t) = C_{TENG}(t + T)$. Capacitance is periodic on the given time interval. For the specific period that is taken into consideration, there is a specific number of repetitive maximum and minim capacitance values. Losses that are present in the practical system have to be accounted for in the theoretical analysis of the circuit comparison. Major losses are due to the voltage threshold of the diodes. Each of the diodes individually and all diodes might be added in series to be able to support higher voltages. Either way, to calculate the losses due to diodes, that is equal to the time period of diode recovery multiplied by the reverse current.

One conclusion that is taken from previous experimental study is that the reliability of data is very important. That is why for this study, an automated and autonomous experimental bench is constructed. In the previous setup, the same circuit topologies were used for the measurements. Nevertheless, the change between the circuits has been done manually. As it has been seen, it was necessary to account for a "human effect" that caused fluctuations in the stability of the setup resulting in a large margin of error.

To reduce interference to the measurement setup and create an environment where it is possible to repeatedly do the same set of measurements, we opted for full automation. Automation in this case encompasses an experimental test bench that can be subjected to different tests at any time without a need for manual manipulations of any of its components. What is created is an integrated system that is capable of running two measurements autonomously. The first reason for the integration of such a sort is because of the reproducibility of data due to TENG. Connecting and disconnecting the transducer from one circuit to another can cause strain to the system in a mechanical sense, therefore, resulting in different results from one experiment to another. The second reason is the motor is used to apply force to the system. In this second test bench, a shaker motor that is controlled through a function

generator. By applying the combination of amplitude and frequency, different displacements are obtained. One of the drawbacks of this motor is the fact that it has less control compared to the linear motor used in the first setup. Nevertheless, it is closer to the realistic case when it is impossible to continuously reproduce the same outputs (apply the same force to the TENG). To sum it up, one reason for needing this integration is the low reproducibility of the force applied by the motor. Repeatability is not possible with the motor. That is, the state of the system depends on its history i.e., applying the magnitude of the force from F1 to F2 will not have the same effect as applying the magnitude from F2 back to F1, hence not the same η and V_{te} are obtained. The main components of the system are represented in Figure 66.

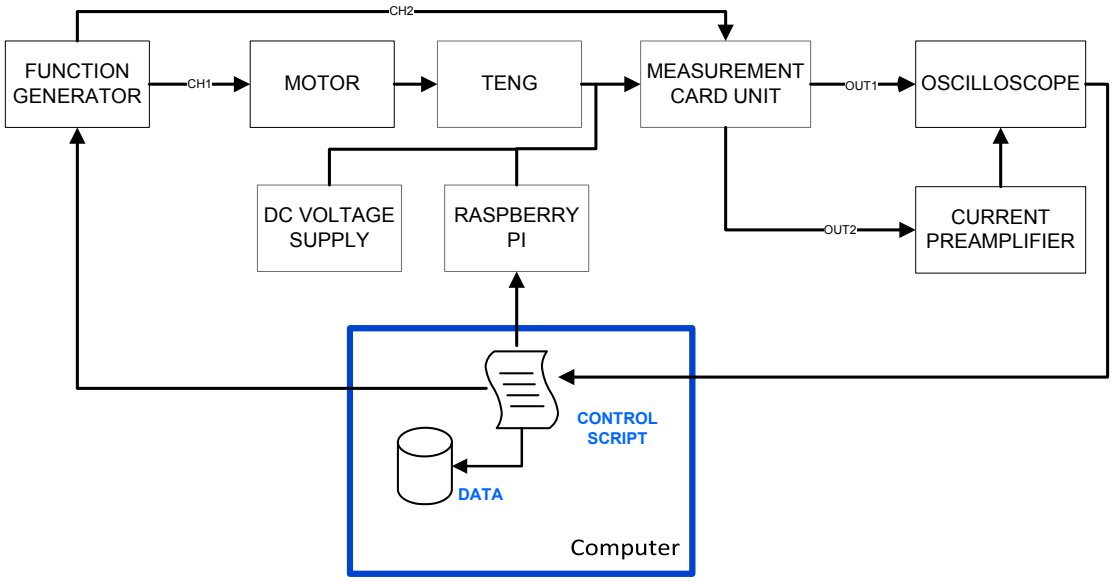

Figure 66: *Block diagram of experimental test bench that measures the η and V_{te}.*

A computer runs the control script and stores the measurement data. An important task of this control script is to maneuver the correct operation of the two circuits present on the measurement card unit and to set input parameters. It achieves this maneuver by communicating with Raspberry Pi which runs a simple script. To understand the measurement setup, we can start observing by following the path starting from the function generator. Its one channel drives the motor. One of the TENG capacitor's plates is connected to it. As a result, TENG is set in motion with controlled input parameters set by the function generator and executed by the motor. Each of its plates is electrically connected to the measurement card unit. In order to determine the active circuit in this unit, relays are used. For the selected relay model to operate, it requires a continuous supply of 5 volts DC to operate. Control of relays is established through their drivers that communicate with a Raspberry Pi. In this way, the Raspberry Pi can set the state of the relay to be either on or off. The second channel

of the function generator is connected directly to the measurement card unit as the carrier signal for η measurements. These measurements are done by collecting voltage data from two points in an active circuit. Voltages are measured and displayed on an oscilloscope by which data is collected and provided to the Python script. V_{te} values are determined by measuring the output voltage of the HW, which is done by measuring the current passing through the output capacitor of the circuit. This is the measurement method that allows for the largest voltage range, highest resolution and repeatability between measurements and lowest losses (compared to other employable voltage measurement methods). The currents are measured with a low noise current preamplifier that has its analog output scaled to a voltage depicted on the oscilloscope. This is a self-sustained system where once all connections are made and TENG is installed, it is possible to set all input parameters and obtain outputs. An image of the created experimental bench is shown in Figure 67. All components that are presented in a block diagram are visible on the image.

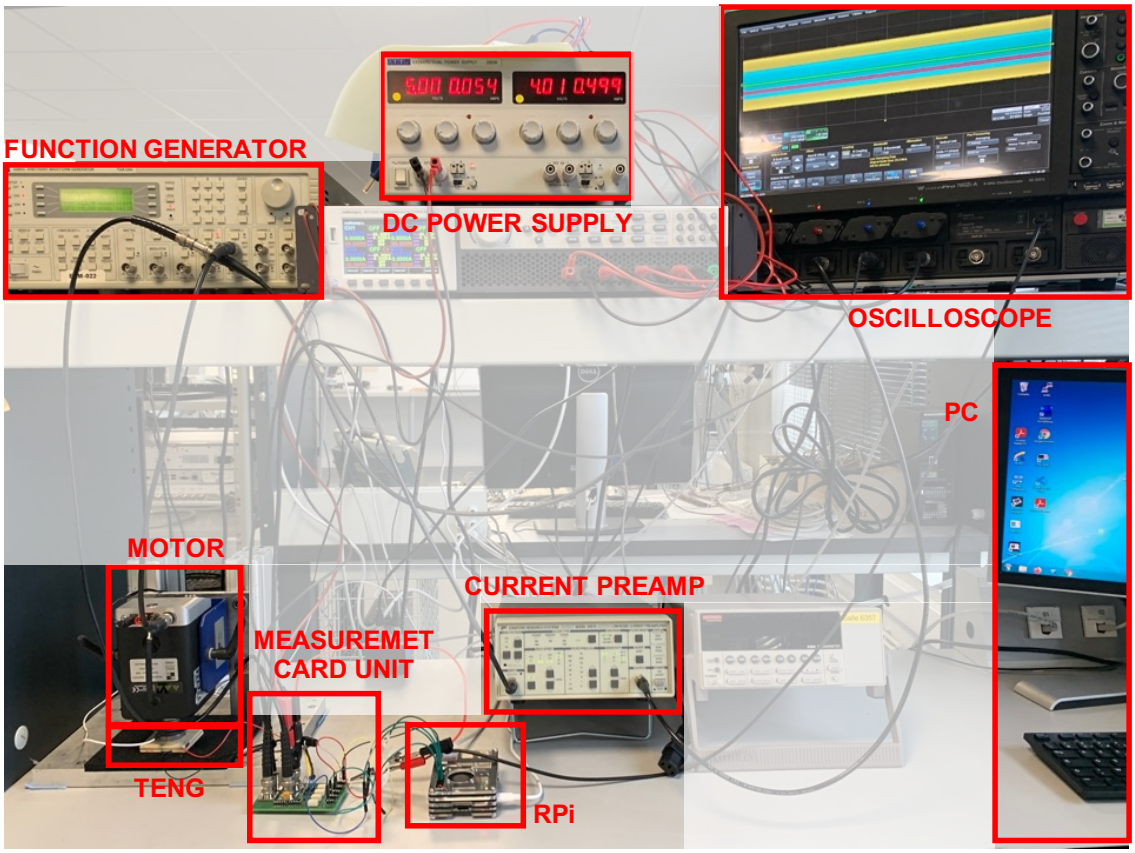

Figure 67: *An image of the test bench that measures the η and V_{te} highlighting used the actuation and measurement equipment.*

V_{te} is characterized by its relationship with applied force and its dynamics in time. To measure V_{te} and hence answer these two questions with empirical models, we can use the HW circuit for which the dynamics is known. It is completely determined by V_{te} and η (as per

equation 81). If values of η are found with one measurement method, it is possible to fix its value and use some other measurement method to determine V_{sat}. For that, a circuit with a known dynamic, like HW, is set by which it is possible to deduce the value of V_{te}. It is important to note that two different measurement methods have to be used for the determination of two variables. To do this, we have built a measurement card that allows us to carry out both measurements. The block in the system that does the measurements is the measurement card unit. It is in fact a circuit board (a customized printed circuit board (PCB)) that can do measurements of η and V_{te} autonomously. One board contains two circuits: dynamic capacitance measurement circuit for η measurements and HW for V_{te} measurements and switching control between the circuits done by relays. The card has 4 relays placed in the circuit as shown in Figure 68a). Combinations of active relays switch between measurements. There are three possible cases:

CASE 1: *Only relay S1 is closed.*
There is contact between the carrier signal and the TENG. As a result, dynamic capacitance measurement circuit forms and η measurements are done (Figure 68c)).

CASE 2: *Relays S2 and S3 are closed.*
S1 is open (open circuit between the carrier and a TENG). Relay S2 is closed connecting the transducer to HW's diodes. To short-circuit the resistor and connect the HW to the ground relays S3 is closed. In this configuration V_{te} measurements are done (Figure 68b)).

CASE 3: *Relays S2, S3 and S4 are closed.*
In this configuration, HW output capacitor C_{st} is discharged by short-circuiting its two terminals through the relays S4 (Figure 68d)).

The diodes have a voltage breakdown at 200 V (limits the scope of the measurements by setting the maximum supported voltage of the system), reverse current at 1nA (below average reverse current reduces losses due to leakage) and power dissipation of 350 mW (contributes to the total power consumption of the system). Monostable (single coil) relays are used that activate at 5V and support up to 220 V_{DC} whose power consumption is determined through coil power that is in this case equal to 140 mW. The relay is controlled by an MDC3105LT1G relay driver that operates at voltages between 3 and 5 volts. It has a power dissipation of 225 mW mostly due to integrated BJT and Zener diode.

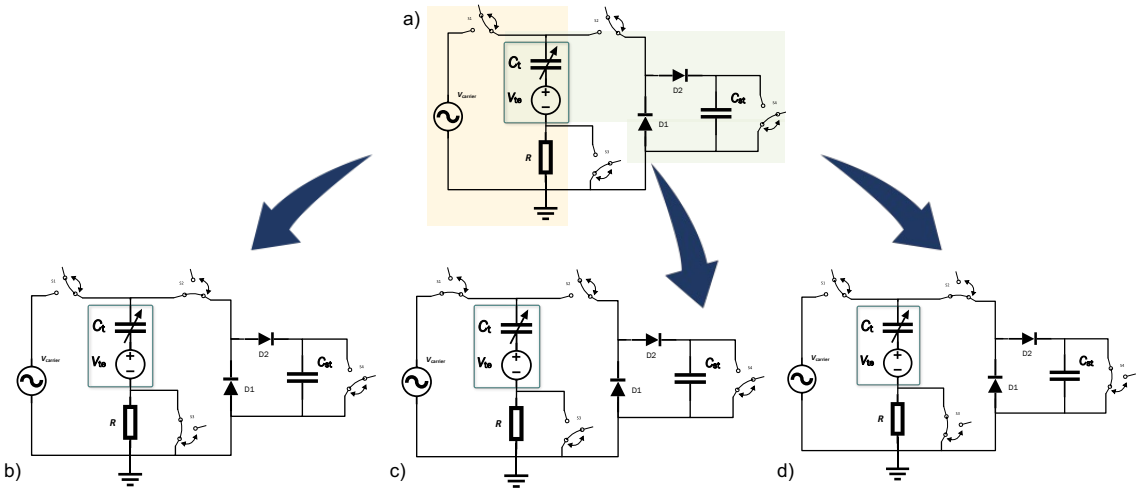

Figure 68: *Schematic representation of components and their connection on the measurement board unit. a) The general schema of the board with all relays open. b) Case 2: S2 and S3 are closed, which corresponds to HW measurements. c) Case 1: S1 is closed forming a dynamic capacitance measurement circuit. d) Case 3: S2, S3 and S4 are closed. This schema discharges the output capacitor after an HW operation.*

The procedure that is taken to exhibit the V_{te} versus force dependency (consequent η vs. F due to direct relationship between V_{te} and η), is the following:

1. set a force value (implicit force setting; directly defining amplitude and frequency of motor) and run a charge-pump experiment for each value,

2. measure η for each force value using its circuit (dynamic capacitance measurement),

3. invert the polarity of the TENG (creates the HW 2 circuit - triboelectric layer is no longer grounded) and measure V_{te} again,

4. confirmation based on data post-processing (calculations done on data for HW 1 and 2) that V_{te} changes with the change of F.

The results of described method measuring V_{sat} are presented in Figure 69. The capacitance ratio varies between 2,2 and 6, which is a large span of C_{max} and C_{min} values for the circuit to operate. The presence of minimum η has been experimentally determined. Even though the used charge pump does not have a specific minimum value of the capacitance ratio that needs to be satisfied for the circuit to operate in a steady state ($\eta > 1$ - as long C_{max} is larger than C_{min} HW is able to operate), it was experimentally determined the circuit's steady state is only reached once generated power is higher than the consumed power due to losses in the circuit. This signifies that η has to be larger enough so that TENG converts enough energy so that HW operates efficiently.

The dashed line corresponds to the theoretically predicted trajectory of output voltage for each η and full lines are the results of measurements. It can be seen that the two are alike. Experimental data forms a curve of the same shape as the theoretical one, with a small margin

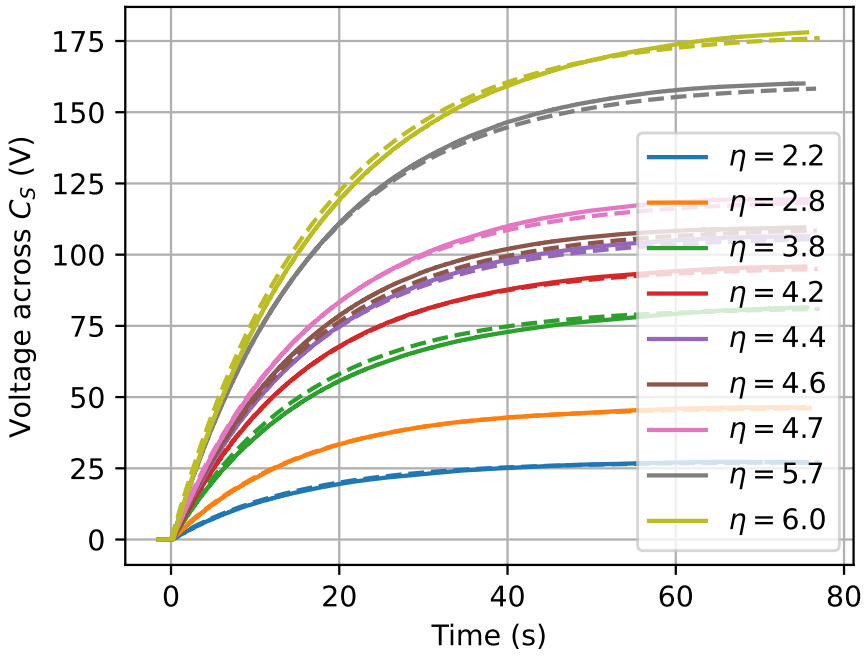

Figure 69: *Comparison on experimentally obtained results for the relationship between η and V_{sat} and their theoretical estimates.*

of error that can be attributed to irregularities in the work of the motor. As hypothesised, the increase in η resulted in increased V_{sat}. The increase is proportional so that saturation voltage is the smallest for the smallest capacitance ratio and proportionally the largest for the highest ratio. For all η values, half-wave rectifier saturates below 200 volts which is the threshold voltage of used components. This indicates adequate component selection and voltage predictions for the experimental bench.

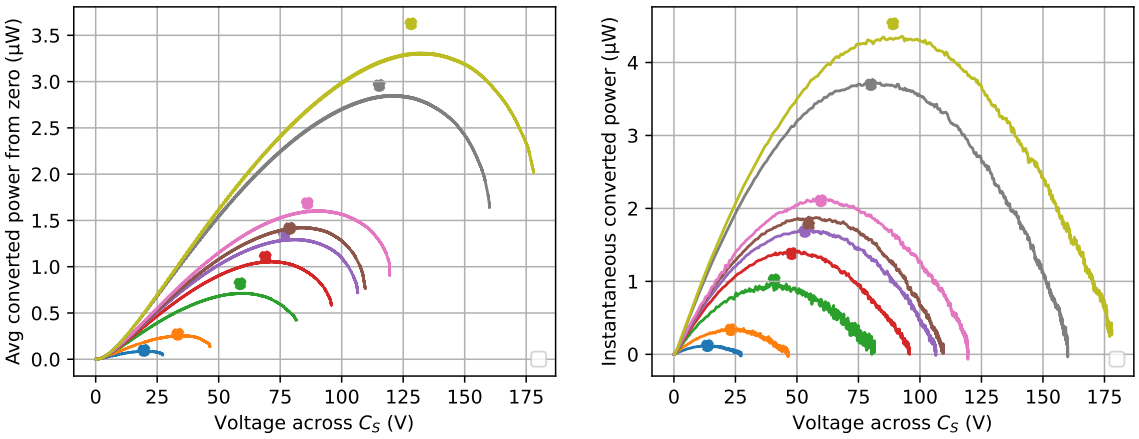

Figure 70: *Graphical representation of results obtained for average and instantaneous power for tested capacitance ratios and their corresponding V_{te} values.*

With obtained data, it is possible to calculate instantaneously and average converted power at the output of the charge pump. As shown in Figure 70b), instantaneous power takes the shape of the reflected quadratic function. As time increases, so does the voltage over the

storage capacitor too, until its peak value after which the instantaneous power descends back to zero W. Experimentally obtained maximum instantaneous power is compared to theoretical values (large clusters of points on the graph) and they do conform well with one another. The shape that instantaneous converted power takes reflects the behaviour of the stable charge pump where it starts operating and energy conversion rates are high until at saturation, the conversion is zero. On the other hand, the average converted energy for each of the η values is shown in Figure 70a). As it has been expected, the largest average energy is converted by the transducer with the highest capacitance ratio and highest saturation voltage.

6 Conclusion and future work

This thesis studies the performance of an energy management system composed of triboelectric kinetic energy generator (TENG) implemented with Bennet's charge doubler. Theoretical analysis supplemented with simulations and experiments is conducted with the goal of reporting the results obtained in studies.

Classic Bennet's doubler supports the application with a TENG having two output electrodes. With the ambition of increasing the amount of converted energy, a modified TENG design is proposed. By adding a third electrode that is fixed, a single capacitive transducer is converted into a double one. An increase in capacitance variation results in a converted energy increase.

To treat obtained output signal, it is common for charge pump circuits to be used as conditioning circuits. While stable charge pumps provide a stable output signal that saturates (resulting in no converted energy at that stage), unstable charge pumps like Bennet's doubler never reach saturation (continuous energy conversion in each cycle). To accommodate the now-modified TENG, a selected conditioning circuit has to be capable of supporting 3-node input. Bennet's doubler is a selected circuit in which a reference capacitor is substituted to fit the second transducer's capacitor. Bennet's charge doubler is a mechanical system whose first electrical model contained a pair of variable capacitors. Moreover, TENG is an electrostatic

kinetic energy harvester that utilizes the triboelectrification effect between its triboelectric layer and electrodes to convert energy. Its electrical equivalent includes a variable capacitance and a DC voltage source. With the goal of implementing double TENG with Bennet's doubler, in branches with variable capacitors two voltage sources have been introduced to the circuit. As it is an active element placed at a relevant node of the circuit, it calls for a complete study of the system.

A newly formed system is first studied through theoretical analysis of Kirchhoff's law and charge conservation law. Derived charge and voltage equations of two TENG's capacitors are interpreted by a charge-voltage (QV) diagram. The cycle of a QV diagram is defined by one mechanical cycle of a TENG. Due to the existence of two TENG's capacitors, two QV cycles are tracked each corresponding to one capacitor. It is concluded that the theoretical analysis of double Bennet is a complex one as it involves multiple parametric analyses of charge and voltage at multiple stages of QV cycle. In those, it has been found that the analysis of one TENG's capacitor cannot be separated from the other one. They are co-dependent and the operation of one has a direct impact on the operation of the other capacitor. The shape of the QV formed by the capacitors implemented in double Bennet differs from the QV cycle of the classic Bennet, as non-linearity is observed at two instances (the instances of large charge transfer).

Spice simulations of the circuits that follow the principles defined by the theoretical analysis were run. QV cycle generated by simulations is compared with the one obtained by calculating derived analytical equations. It has been found that calculated and simulated QV cycles are an almost perfect match. This has led to a continuation of the research on the system through experiments. For the experiments, a TENG is constructed whose motion of the middle plate is controlled by a linear motor. A characterisation of the TENG is done by connecting it to half-wave and full-wave rectifiers to obtain data necessary for characterising the capacitance ratio and voltage of the triboelectric layer. As the value of the capacitance ratio is a necessary condition that has to be satisfied for the correct operation of Bennet's doubler, it has been further examined. By performing dynamic capacitance measurements exact shape and values of capacitance are determined. This method generates a precise $C_{\max}$ and $C_{\min}$ measurements for two transducer's capacitors under test and consequently precise capacitance ratio. Experiments measuring outputs of classic Bennet and double Bennet are done. From obtained results, the superiority of double Bennet is established. For the same capacitance ratio and range of capacitances, double Bennet takes less time to reach equally high voltages. Capabilities of the constructed system are limited by the breakdown voltages

of diodes used in the system. Thus, double Bennet's output voltage is measured to its limits, effectively reaching 1 kV with an exponential increase in a span of 26 seconds.

Obtained experimental results have been compared to simulations results of classic and double Bennets output voltage. It was found that the shape of the curve formed by the experimental test indeed does follow the envelope of the simulated results, for both circuits. With the experimental tests, it has been concluded that there is a level of uncertainty that might be caused by the manual assembly of the transducer and manual switches between measurement circuits. To address this problem, a second separate experimental bench is created with the goal of automatic measurements of capacitance ratio η and characterisation of the triboelectric layer (measurements of V_{te}). A custom measurement board, integrating dynamic capacitance measurement and HW circuits, is externally controlled through a script providing a unique possibility of performing multiple iterations of measurements without interruption. This test bench has given insight into the importance of uninterrupted measurements for generating of constant results. While doing the characterisation measurements, the presence of the "memory effect" of the triboelectric layer has been noticed. It refers to the non-ideal relationship between applied force to the triboelectric layer and measured V_{te}. It is related to the material properties of implemented triboelectric layer and mechanisms that take place when charges are inplanted into the layer.

To manage such high voltages at the output of the conditioning circuit and low loss power transfer from the conditioning circuit to the Buck converter a micro-plasma MEMS switch is proposed to be used. The MEMS switch composed of two conductors placed at controlled distances from one another is guided by Paschen's law. It defines the voltage at which a breakdown will occur for the defined gap and pressure to which conductors are submitted to. The breakdown voltage is the voltage at which a plasmonic conduction channel between conductors forms. Plasma discharge is ignited by the formation of a strong electric field between two conductors of the switch, for which high voltages are necessary. Exponentially increasing high voltages of Bennet are used to the advantage of ensured activation of the micro-plasma switch. In this thesis, a range of switches is fabricated with gaps of 5, 7 and 9 $\mu\mathrm{m}$ and designs with single and multiple fingers and possible extrusions to design. Preliminary experimental tests show that the "double TENG – double Bennet – plasma switch" system operates within the range of hypothesized voltages. Nevertheless, conducted experiments created significant damage to tested samples as the current passing through them is overbearing for the structure.

Aspiration for future work on the system involves further experimental research. On the initial experimental bench, the first goal is to record an experimental QV cycle that can be

compared with ones obtained in simulations and analytical equations. In that way, a research analysis of the circuit would be completed. It is planned to test the performance of the circuit with different variations of TENG. This involves the possible implementation of sliding or a rotational TENG. The variation in geometry of the tested transducer would widen the specter of possible realistic usages of the circuit.

The automatized experimental bench can be used for the determination of the presence and severity of V_{te} decay as an electrical property of the used triboelectric layer, for different materials and their thicknesses. The final objective of the automatic experimental bench is the determination of an empirical model linking input force, voltage and power dynamics, where the parameters of the model are: peak pressure, device geometry and triboelectric layer parameters like the material itself and its thickness.

With the goal of forming an energy-efficient management system, a continuation of research on a plasma switch is imperative. The selection of materials used to fabricate them has to be analysed so that samples are capable of supporting high voltages and bursts of current for extended periods of time. By increasing the thickness of the box layer of the SOI wafer, the levels of supported voltages and currents drastically increase. It is necessary to continue conducting tests on fabricated samples so that all gap and design variations of the switch can be characterized and their full potential discovered.

List of publications and awards

Published conference proceedings

N. Hodzic, D. Galayko, S.-W. Kim, and P. Basset. Unstable charge-pump for signal rectification of sliding tribo-electret generators with interdigitated grating electrodes. In *2019 19th International Conference on Micro and Nanotechnology for Power Generation and Energy Conversion Applications (PowerMEMS)*, pages 1–4. IEEE.

N. Hodzic, A. Delbani, A. Karami, D. Galayko and P. Basset. Bennet's Doubler With Double Capacitive TENG for Kinetic Energy Harvesting. In *2021 10th National Days on Energy Harvesting and Storage (JNRSE)*.

N. Hodzic, T. Alves, J-M. Laheurte and P. Basset. Substrate Capacitance Calculation in Linear Motion-Driven Electrostatic Kinetic Energy Harvester. In *2019 9th National Days on Energy Harvesting and Storage (JNRSE)*.

A. Delbani , A. Karami, D. Galayko, **N. Hodzic**, S. Vaidyanathan, M. Kane and P. Basset Triboelectric-Powered System For Pedestrian And Vehicle Detection With Wireless Data Transmission. In *2022 21st International Conference on Micro and Nanotechnology for Power Generation and Energy Conversion Applications (PowerMEMS)*.

P. Basset, H. Zhang, F. Marty, A. Delbani, **N. Hodzic**, A. Karami, and D. Galayko. High-voltage micro-plasma switch for efficient power management of triboelectric kinetic energy harvesters. In *2020 IEEE International Electron Devices Meeting (IEDM)*, pages 37.4.1–37.4.4. IEEE.

H. Zhang, F. Marty, D. Galayko, **N. Hodzic**, and P. Basset. High-voltage MEMS plasma switch for boosting the energy transfer efficiency in triboelectric nanogenerators. In *2020 IEEE 33rd International Conference on Micro Electro Mechanical Systems (MEMS)*, pages 610–613. IEEE.

Awards

- 1st (first) place at Symposium of Postgraduate Research in electrical engineering at the 13. DAYS of BHAAAs (June 2022)
- Outstanding Paper Award at JNRSE 2021 (June 2021)
- Symposium Best Presentation Award at Spring MRS Nanogenerators and Piezotronics Symposium (April 2021)
- Best Poster Presentation Award at JNRSE 2019 (May 20219)

Résumé détaillé

Le processus de collecte d'énergie consiste à convertir l'énergie présente dans notre environnement qui est inutilisée en énergie électrique utilisable. Les transducteurs sont des dispositifs qui convertissent cette énergie d'une forme à une autre. Ils sont guidés par la loi de conservation de l'énergie qui prévoit que l'énergie ne peut être ni créée ni perdue, mais transformée d'une forme à une autre. En fonction des matériaux utilisés et de la spécificité de leur conception, ils peuvent capter différentes formes d'énergie et les convertir en énergie électrique. Le concept repose sur l'utilisation de l'énergie ambiante, plutôt redondante, qui permet de produire de petites quantités d'énergie électrique par rapport aux sources traditionnelles. Les capteurs spécifiquement conçus pour convertir l'énergie et la stocker en vue d'une utilisation ultérieure, comme par exemple pour alimenter des composants électroniques disponibles dans le commerce, sont des récupérateur d'énergie (RE). Pour générer suffisamment d'énergie, la transduction continue dans les récupérateur est encouragée afin d'en faire un élément autosuffisant d'un dispositif électronique où la sortie de ce dispositif doit être conforme aux normes commerciales des signaux d'entrée. Par conséquent, il est nécessaire de gérer l'énergie récoltée de manière à ce qu'elle soit compatible avec la charge qu'elle alimente. Si le signal du récupérateur d'énergie n'est pas correctement traité, le signal d'entrée pour le composant électronique sera erroné et la transduction sera sans utilité. Il est donc très important de faire traiter le signal. Il y a plusieurs étapes à suivre pour s'assurer que le signal de sortie est compatible avec les composants électroniques disponibles dans le commerce.

Les récupérateurs d'énergie mécanique électrostatique (eKEH) sont alimentés par l'énergie mécanique sous forme de vibrations et sont basés sur le concept d'un condensateur et de ses paramètres variables induisant une conversion d'énergie. En général, ils sont composés de deux plaques conductrices placées face à face. Les plaques sont placées à une distance contrôlée qui peut être remplie d'air, de vide ou d'un matériau diélectrique spécifiquement choisi. Un condensateur inerte, d'un point de vue électrostatique, est considéré comme un élément à charge neutre. Il y a une quantité égale de changement sur les deux plaques conductrices. Une plaque est chargée positivement et l'autre est chargée négativement. Une force externe, provoquée par l'exercice d'une énergie mécanique sur le transducteur, affecte le condensateur de transduction de manière à faire varier une propriété définissant capacité. Pour ce faire, la conception du condensateur classique est modifiée de sorte qu'une de ses plaques est fixe et l'autre est mobile. Les deux paramètres qui peuvent être modifiés par une force appliquée à la structure sont A, la surface effective des électrodes, et d, la distance qui les sépare.

Un eKEH peut être soumis à des stimuli externes de n'importe quelle direction. En fonction de sa conception, le stimulus se propage vers un mécanisme de transduction de différentes manières, la force qui lui est appliquée pouvant être latérale, transversale ou rotative. En fonction de la direction de la force appliquée, les eKEH peuvent être classées dans les catégories suivantes : les eKEH à chevauchement dans le plan, les eKEH à fermeture de l'espace et les eKEH à rotation. Pour lancer le processus de transduction, le condensateur doit être polarisé par une source de tension continue. Cela permet de créer une différence de potentiel entre les deux plaques du condensateur et de créer des champs électriques variables. Alimenter un transducteur avec une tension continue au stade applicatif de la recherche et de la mise en œuvre pourrait être présenté comme un inconvénient. En conséquence, les chercheurs ont opté

pour une solution de construction permettant aux eKEH de disposer d'une tension intégrée. Pour ce faire, ils utilisent des matériaux qui présentent de bonnes propriétés d'accumulation et de stockage des charges. Ces matériaux sont appelés électrets. Grâce à leur propriété de stockage de la charge, ils peuvent servir de sources de tension permanentes. Pour que la conversion d'énergie ait lieu, la couche doit être préchargée en utilisant des rayons X doux, un faisceau électronique ou une décharge corona. De cette façon, la couche d'électret peut stocker la charge dans sa structure. Les scientifiques ont rapidement commencé à explorer un autre moyen de charger la couche d'électret, à savoir le mouvement mécanique naturel de l'eKEH et l'utilisation du processus de triboélectrification. Ainsi, certains eKEH ont évolué en nanogénérateurs triboélectriques (TENG), qui constituent une sous-famille d'eKEH. Un TENG peut être décrit comme un transducteur capacitif variable doté d'une couche triboélectrique supplémentaire.

Les électrets sont des matériaux diélectriques spécifiques ayant la capacité d'accumuler une charge électrique pendant une durée relativement longue, ce qui les rend électriquement équivalents à un aimant permanent. Comme mentionné, pour stocker ou injecter des charges dans les électrets, on peut utiliser des phénomènes de triboélectrification. Il s'agit d'une forme d'électrification par contact au cours de laquelle deux matériaux entrent en contact et la force de friction entre les deux transfère les charges de l'un à l'autre, après quoi les deux peuvent être séparés.

Le modèle électrique du système mécanique est rapporté par Hinchet et al. dans [4] qui ont dérivé l'équation de tension du TENG à partir des lois de Kirchhoff et de Gauss en formant l'équation 5. V_{TE} correspond à la source de tension constante générée par la triboélectrification. Elle dépend uniquement des caractéristiques de la couche triboélectrique (épaisseur et densité de charge) et non des paramètres de conception de la TENG, ce qui lui confère une valeur constante. Pour cette raison, V_{TE} correspond à une source de tension continue. Le condensateur variable CTENG comprend l'expression compensant le mouvement mécanique car il affecte directement la variation de celui-ci.

Le doubleur de Bennet est un système mécanique qui a été inventé en 1787 par Abraham Bennet [36]. Ce système mécanique a connu une renaissance grâce à son équivalent électrique rapporté pour la première fois par de Queiroz dans [37]. La première itération du doubleur de Bennet se composait d'un condensateur variable, de trois interrupteurs, d'un condensateur de référence et d'un condensateur de stockage. Après que son comportement ait été étudié d'un point de vue électrique et dans un but de réduction des pertes et augmentation de la vitesse du circuit, les interrupteurs ont été remplacés par des diodes. Le modèle de départ a commencé à changer chaque élément à des fins d'optimisation et la source de tension initiale a été remplacée par un condensateur de stockage, ce qui a fait du doubleur de Bennet un circuit de redressement possible pour les récoltes d'énergie. À ce stade, le circuit a été étudié uniquement du point de vue de l'électronique, sans aucune application spécifique pour les TENG. Comme les autres pompes de charge, le doubleur de Bennet a une condition nécessaire pour η, qui est égal à 1,56. Le caractère unique de ce circuit vient du fait qu'il est instable, c'est-à-dire qu'il n'a pas un état de fonctionnement optimal pour la conversion de charge. Sa caractéristique la plus notable est qu'il présente une augmentation exponentielle. Elle commence dès la mise en route du circuit et se poursuit à l'infini. En théorie, elle n'a pas de limite. En pratique, le facteur limitant est la tension maximale supportée les condensateurs

et les diodes utilisés. Une augmentation exponentielle de la charge et de la tension signifie que les cycles QV du doubleur de Bennet ne sont pas bloqués par une tension ou une charge à un moment donné. La surface des cycles QV augmente d'un cycle mécanique à l'autre, ce qui accroît l'énergie convertie par cycle. La réduction du critère de rapport minimal Cmax-Cmin et l'augmentation exponentielle de l'énergie convertie par cycle expliquent pourquoi ce circuit est favorable aux autres pompes de charge.

L'hypothèse suppose que, par l'augmentation de la capacité totale à varier et l'application d'un circuit de conditionnement efficace, la puissance convertie est augmentée. L'augmentation de la capacité à varier se fait en augmentant la taille du transducteur ou en modifiant sa géométrie. Si l'espace est limité, ce qui est le cas dans la plupart des cas, l'augmentation de la taille est possible. La modification de la géométrie peut être longue à mettre au point d'un point de vue mécanique, ne la rendant pas la plus efficace. En conservant la géométrie et en ajoutant une autre plaque ayant les mêmes caractéristiques physiques dans le même espace confiné, on peut concevoir un transducteur ayant une capacité variée plus élevée. Ce nouveau transducteur possède trois nœuds de sortie, contre deux traditionnellement. Le changement du nombre de sorties oblige à mettre en œuvre des circuits différents qui peuvent ne pas être adaptés aux récupérateurs d'énergie. Néanmoins, le doubleur de Bennet permet des substitutions possibles dans sa topologie. Le doubleur de Bennet est un circuit bien étudié et appliqué pour de nombreux transducteurs et TENGs. Cette thèse explore un ajustement de la conception du transducteur et une adaptation du doubleur de Bennet qui augmentent de manière significative les taux de conversion d'énergie et améliorent les performances du système de conversion d'énergie.

La théorie du double Bennet est définie par une analyse du système "double TENG" - "double Bennet". Elle comprend l'analyse du circuit du double Bennet dans cette configuration spécifique. Les niveaux de tension et le flux de charge dans les branches du circuit sont les paramètres cruciaux sur lesquels se base l'analyse, ce qui entraîne l'application de la loi de tension de Kirchhoff et de la loi de conservation de la charge. Les résultats sont résumés sur un graphique de cycle QV. Auparavant, trois architectures différentes de TENG ont été présentées. Chacune d'entre elles peut être convertie en un double TENG, cependant pour présenter la théorie du double Bennet, un système de fermeture de l'espace est choisi. Pour mener l'analyse théorique du double Bennet, un ensemble de contraintes initiales est défini : Tous les condensateurs du circuit sont entièrement déchargés. Chaque couche triboélectrique mise en œuvre dans le système est totalement saturée. En d'autres termes, les Vte ont des valeurs constantes. Le rapport de capacité η est suffisamment grand pour amorcer le circuit. Le Double Bennet fonctionne en régime permanent. L'analyse théorique peut être appliquée à n'importe quel point de fonctionnement d'un système "double TENG" - "double Bennet". Par conséquent, un énième cycle de l'opération est pris pour cette étude.

Le TENG est construit de manière à ce qu'une plaque mobile soit placée entre deux plaques fixes. La plaque mobile oscille ensuite sous l'effet d'un stimulus mécanique externe. Il est naturel de conclure que la forme que prend la variation de la capacité est influencée par la forme du mouvement mécanique. Dans le cas d'un TENG à fermeture automatique, il s'agit de la fonction cosinus. Un cycle mécanique de fonctionnement du TENG avec cette topologie est défini par une itération C_{max} - C_{min} - C_{max} pour C_{t+}, et une itération C_{min} - C_{max} - C_{min} pour C_{t-}. Par conséquent, le cycle de l'un des condensateurs est décalé par rapport

à l'autre de la moitié du cycle. Cela signifie que, alors que C_{t+} est défini par une fonction cosinus classique, le C_{t-} est décalé d'une portion T/2 du cycle, soit une demi-période. Les équations 10 et 11 contiennent les expressions des deux condensateurs.

Analyse du circuit du double Bennet

De Ai à Bi : On considère que le cycle mécanique commence avec $C_{t+} = C_{max}$ et $C_{t-} = C_{min}$. L'instant initial est défini comme le point Ai. A cet instant, les deux condensateurs sont équipotentiels. La topologie du circuit que TENG forme avec le reste du doubleur de Bennet est définie par la conduction ou l'isolation des diodes. Initialement, aucune des diodes n'est active, ergo le transducteur est déconnecté du reste du circuit. Au moment où le point Ai est défini, la stimulation mécanique du système commence. Comme le transducteur est déconnecté électriquement, tous les changements qui se produisent dans le système sont contenus dans celui-ci. On peut en déduire que les niveaux de charge restent inchangés dans ce cas. C_{t+} commence avec une capacité maximale, ce qui signifie qu'à partir du point Ai, elle va diminuer. La diminution de la capacité entraîne naturellement une augmentation de la tension aux nœuds de C_{t+} (tension $V_{t+|B}$). D'autre part, le C_{t-} commence le cycle avec une capacité minimale qui ne peut qu'augmenter, ce qui entraîne une diminution de la tension (tension $V_{t-|B}$). Avec la progression du mouvement mécanique, les nœuds du transducteur, qui avaient auparavant un potentiel égal, créent une différence de potentiel croissante entre eux. La différence de potentiel entre les nœuds induit la mise en conduction d'une des diodes. Ce moment est appelé le point Bi, qui est le premier point de changement dans le cycle QV.
De Bi à Di : Au point de changement Bi, la première diode conductrice est la diode D2. Cela se fait car la différence de tension entre le noeud de sortie et l'une des plaques fixes dépasse la valeur nécessaire pour que D2 soit conductrice. Cette diode étant allumée, les trois condensateurs sont connectés en série. L'avancement de l'énergie mécanique appliquée qui déplace l'électrode mobile continue à diminuer Ct+ jusqu'à ce qu'il atteigne son minimum $V_{t+|D} = C_{min}$ et C_{t-} à augmenter jusqu'à son maximum $V_{t-|D} = C_{max}$. Il s'agit d'un point critique dans l'évolution de la capacité qui provoque un changement dans le cycle, appelé point Di. La configuration en série formée entre les condensateurs crée les conditions pour que le flux de charges commence. TENG, en tant que dispositif physique, possède deux condensateurs qui ne peuvent pas être séparés l'un de l'autre. Par conséquent, les équations pour le segment de Bi à Di ne peuvent pas être évaluées séparément. Pour calculer et tracer la trajectoire de QV dans ce segment, il est nécessaire d'utiliser des équations paramétriques dépendantes du temps pour la capacité et la tension. Pour ce faire, les équations 23, 24 et 25 sont modifiées de façon à ce que chaque variable définie et calculée à cette occasion devienne dépendante du temps. Ceci inclut la capacité et les tensions en ce laps de temps.
De Di à Ei : Avec l'accumulation de charge dans le condensateur Cst, la tension V_{st} augmente et la différence de potentiel entre la sortie et le point TENG diminue jusqu'à ce que la diode D2 s'éteigne au moment Di. A ce stade, le TENG se déconnecte du circuit de redressement car aucune diode n'est conductrice à cet instant. Néanmoins, la stimulation externe continue à être appliquée au système car le cycle QV continue également d'évoluer. Le mouvement continu de l'électrode mobile incite C_{t+} et C_{t-} à passer par deux événements transitoires avant de revenir respectivement à C_{max} et C_{min}. Entre le moment Di et Ei, le TENG est électriquement séparé du reste, ce qui entraîne une stagnation des quantités de charge accumulées dans les condensateurs des transducteurs. Proportionnellement, avec la variation

de la capacité causée mécaniquement, V_{t+} augmente et V_{t-} diminue. Comme le TENG est électriquement séparé des autres condensateurs du circuit, la loi de conservation de la charge est applicable car leurs niveaux ne doivent pas être modifiés à ce stade. Les variations de capacité, qui sont inversées pour l'exemple de Ai à Bi, entraînent une diminution de la tension sur C_{t+} et une augmentation de la tension sur C_{t-}.
De Ei à Fi : Comme indiqué précédemment, au point Ei, le potentiel des deux condensateurs TENG s'égalise. Une fois que les deux s'approchent des V_{st}, la diode D1 conduit. Les deux condensateurs sont connectés en parallèle fermant la boucle et provoquant la réapparition de l'échange de charge, néanmoins dans la direction opposée. Une inversion des occurrences au point Bi où V_{t+} a libéré des charges au reste du circuit et V_{t-} en a accumulé une partie a lieu au point Ei. Entre Ei et Fi, V_{t+} absorbe et accumule maintenant les charges des autres condensateurs du circuit et V_{t-} les libère. La charge est envoyée de C_{t-} vers C_{t+}. Comme il n'y a que deux condensateurs dans le circuit.
De Fi à Ai+1 : Pendant que D1 conduit, les tensions des deux TENG passent à V_{st} et au moment où les trois tensions s'égalisent, la diode D3 commence aussi être conductrice. Maintenant, avec deux diodes allumées, le Cst est ajouté en parallèle à C_{t+} et C_{t-}. La même configuration est conservée jusqu'à la fin du cycle de conversion d'énergie. Dans l'intervalle Fi à Ai+1, C_{t+} et C_{t-} terminent leurs variations vers Cmax et Cmin, respectivement. C_{t-} continue à céder les charges qui sont maintenant partagées entre C_{t+} et Cst, et la tendance à laquelle cela se produit diffère de la période précédente car le circuit a changé. La loi de conservation des charges définit le nombre total de charges qui ont traversé les ensembles de boucles nouvellement formés comme $Q_{tot|F} = Q_{tot|A^{i+1}}$. En tenant compte de la connexion parallèle de trois condensateurs, on peut conclure qu'ils se trouvent au point équipotentiel.

L'analyse théorique du double Bennet donne un aperçu complet de la complexité du comportement de ce circuit. Pour connaître les limites du circuit et vérifier la précision de l'analyse effectuée, des simulations du circuit électrique sont réalisées. Les simulations électriques sont réalisées à l'aide de LTspice qui est un programme de résolution de circuits. Les caractéristiques du TENG doivent être présentées comme des paramètres électriques qui utilisent leur modèle électrique équivalent (une source DC et un condensateur).

Les variables qui doivent être étudiées sont la charge et la tension des condensateurs de TENG. Considérant que les simulations sont faites pour le système en régime permanent, n'importe quelle instance temporelle de la période simulée peut être prise pour observation. L'intervalle de temps choisi est de 1 seconde. Tout d'abord, les courbes de charge sur C_{t+} et C_{t-} sont observées pour la période sélectionnée. En conséquence du mouvement mécanique, le comportement symétrique antiphasique du système se transpose également dans la forme de la courbe de charge.

La simulation est exécutée pendant une période de 40 secondes et la charge sur C_{t+} est l'un des résultats de la simulation. On constate une augmentation exponentielle de la charge accumulée dans le condensateur du TENG. L'inférence générale sur la progression de la charge dans le temps a également été corroborée par des simulations. Le double Bennet maintient sa caractéristique primaire d'augmentation exponentielle de la quantité de charges et il a été prouvé que le système "double TENG" - "double Bennet" présente effectivement les caractéristiques prévues.

Examinons la tension de sortie du système actuel, c'est-à-dire la tension du condensateur

de sortie du double Bennet, Cst. Il est clair qu'il y a une augmentation exponentielle distincte et significative de la tension au fil du temps. La tension de sortie démarre lentement pour atteindre une tension d'environ 100 V dans les 15 premières secondes de fonctionnement. Ainsi, dans les 15 secondes suivantes, le comportement exponentiel se traduit par des niveaux de tension atteignant 450 V. En 37 secondes, elle a atteint 1000 volts, ce qui montre qu'à des tensions plus élevées, les tensions de démarrage cycle à cycle augmentent brusquement.

Enfin, la charge et la tension caractérisées du TENG sont simulées l'une contre l'autre pour former un cycle de QV. Trois instances du cycle de C_{t+} sont représentées. La forme simulée correspond bien à la forme du cycle QV généré par les dérivations théoriques. Les cinq phases du cycle sont identifiées. Chacune contient une phase de charge constante et de tension variable. Lorsque les niveaux de charge changent, sa relation non linéaire avec la tension se reflète sur la forme de la deuxième, quatrième et cinquième phase du cycle. Comme la simulation est effectuée sur un intervalle court et que la tendance à l'augmentation n'est pas claire, la présence d'un cycle est établie. Trois cycles QV simulés sont définis où chacun fixe une nouvelle tension plus élevée.

Les résultats de la simulation sont comparés aux résultats obtenus en calculant les équations analytiques. La ligne bleue (dérivée) suit largement la ligne rouge (simulée) avec de faibles écarts. Pour les instances de charge constante, la correspondance est parfaite. Cependant, l'inadéquation se produit dans les segments non linéaires. L'écart le plus important se situe au point Di du cycle QV auquel les calculs prédisent une baisse de tension plus forte. Dans le fragment Ei - Fi -Ai+1 du cycle, les deux courbes suivent les mêmes tendances avec de légères déviations qui peuvent être négligées en raison de l'ordre de grandeur en question (la charge étant de l'ordre du nano coulomb).

Expérimences sur le double Bennet

Sur la base de l'évaluation de la disponibilité des matériaux, du fonctionnement et de l'équipement de mesure du laboratoire où l'analyse expérimentale doit être menée, il a été conclu qu'il était préférable de fabriquer et de mener les expériences de double Bennet avec une TENG à fermeture d'espace. L'objectif initial de l'analyse expérimentale est de valider le comportement du double Bennet qui a été établi par l'analyse et la simulation. Pour ce faire, un TENG de taille significative est conçu dans l'intention de servir de preuve de concept. En augmentant la taille du dispositif, l'échelle de l'énergie convertie et d'autres paramètres, y compris les variables parasites, augmentent proportionnellement, ce qui ouvre une fenêtre plus large pour la détection, l'élaboration et l'élimination des composants nécessaires.

Sur le dessus du support, une feuille de cuivre de 9 cm par 9 cm est collée. Pour achever la construction du TENG, il est nécessaire de déposer le matériau triboélectrique. Pour ce faire, des feuilles de polytétrafluoroéthylène (PTFE) sont collées sur un ruban adhésif double face. Ce matériau électret est chimiquement résistant et peu sensible à l'usure mécanique avec l'un des coefficients de friction les plus faibles de tous les solides. Une couche de 100 m de PTFE est déposée sur deux plaques de cuivre du TENG.

Pour caractériser le dispositif fabriqué, il est nécessaire d'obtenir des données sur ses propriétés capacitives, ainsi que sur les propriétés de la couche triboélectrique. La capacité est caractérisée par la détermination de ses valeurs minimales et maximales et de la forme que prend la capacité. Les valeurs limites sont importantes pour déterminer le rapport de capacité (η) qui joue un rôle majeur car sa valeur détermine si la condition initiale de démarrage

des circuits est satisfaite ou non. La quantification de la tension de surface de la couche triboélectrique représente la caractérisation électrique.

Une fois l'ordre de grandeur de Cmax et Cmin obtenu, le comportement exact de deux condensateurs est enregistré à l'aide de la méthode de la capacité dynamique ou autrement appelée méthode du déphasage . Cette méthode génère une courbe de forme de capacité et donne les valeurs de capacité dans un intervalle de temps spécifié. Cette méthode fournit des informations sur la valeur de la capacité en se basant sur le déphasage obtenu entre un signal porteur et le signal mesuré. Pour obtenir ce déphasage, on utilise un circuit résistance-capacité (RC) où le condensateur fixe est remplacé par l'un des condensateurs du TENG. Lorsqu'un signal alternatif de fréquence et d'amplitude spécifique est envoyé au circuit RC de filtrage, le condensateur crée un déphasage du signal envoyé qui est ensuite enregistré. Le déphasage est mesuré comme la différence entre les points d'intersection des deux signaux.

La capacité approximative est d'environ 550 pF pour le Cmax. En calculant la résistance à partir de l'équation 66, la valeur choisie est de 56 k. La sortie du circuit est connectée à l'oscilloscope avec une sonde de 10 M à laquelle est également connecté le signal d'entrée. Dès qu'au moins trois révolutions Cmax - Cmin - Cmax sont présentes sur l'écran de l'oscilloscope, les données sont acquises. Il est impératif de visualiser et de traiter plus d'une révolution de capacité pour éviter d'utiliser le signal qui contient une anomalie ou un fonctionnement défectueux du TENG. La stabilité du signal obtenu est cruciale. Le post-traitement des données est effectué à l'aide d'un script Python où deux signaux sont alimentés et le script traite les données selon les équations 60 à 65. A la fin du processus, il fournit un tracé de la capacité et un fichier contenant les données tracées. Pour le TENG fabriqué, les résultats des mesures sont les suivants : Cmax = 500pF et Cmin = 55pF pour le condensateur gauche (appelé CTENG+), et Cmax = 560pF et Cmin = 55pF pour le condensateur droit (appelé CTENG-). Les écarts entre deux condensateurs sont naturels et sont présents en raison de l'erreur humaine, car le transducteur est fabriqué et placé dans le système à la main. Deux condensateurs sont symétriques et atteignent des valeurs maximales et minimales similaires. Cela permet de conclure que les deux condensateurs de ce transducteur sont symétriques et oscillent en phase opposée.

La capacité minimale calculée pour la dimension d'un seul condensateur TENG est de 50 pF, alors que la valeur mesurée est de 55 pF. L'écart entre la valeur calculée et la valeur mesurée est de 5 pF. Cela montre qu'aux faibles valeurs de capacité, lorsque le condensateur est le plus susceptible d'accumuler les parasites de l'environnement et du système lui-même, les condensateurs TENG sont plutôt stables et fidèles à leur valeur minimale. La capacité maximale calculée est de 1 nF et les capacités mesurées sont de 500 pF et 550 pF, ce qui montre des écarts plus importants. Même si la différence est assez importante, elle n'est pas inattendue car le dispositif est construit à la main et des imperfections dans la stratification peuvent avoir modifié la plus petite distance estimée entre deux plaques. Comme on le sait, pour calculer la capacité maximale, on considère la distance minimale entre deux plaques.

Le condensateur est ajouté en parallèle au condensateur du TENG de sorte que sa valeur contribue à la fois à Cmax et à Cmin, avec un impact significatif sur Cmin, car sa valeur est la plus petite. La valeur du condensateur sélectionné qui est ajouté de chaque côté du TENG (aux deux condensateurs pour que leur symétrie soit conservée lors des expériences) est Cpara = 33pF. Cela porte les rapports de capacité à $\eta_{TENG+} = 6$ et $\eta_{TENG-} = 6, 6$.

Estimation de Vte et η

L'estimation de Vte est la deuxième étape de la caractérisation électrique du TENG. La condition initiale pour le fonctionnement du circuit est que la couche triboélectrique soit complètement saturée. L'appareil qui mesure la densité de la charge de surface est disponible, mais il exige que la sonde de détection soit très proche de la couche triboélectrique. Par conséquent, il est impossible d'effectuer des mesures lorsque le TENG est actif et que ses plaques sont positionnées perpendiculairement les unes aux autres. En supposant que la couche triboélectrique soit complètement saturée et stabilisée, il serait nécessaire de retirer physiquement la plaque avec la couche, de faire la mesure avec l'appareil et de le remettre dans son état initial. Il est impossible d'effectuer les mesures sans tempérer avec les couches. Pour cette raison, on utilise des mesures de la tension de sortie d'un redresseur. Auparavant, on a mesuré η. En plus de cela, une fois que la tension de saturation du circuit pleine onde est connue, il est possible de calculer la valeur de la tension de surface de la couche triboélectrique, Vte.

La procédure pour mesurer la tension de sortie du redresseur pleine onde consiste à réaliser l'expérience avec l'un des condensateurs du TENG, après quoi il est déconnecté et le condensateur restant est connecté pour les mesures. Le condensateur de sortie choisi a une valeur fixe connue de 10 nF. Pour mesurer la tension sur ce condensateur, on mesure une charge à travers sa branche. Comme la valeur du condensateur est connue et constante, la relation V $=$ Q/C permet d'obtenir la tension du condensateur de sortie. L'appareil utilisé pour mesurer la charge est l'électromètre Keithley 6514 en configuration "Q". Les valeurs calculées dans les équations 70 et 71 confirment l'hypothèse selon laquelle les deux couches triboélectriques contribuent de manière égale au fonctionnement du TENG. La différence d'environ 40 V peut être négligée du fait que les couches ont été déposées à la main.

Comparaison des performances de Bennet classique et double

La comparaison des deux doubleurs de Bennet se fait en comparant les tensions de sortie au niveau du condensateur de stockage de 10 nF à la sortie. Les courbes sont restreintes à 400 V, comme mentionné précédemment, ce qui limite la portée de la comparaison à des tensions inférieures. On s'attend à ce que les deux circuits aient les mêmes capacités à atteindre des tensions élevées et qu'ils aient tous deux une augmentation exponentielle. Si l'on considère uniquement les condensateurs utilisés, la différence entre les deux circuits vient du fait que le condensateur de référence fixe est maintenant variable, mais toujours dans la même gamme. On peut conclure que la présence de la deuxième couche triboélectrique dans le TENG est bénéfique à son rendement.

Il est clair que même dans les premiers stades de son fonctionnement, le double Bennet est plus performant que le Bennet classique. Si l'on considère le temps qu'il faut à chacun pour atteindre 400 V, il est clair que le double Bennet met moins de temps pour atteindre la même tension. Si l'on fait la moyenne de la tension de sortie entre deux Bennet classiques, il faudrait 16,5 secondes pour atteindre 400 V, soit plus que les 15 secondes que celles nécessaires au double Bennet. Ces 15 secondes incluent 0,66 seconde de période transitoire, ce qui réduit le temps à 14,33 secondes, ce qui est plus que significatif.

Nous avons vu que le véritable potentiel du double Bennet se manifeste à des tensions encore plus élevées en raison de son démarrage exponentiel très brusque et de sa forte augmentation de tension. Ceci permet de conclure que les deux circuits ont les mêmes capacités à atteindre

dre des tensions élevées - pas de point de saturation et augmentation exponentielle. L'ajout d'un deuxième condensateur TENG a accéléré l'augmentation. Par conséquent, lorsque le temps est compté, le double Bennet est un circuit plus rapide.

La tension de sortie n'est qu'un des aspects qui caractérisent les performances d'un circuit comme le doubleur de Bennet. Il est nécessaire de se concentrer sur les observations des niveaux de charge qui complètent la tension et qui, dans ce cas, reflètent directement la quantité d'énergie qui est effectivement convertie de sa forme mécanique en énergie électrique. Les expériences qui suivent simultanément la tension et la distribution de la charge dans le circuit sont en cours de réalisation et les résultats sont prévus dans un avenir proche. Interrupteur MEMS à plasma haute tension Dans un premier temps, le premier et le deuxième bloc du système de conversion et de gestion de l'énergie ont été élaborés. L'énergie de l'environnement a été convertie en un signal électrique conditionné. Le doubleur de Bennet produit des tensions élevées à sa sortie. Il est impératif de construire un circuit qui régule et diminue les tensions à des niveaux (3,3 V ou 5 V) qui permettent au système d'être associé aux composants électroniques disponibles dans le commerce. La solution proposée consiste à utiliser un convertisseur Buck. Pour gérer le transfert des charges accumulées du condensateur de stockage de sortie du double Bennet aux nœuds d'entrée du convertisseur Buck, un élément de contrôle est implémenté comme un pont entre les deux. On y présente l'utilisation d'un commutateur MEMS à micro-plasma haute tension comme élément de contrôle pour le système de conversion et de gestion de l'énergie. Une fois que la connexion entre deux conducteurs est établie, les conducteurs commencent à conduire et à transférer l'énergie d'un nœud (anode) à un autre (cathode). Diverses méthodes peuvent être utilisées pour former un contact. Il peut s'agir de placer mécaniquement un matériau conducteur à connecter (interrupteurs mécaniques comme les boutons poussoirs et les relais) ou d'utiliser les propriétés semi-conductrices des matériaux constitutionnels (interrupteurs électroniques sans contact comme les transistors et les MOSFET). Un autre type d'interrupteurs qui est proposé par cette thèse sont les interrupteurs à éclateur. Leur principe de conduction est basé sur la formation d'un canal de conduction par plasma entre deux conducteurs. Pour que le plasma forme un canal de conduction, ou en d'autres termes pour qu'une décharge ait lieu, un fort champ électrique formé par des tensions élevées aux extrémités des conducteurs est nécessaire. À une tension élevée, un courant passe à travers deux électrodes conductrices en raison de la rupture électrique dans un gaz spécifique à une pression spécifique. L'environnement dans lequel l'anode et la cathode sont placées joue un rôle important dans le niveau de contrôle et les caractéristiques de l'interrupteur. Au départ, des sources de micro-plasma ont été développées, mais le contrôle des tensions supportées et du fonctionnement général du commutateur était faible, voire inexistant. Grâce à la qualité et à la précision des processus de fabrication des MEMS, il a été possible de contrôler avec précision l'espace entre les électrodes et donc de contrôler les tensions d'actionnement en utilisant le micro plasma. La figure montre le principe général de fonctionnement d'un interrupteur à plasma qui est ensuite traduit à l'échelle micro. La taille des micro-écarts peut varier de 100 m à des valeurs élevées dans la gamme des nm. Les pressions auxquelles une décharge de plasma peut se former pour les distances d'espacement mentionnées vont du vide poussé à la pression atmosphérique. La loi de Paschen est un principe physique qui définit la relation entre l'écart anode-cathode, la pression et la tension à laquelle le plasma se forme et conduit.

Le choix de la conception des interrupteurs MEMS a été motivé par les travaux réalisés précédemment sur ce sujet [22]. Deux modèles de interrupteurs anode-cathode fixes sont conçus et fabriqués. Chaque dice contient deux interrupteurs à éclateur. La première conception contient une seule structure rectangulaire (un doigt) allant de l'anode à la cathode. Les extrémités des deux sont plates, ce qui donne une géométrie de plaque à plaque. Le deuxième modèle, placé sur le même dice, présente une légère variation par rapport au premier. Au niveau de la bande où l'anode et la cathode sont les plus proches, un ensemble d'intrusions en forme de triangle a été ajouté des deux côtés. Le deuxième modèle a plusieurs doigts. Trois doigts sont attachés à l'anode et les deux autres à la cathode. Cette conception fournit une surface beaucoup plus grande pour que la décharge se produise. Ces modèles ont été utilisés comme base pour créer des variations dans la conception. Elles sont représentées par la modification de l'écart entre l'anode et la cathode. Les valeurs sélectionnées sont 5, 7 et 9 m. Cela fixe les valeurs prédites du claquage juste au niveau de la région du plateau de la courbe de Paschen.

La méthode de test des interrupteurs fabriqués commence par l'établissement de leurs tensions d'actionnement. Bien que la loi de Paschen prédise les tensions de claquage, il est connu qu'elle s'écarte de sa forme originale et atteint le plateau pour les dimensions d'entrefer qui sont étudiées dans cette thèse. La détermination des tensions d'actionnement réelles par des expériences est un impératif pour déterminer l'exactitude des calculs ainsi que la qualité du processus de fabrication. Toutes les variations des commutateurs fabriqués ont été soumises au test, cependant l'échantillon de interrupteur sélectionné qui est utilisé pour montrer les résultats des expériences réalisées est la conception avec des structures en forme de peigne avec des extrusions.

Le circuit de test est composé d'un TENG qui est connecté à un redresseur demi-onde. Au condensateur de sortie du redresseur est connecté l'interrupteur testé, à la sortie duquel est connecté un capaciteur. Ce signal est alimenté par un amplificateur opérationnel (OPA) en configuration suiveur afin que le signal de sortie puisse être observé sur un oscilloscope. Au lieu d'utiliser un seul condensateur à la sortie du redresseur et du commutateur, on utilise des diviseurs de tension capacitifs. Le raisonnement derrière l'utilisation de ces configurations spécifiques est basé sur les capacités de l'équipement de mesure, à savoir, l'électromètre dans la configuration de tension et les tensions de support de l'OPA. Le choix d'un circuit redresseur demi-onde pour le premier essai a pour but d'alimenter le commutateur avec des tensions qui atteindront la saturation. Dans la deuxième itération d'expériences, le doubleur de Bennet comme circuit redresseur est utilisé pour tester réellement le système proposé.

Le paramètre qui peut affecter l'échantillon fabriqué est le courant car il a tendance à augmenter de manière significative une fois que l'arc est formé et que les électrons commencent à circuler. Par conséquent, il est essentiel d'établir les capacités de certains modèles de interrupteur en mettant en œuvre une pompe de charge stable. Une fois qu'il est établi que le interrupteur est capable de gérer des tensions élevées mais contrôlées, il peut être soumis au système alimenté par un doubleur de Bennet qui présente une augmentation exponentielle continue de la tension et du nombre de charges accumulées au niveau du condensateur de sortie.

Lorsque le condensateur de sortie du redresseur demi-onde se charge, la courbe qui le représente prend la forme attendue. Une fois que la tension sur le condensateur, qui est en

même temps l'anode de l'interrupteur, a atteint 350V, une décharge plasma se produit et le condensateur de sortie est déchargé dans le condensateur après l'interrupteur.

Les échantillons contenant des structures en forme de peigne sont capables de s'activer de manière répétée aux mêmes tensions avec une décharge partielle. Les résultats des premières expériences ont montré que la méthodologie utilisée pour la conception et la fabrication des interrupteurs à plasma est conforme à leur comportement prédit. Une fois que les échantillons à doigt unique ont été soumis au même test, ils ont montré une certaine vulnérabilité dans les choix de conception. En effet, après quelques actionnements stables de l'interrupteur, la tension d'actionnement augmentait de manière significative. En considérant que les interrupteurs n'ont pas été interférés, l'explication possible de ce comportement inhabituel serait un endommagement de la structure.

La possibilité d'un endommagement structurel du commutateur a été étudiée en plaçant les échantillons sous le microscope et en observant la géométrie. Une fois l'hypothèse initiale confirmée, la gravité et la nature des dommages ont été évaluées au microscope électronique. La figure 58 montre une image rapprochée de la déformation de la cathode et de l'anode. Il a été compris qu'en raison du processus de formation de l'arc, des électrons sont projetés dans la cathode. Comme la décharge est concentrée à un endroit de l'espace, le flux d'électrons pénètre le matériau sur une très petite surface. Les effets secondaires des dommages proviennent de la libération thermique pendant la décharge. La combinaison de ces effets aboutit à des échantillons dont la cathode et l'anode sont fusionnées ou dont l'entrefer est agrandi. Le comportement enregistré de la tension de sortie est une réponse naturelle au changement de l'écart entre l'anode et la cathode. L'augmentation de l'écartement entraîne une augmentation de la tension de claquage.

Bibliography

[1] J W Matiko, N J Grabham, S P Beeby, and M J Tudor. Review of the application of energy harvesting in buildings. *Measurement Science and Technology*, 25(1):012002, January 2014.

[2] Gonzalo del Castillo-García, Elena Blanco-Fernandez, Pablo Pascual-Muñoz, and Daniel Castro-Fresno. Energy harvesting from vehicular traffic over speed bumps: a review. *Proceedings of the Institution of Civil Engineers - Energy*, 171(2):58–69, May 2018.

[3] S P Beeby, M J Tudor, and N M White. Energy harvesting vibration sources for microsystems applications. *Measurement Science and Technology*, 17(12):R175–R195, December 2006.

[4] Cheuk-Wang Yau, Tyrone Tai-On Kwok, Chi-Un Lei, and Yu-Kwong Kwok. Energy Harvesting in Internet of Things. In Beniamino Di Martino, Kuan-Ching Li, Laurence T. Yang, and Antonio Esposito, editors, *Internet of Everything*, pages 35–79. Springer Singapore, Singapore, 2018. Series Title: Internet of Things.

[5] Farnell element14. Calculating Battery Life in IoT Applications, May 2017.

[6] A.S. Holmes, G. Hong, K.R. Pullen, and K.R. Buffard. Axial-flow microturbine with electromagnetic generator: design, CFD simulation, and prototype demonstration. In *17th IEEE International Conference on Micro Electro Mechanical Systems. Maastricht MEMS 2004 Technical Digest*, pages 568–571, Maastricht, Netherlands, 2004. IEEE.

[7] Sijun Du, Yu Jia, Chun Zhao, Gehan A. J. Amaratunga, and Ashwin A. Seshia. A Nail-Size Piezoelectric Energy Harvesting System Integrating a MEMS Transducer and a CMOS SSHI Circuit. *IEEE Sensors Journal*, 20(1):277–285, January 2020.

[8] Kinetron.

[9] Perpetuum.

[10] Ronan Hinchet, Ali Ghaffarinejad, Yingxian Lu, Javad Yavand Hasani, Sang-Woo Kim, and Philippe Basset. Understanding and modeling of triboelectric-electret nanogenerator. *Nano Energy*, 47:401–409, May 2018.

[11] Junrui Liang and Wei-Hsin Liao. Impedance matching for improving piezoelectric energy harvesting systems. page 76430K, San Diego, California, USA, March 2010.

[12] Liao Wu, Peidong Zhu, and Minghua Xie. A Self-Powered Hybrid SSHI Circuit with a Wide Operation Range for Piezoelectric Energy Harvesting. *Sensors*, 21(2):615, January 2021.

[13] E. Arroyo and A. Badel. Electromagnetic vibration energy harvesting device optimization by synchronous energy extraction. *Sensors and Actuators A: Physical*, 171(2):266–273, November 2011.

[14] Philippe Basset. *Electrostatic kinetic energy harvesting*. ISTE Ltd/John Wiley and Sons Inc, Hoboken, NJ, 2016.

[15] Yunlong Zi, Jie Wang, Sihong Wang, Shengming Li, Zhen Wen, Hengyu Guo, and Zhong Lin Wang. Effective energy storage from a triboelectric nanogenerator. *Nature Communications*, 7(1):10987, April 2016.

[16] Xiaoliang Cheng, Liming Miao, Yu Song, Zongming Su, Haotian Chen, Xuexian Chen, Jinxin Zhang, and Haixia Zhang. High efficiency power management and charge boosting strategy for a triboelectric nanogenerator. *Nano Energy*, 38:438–446, August 2017.

[17] Hemin Zhang, Frédéric Marty, Xin Xia, Yunlong Zi, Tarik Bourouina, Dimitri Galayko, and Philippe Basset. Employing a MEMS plasma switch for conditioning high-voltage kinetic energy harvesters. *Nature Communications*, 11(1):3221, December 2020.

[18] Simiao Niu, Xiaofeng Wang, Fang Yi, Yu Sheng Zhou, and Zhong Lin Wang. A universal self-charging system driven by random biomechanical energy for sustainable operation of mobile electronics. *Nature Communications*, 6(1):8975, December 2015.

[19] N M White and J D Turner. Thick-film sensors: past, present and future. *Measurement Science and Technology*, 8(1):1–20, January 1997.

[20] R. Geigy, L. Jenni, M. Kauffmann, R. J. Onyango, and N. Weiss. Identification of T. brucei-subgroup strains isolated from game. *Acta Tropica*, 32(3):190–205, 1975.

[21] Mahmoud M. Magdy, Ahmed M. R. Fath El-Bab, and Samy F. M. Assal. Design Methodology of a Micro-Scale 2-DOF Energy Harvesting Device for Low Frequency and Wide Bandwidth. *Journal of Sensor Technology*, 04(02):37–47, 2014.

[22] P.D. Mitcheson, G.K. Rao, A.S. Holmes, and T.C. Green. Energy Harvesting From Human and Machine Motion for Wireless Electronic Devices. *Proceedings of the IEEE*, 96(9):1457–1486, September 2008.

[23] Yingxian Lu, Frédéric Marty, Dimitri Galayko, Jean-Marc Laheurte, and Philippe Basset. A power supply module for autonomous portable electronics: ultralow-frequency MEMS electrostatic kinetic energy harvester with a comb structure reducing air damping. *Microsystems & Nanoengineering*, 4(1):28, December 2018.

[24] Ya Yang, Hulin Zhang, Jun Chen, Qingshen Jing, Yu Sheng Zhou, Xiaonan Wen, and Zhong Lin Wang. Single-Electrode-Based Sliding Triboelectric Nanogenerator for Self-Powered Displacement Vector Sensor System. *ACS Nano*, 7(8):7342–7351, August 2013.

[25] J. Boland, Yuan-Heng Chao, Y. Suzuki, and Y.C. Tai. Micro electret power generator. In *The Sixteenth Annual International Conference on Micro Electro Mechanical Systems, 2003. MEMS-03 Kyoto. IEEE*, pages 538–541, Kyoto, Japan, 2003. IEEE.

[26] J Nakano, K Komori, Y Hattori, and Y Suzuki. MEMS Rotational Electret Energy Harvester for Human Motion. *Journal of Physics: Conference Series*, 660:012052, December 2015.

[27] Tomoya Miyoshi, Mitsuru Adachi, Kuniko Suzuki, Yiran Liu, and Yuji Suzuki. Low-profile rotational electret generator using print circuit board for energy harvesting from arm swing. In *2018 IEEE Micro Electro Mechanical Systems (MEMS)*, pages 230–232, Belfast, January 2018. IEEE.

[28] Yeon Joo Kim, Jaejun Lee, Sangwon Park, Chanho Park, Cheolmin Park, and Heon-Jin Choi. Effect of the relative permittivity of oxides on the performance of triboelectric nanogenerators. *RSC Adv.*, 7(78):49368–49373, 2017.

[29] K. Yamashita, M. Honzumi, K. Hagiwara, Y. Iguchi, and Y. Suzuki. Vibration-driven MEMS energy harvester with vacuum UV-charged vertical electrets. In *2011 16th International Solid-State Sensors, Actuators and Microsystems Conference*, pages 2630–2633, Beijing, China, June 2011. IEEE.

[30] Yuji Suzuki, Daigo Miki, Masato Edamoto, and Makoto Honzumi. A MEMS electret generator with electrostatic levitation for vibration-driven energy-harvesting applications. *Journal of Micromechanics and Microengineering*, 20(10):104002, October 2010.

[31] T. Takahashi, M. Suzuki, T. Nishida, Y. Yoshikawa, and S. Aoyagi. Application of paraelectric to a miniature capacitive energy harvester realizing several tens micro watt — Relationship between polarization hysteresis and output power. In *2013 IEEE 26th International Conference on Micro Electro Mechanical Systems (MEMS)*, pages 877–880, Taipei, Taiwan, January 2013. IEEE.

[32] Lokesh Dhakar, F. E. H. Tay, and Chengkuo Lee. Skin based flexible triboelectric nanogenerators with motion sensing capability. In *2015 28th IEEE International Conference on Micro Electro Mechanical Systems (MEMS)*, pages 106–109, Estoril, Portugal, January 2015. IEEE.

[33] Lokesh Dhakar, Xuechuan Shan, Zhiping Wang, Bin Yang, Francis Eng Hock Tay, Chun-Huat Heng, and Chengkuo Lee. Scalable fabrication of triboelectric nanogenerators for commercial applications. *Journal of Physics: Conference Series*, 660:012032, December 2015.

[34] Xiaoyi Li, Guoqiang Xu, Xin Xia, Jingjing Fu, Longbiao Huang, and Yunlong Zi. Standardization of triboelectric nanogenerators: Progress and perspectives. *Nano Energy*, 56:40–55, February 2019.

[35] S Boisseau, G Despesse, and A Sylvestre. Optimization of an electret-based energy harvester. *Smart Materials and Structures*, 19(7):075015, July 2010.

[36] Simiao Niu, Yu Sheng Zhou, Sihong Wang, Ying Liu, Long Lin, Yoshio Bando, and Zhong Lin Wang. Simulation method for optimizing the performance of an integrated triboelectric nanogenerator energy harvesting system. *Nano Energy*, 8:150–156, September 2014.

[37] Ali Ghaffarinejad, Javad Yavand Hasani, Ronan Hinchet, Yingxian Lu, Hemin Zhang, Armine Karami, Dimitri Galayko, Sang-Woo Kim, and Philippe Basset. A conditioning circuit with exponential enhancement of output energy for triboelectric nanogenerator. *Nano Energy*, 51:173–184, September 2018.

[38] Armine Karami, Dimitri Galayko, and Philippe Basset. Series-Parallel Charge Pump Conditioning Circuits for Electrostatic Kinetic Energy Harvesting. *IEEE Transactions on Circuits and Systems I: Regular Papers*, 64(1):227–240, January 2017.

[39] A. Bennet. *New Experiments on Electricity: Wherein the Causes of Thunder and Lightning as Well as the Constant State of Positive Or Negative Electricity in the Air Or Clouds, are Explained : with Experiments on Clouds of Powders and Vapours Artificially Diffused in the Air : Also a Description of a Doubler of Electricity, and of the Most Sensible Electrometer Yet Constructed : with Other New Experiments and Discoveries in the Science Illustrated by Explanatory Plates*. J. Drewry, 1789.

[40] Antonio Carlos M. de Queiroz. Electrostatic vibrational energy harvesting using a variation of Bennet's doubler. In *2010 53rd IEEE International Midwest Symposium on Circuits and Systems*, pages 404–407, Seattle, WA, USA, August 2010. IEEE.

[41] M.A. Ben Ouanes, H. Samaali, D. Galayko, P. Basset, and F. Najar. A new type of triboelectric nanogenerator with self-actuated series-to-parallel electrical interface based on self-synchronized mechanical switches for exponential charge accumulation in a capacitor. *Nano Energy*, 62:465–474, August 2019.

[42] Antonio Carlos M. de Queiroz and Marcelo Domingues. Analysis of the doubler of electricity considering a resistive load. In *2013 IEEE 56th International Midwest Symposium on Circuits and Systems (MWSCAS)*, pages 45–48, Columbus, OH, USA, August 2013. IEEE.

[43] E Lefeuvre, S Risquez, J Wei, M Woytasik, and F Parrain. Self-Biased Inductor-less Interface Circuit for Electret-Free Electrostatic Energy Harvesters. *Journal of Physics: Conference Series*, 557:012052, November 2014.

[44] Vitaly Dorzhiev, Armine Karami, Philippe Basset, Frederic Marty, Valery Dragunov, and Dimitri Galayko. Electret-Free Micromachined Silicon Electrostatic Vibration Energy

Harvester With the Bennet's Doubler as Conditioning Circuit. *IEEE Electron Device Letters*, 36(2):183–185, February 2015.

[45] V.P. Dragunov, D.I. Ostertak, and R.E. Sinitskiy. New modifications of a Bennet doubler circuit-based electrostatic vibrational energy harvester. *Sensors and Actuators A: Physical*, 302:111812, February 2020.

[46] Longjie Li, Jiangtao Li, and Zheng Zhao. Effect of switch parameters and polarity on the repetitive performance of a corona-stabilized switch viewed from behavior of space charge. *Physics of Plasmas*, 27(4):043509, April 2020.

[47] P. Carazzetti, Ph. Renaud, and H. R. Shea. Experimental study of electrical breakdown in MEMS devices with micrometer scale gaps. page 688404, San Jose, CA, February 2008.

[48] Guodong Meng and Yonghong Cheng. Electrical Breakdown Behaviors in Microgaps. In Steven H. Voldman, editor, *Electrostatic Discharge - From Electrical breakdown in Micro-gaps to Nano-generators*. IntechOpen, October 2019.

[49] S.L. Moran and L.W. Hardesty. High-repetition-rate hydrogen spark gap. In *Nineteenth IEEE Symposium on Power Modulators*, pages 227–231, San Diego, CA, USA, 1990. IEEE.

[50] S.J. MacGregor, S.M. Turnbull, F.A. Tuema, and O. Farish. Factors affecting and methods of improving the pulse repetition frequency of pulse-charged and DC-charged high-pressure gas switches. *IEEE Transactions on Plasma Science*, 25(2):110–117, April 1997.

[51] J.M. Koutsoubis and S.J. MacGregor. Effect of gas type on high repetition rate performance of a triggered, corona stabilised switch. *IEEE Transactions on Dielectrics and Electrical Insulation*, 10(2):245–255, April 2003.

[52] J. W. Nam, H. Rahaman, and S. H. Nam. Investigation a microplasma assisted spark gap pulser. In *2010 IEEE International Power Modulator and High Voltage Conference*, pages 545–548, Atlanta, GA, USA, May 2010. IEEE.

[53] H. Rahaman, J. W. Nam, S. H. Nam, and K. Frank. A miniaturized spark gap switch in the regime of high repetition rate. In *2010 IEEE International Power Modulator and High Voltage Conference*, pages 385–387, Atlanta, GA, USA, May 2010. IEEE.

[54] Faisal K. Chowdhury, Yuying Zhang, and M. Tabib-Azar. Fabrication and characterization of 3D micro-plasma field effect transistors. In *2013 IEEE 26th International Conference on Micro Electro Mechanical Systems (MEMS)*, pages 669–672, Taipei, Taiwan, January 2013. IEEE.

[55] Kurt Zuber. Über die Verzögerungszeit bei der Funkenentladung. *Annalen der Physik*, 381(2-3):231–260, 1925.

[56] M. v. Laue. Bemerkung zu K. Zubers Messung der Verzögerungszeiten bei der Funkenentladung. *Annalen der Physik*, 381(2-3):261–265, 1925.

[57] Momcilo M Pejovic, Goran S Ristic, and Jugoslav P Karamarkovic. Electrical breakdown in low pressure gases. *Journal of Physics D: Applied Physics*, 35(10):R91–R103, May 2002.

[58] Yu. Z. Ionikh, A. V. Meshchanov, and D. O. Ivanov. Dependence of the Breakdown Potential on the Voltage Rise Rate in a Long Discharge Tube at Low Pressure. *Technical Physics*, 64(7):950–956, July 2019.

[59] A I Shishpanov, D O Ivanov, and S A Kalinin. Collision of ionization waves in long discharge tubes. *Plasma Research Express*, 1(2):025004, May 2019.

[60] M F Gendre, M Haverlag, and G M W Kroesen. Optical and electrostatic potential investigations of electrical breakdown phenomena in a low-pressure gas discharge lamp. *Journal of Physics D: Applied Physics*, 43(23):234004, June 2010.

[61] Yangyang Fu, Peng Zhang, and John P. Verboncoeur. Gas breakdown in atmospheric pressure microgaps with a surface protrusion on the cathode. *Applied Physics Letters*, 112(25):254102, June 2018.

[62] Yangyang Fu, Janez Krek, Peng Zhang, and John P. Verboncoeur. Gas Breakdown in Microgaps With a Surface Protrusion On the Electrode. *IEEE Transactions on Plasma Science*, 47(5):2011–2019, May 2019.

[63] Yangyang Fu, Peng Zhang, Janez Krek, and John P. Verboncoeur. Gas breakdown and its scaling law in microgaps with multiple concentric cathode protrusions. *Applied Physics Letters*, 114(1):014102, January 2019.

[64] Simon Ang and Alejandro Oliva. *Power-Switching Converters, Third Edition*. CRC Press, Boca Raton, FL, third edition edition, 2010. OCLC: 1027760048.

Appendix A

:

Full derivations of theoretical analysis

Capacitance

$$C_{\mathrm{t}+}(t) = \frac{\varepsilon_0 s}{\frac{d_{\mathrm{die}}}{\varepsilon_r} + \frac{X_{\max}}{2} - \frac{X_{\max}}{2}\cos(2\pi f t)}$$

$$C_{\mathrm{t}-}(t) = \frac{\varepsilon_0 s}{\frac{d_{\mathrm{die}}}{\varepsilon_r} + \frac{X_{\max}}{2} - \frac{X_{\max}}{2}\cos\left(2\pi f t + \frac{T}{2}\right)}$$

To uniformly represent and easily maneuver the capacitance values throughout further, more complex expressions, the two equations are normalized starting with $C_{\mathrm{t}+}$.

$$C_{\mathrm{t}+}(t) = \frac{\varepsilon_0 s}{\frac{d_{\mathrm{die}}}{\varepsilon_r} + \frac{X_{\max}}{2} - \frac{X_{\max}}{2}\cos(2\pi f t)}$$

$$C_{\mathrm{t}+}(t) = \frac{\varepsilon_0 s}{\frac{2d_{\mathrm{die}} + \varepsilon_r X_{\max} - \varepsilon_r X_{\max}\cos(2\pi f t)}{2\varepsilon_r}}$$

$$C_{\mathrm{t}+}(t) = \frac{\varepsilon_0 s}{\frac{2d_{die} + \varepsilon_r X_{max}}{2\varepsilon_r} - \frac{\varepsilon_r b X_{max}}{2\varepsilon_r}\cos(2\pi f t)}$$

$$C_{\mathrm{t}+}(t) = \frac{\frac{2\varepsilon_0\varepsilon_r s}{2d_{\mathrm{die}} + \varepsilon_r X_{\max}}}{1 - \frac{X_{\max}}{2(2d_{die} + \varepsilon_r X_{\max})}\cos(2\pi f t)}$$

$$C_{\mathrm{t}+}(t) = \frac{C_0}{1 - \alpha\cos(2\pi f t)}$$

Where nominal capacitance C_0 substitutes

$$C_0 = \frac{2\varepsilon_0\varepsilon_r s}{2d_{\mathrm{die}} + \varepsilon_r X_{\max}}$$

and a numeric parameter α equals

$$\alpha = \frac{X_{\max}}{2(2d_{\mathrm{die}} + \varepsilon_r X_{\max})}$$

.

Using the same method, $C_{\mathrm{t}-}$ is normalized to a similar expression.

$$C_{\mathrm{t}-}(t) = \frac{C_0}{1 + \alpha\cos(2\pi f t)}$$

where the parameters C_0 and α are the same as for $C_{\mathrm{t}+}(t)$.

QV Cycle

From A^i to B^i

$$Q^i_{\mathrm{t}+|\mathrm{A}} = Q^i_{\mathrm{t}+|\mathrm{B}}$$

$$C^i_{\mathrm{t}+|\mathrm{A}}(V^i_{\mathrm{t}+|\mathrm{A}} - V_{\mathrm{te}+}) = C_{\max}(V^i_{\mathrm{t}+|\mathrm{A}} - V_{\mathrm{te}+}) = C^i_{\mathrm{t}+|\mathrm{A}}(V^i_{\mathrm{t}+|\mathrm{B}} - V_{\mathrm{te}+})$$

$$\rightarrow C^i_{\mathrm{t+|B}} = C^i_{\mathrm{t+|A}} \frac{V^i_{\mathrm{t+|A}} - V_{\mathrm{te+}}}{V^i_{\mathrm{t+|B}} - V_{\mathrm{te+}}} = \frac{C_{\max}(V^i_{\mathrm{t+|A}} - V_{\mathrm{te+}})}{V^i_{\mathrm{t+|B}} - V_{\mathrm{te+}}} = C^*$$

Form the initial conservation of charge equality we can also extract the expression for the potential at point $B^i ti$.

$$\rightarrow V^i_{\mathrm{t+|B}} = (V^i_{\mathrm{t+|A}} - V_{\mathrm{te+}}) \frac{C_{\max}}{C_{\mathrm{t+|B}}} + V_{\mathrm{te+}}$$

Same as it happens with C_t+ the C_t- has the similar occurrences in the period. Following equations define it as

$$Q^i_{\mathrm{t-|A}} = Q^i_{\mathrm{t-|B}}$$

$$C^i_{\mathrm{t-|A}}(V^i_{\mathrm{t-|A}} - V_{\mathrm{te-}}) = C_{\min}(V^i_{\mathrm{t+|A}} - V_{\mathrm{te-}}) = C^i_{\mathrm{t-|B}}(V^i_{\mathrm{t-|B}} - V_{\mathrm{te-}})$$

$$\rightarrow C^i_{\mathrm{t-|B}} = C^i_{\mathrm{t-|A}} \frac{V^i_{\mathrm{t-|A}} - V_{\mathrm{te-}}}{V^i_{\mathrm{t-|B}} - V_{\mathrm{te-}}} = \frac{C_{\min}(V^i_{\mathrm{t+|A}} - V_{\mathrm{te-}})}{V^i_{\mathrm{t-|B}} - V_{\mathrm{te-}}} = C^{**}$$

Following the method applied to $C_{\mathrm{t+}}$, expression for the potential at point $B^i ti$ for $C_{\mathrm{t-}}$ is as follows.

$$\rightarrow V^i_{\mathrm{t-|B}} = (V^i_{\mathrm{t-|A}} - V_{\mathrm{te-}}) \frac{C_{\min}}{C_{\mathrm{t-|B}}} + V_{\mathrm{te-}}$$

From B^i to D^i By the law of conservation of charge over the TENG between points A^i to D^i:

$$C_{\min}(V - V_{\mathrm{te-}}) + C_{\max}(V - V_{\mathrm{te+}}) = C_{\min}(V^i_{\mathrm{t+|D}} - V_{\mathrm{te+}}) + C_{\max}(V^i_{\mathrm{t-|D}} - V_{\mathrm{te-}}) \tag{82}$$

The second node for which the circuit that provides information about charge distribution is the node between two parts of the TENG:

$$C_{\mathrm{st}} V - C_{\min}(V - V_{\mathrm{te-}}) = V^i_{\mathrm{st|D}} C_{\mathrm{st}} - C_{\max}(V^i_{\mathrm{t-|D}} - V_{\mathrm{te-}}) \tag{83}$$

Looking at the circuit when D_2 is ON, it is possible to write Kirchhoff's voltage law as follows:

$$V^i_{\mathrm{t+|D}} = V^i_{\mathrm{t-|D}} + V^i_{\mathrm{st|D}} + \Delta V \tag{84}$$

Where $\Delta V = V_{\mathrm{te+}} - V_{\mathrm{te-}}$. These three equations are providing enough information to define TENG's voltages at point D^i. The expressions simplify if we substitute voltages over the TENG capacitors at point A^i with

$$\alpha = V^i_{\mathrm{t+|A}} - V_{\mathrm{te+}}$$

$$\beta = V^i_{\mathrm{t+|A}} - V_{\mathrm{te-}}$$

which transform the initial equations into:

$$C_{\max}\alpha + C_{\min}\beta = C_{\min}(V^i_{\mathrm{t+|D}} - V_{\mathrm{te+}}) + C_{\max}(V^i_{\mathrm{t-|D}} - V_{\mathrm{te-}}) \tag{82}$$

$$C_{\mathrm{st}}V^i_{\mathrm{t+|A}} - C_{\min}\beta = C_{\mathrm{st}}V^i_{\mathrm{st|D}} - C_{\max}(V^i_{\mathrm{t-|D}} - V_{\mathrm{te-}}) \tag{83}$$

From the equation (3) the expression for $V^i_{\mathrm{st|D}}$ which than can be neutralized in equations (1) and (2).

$$V^i_{\mathrm{t+|D}} = V^i_{\mathrm{t-|D}} + V^i_{\mathrm{st|D}} - \Delta V \rightarrow V^i_{\mathrm{st|D}} = V^i_{\mathrm{t+|D}} - V^i_{\mathrm{t-|D}} + \Delta V \tag{84}$$

Resolving this set of the equations defines the three circuit capacitors' voltages as:

$$V_{t+|D} = \frac{C_{\max}C_{\min}V_{\mathsf{te+}} + {C_{\max}}^2\alpha + C_{\min}C_{\mathsf{st}}(V_{\mathsf{te+}} + \beta) + C_{\max}C_{\mathsf{st}}(V^i_{\mathrm{t+|A}} + V_{\mathsf{te-}} + \alpha - \Delta\mathsf{V})}{C_{\min}C_{\mathsf{st}} + C_{\max}(C_{\min} + C_{\mathsf{st}})}$$

$$V_{t-|D} = \frac{C_{\max}C_{\min}V_{\mathsf{te-}} + C_{\max}C_{\mathsf{st}}(V_{\mathsf{te-}} + \alpha) + {C_{\min}}^2\beta + C_{\min}C_{\mathsf{st}}(-V^i_{\mathrm{t+|A}} + V_{\mathsf{te+}} + \beta + \delta\mathsf{V})}{C_{\min}C_{\mathsf{st}} + C_{\max}(C_{\min} + C_{\mathsf{st}})}$$

$$V_{\mathsf{st}|D} = \frac{C_{\max}C_{\mathsf{st}}V + {C_{\max}}^2\alpha + C_{\min}(C_{\mathsf{st}}V^i_{\mathrm{t+|A}} - C_{\min}\beta) + C_{\max}C_{\min}(V_{\mathsf{te+}} - V_{\mathsf{te-}} + \delta\mathsf{V})}{C_{\min}C_{\mathsf{st}} + C_{\max}(C_{\min} + C_{\mathsf{st}})}$$

$$Q^i_{AD+} = C_{max}(V^i_{t+|A} - V_{te+}) - C_{min}(V^i_{t+|D} - V_{te+})$$

$$Q^i_{AD+} = -\frac{C_{\mathsf{st}}(C_{\max}C_{\min}(V^i_{\mathrm{t+|A}} - 2V_{\mathsf{te+}} + 2V_{\mathsf{te\text{-}}}) + C^2_{\max}(V_{\mathsf{te+}} - V^i_{t+|A}) + C^2_{\min}(-V_{\mathsf{te\text{-}}} + V^i_{t+|A}))}{C_{\min}C_{\mathsf{st}} + C_{\max}(C_{\min} + C_{\mathsf{st}})}$$

The charge $\Delta Q^i_{\mathrm{AD+}}$ is (equally??) distributed across the other two circuit's capacitors $C_{\mathrm{t-}}$ and C_{st} as they are connected in series with $C_{\mathrm{t+}}$. As established earlier, $C_{\mathrm{t-}}$ and $C_{\mathrm{t+}}$ are equal, yet antiphasic(??) capacitors leading to the conclusion that $C_{\mathrm{t-}}$ is passing through charge exchange phase same as its opposing transducer capacitor. Therefore, these TENG's capacitors variations cause additional charge transfer to C_{st}.

$C_{\mathrm{t+}}$ and $C_{\mathrm{t-}}$ having equal and (anti)symmetrical variations results in same amount of charge that is transferred to $C_{\mathrm{t-}}$ from $C_{\mathrm{t+}}$ to be transferred from it due to its own QV cycle evolution. In addition to $\frac{\Delta Q^i_{\mathrm{AD+}}}{2}$ transferred to C_{st}, an additional $\frac{\Delta Q^i_{\mathrm{AD-}}}{2}$ is added to the charge of C_{st}. Keeping in mind that $\Delta Q^i_{\mathrm{AD-}} = \Delta Q^i_{\mathrm{AD+}}$ the charge of C_{st} is increased by $\Delta Q^i_{\mathrm{AD+}}$.

Parametric expressions

$$C_{\max}(V^i_{\mathrm{t+|A}} - V_{\mathrm{te+}}) + C_{\min}(V^i_{\mathrm{t+|A}} - V_{\mathrm{te-}}) = C_{\mathrm{t+|BD}}(t)(V^i_{\mathrm{t+|BD}}(t) - V_{\mathrm{te+}}) + C_{\mathrm{t-|BD}}(t)(V^i_{\mathrm{t-|BD}}(t) - V_{\mathrm{te-}})$$

$$C_{\mathrm{st}} V^i_{\mathrm{t+|A}} - C_{\min}(V^i_{\mathrm{t+|A}} - V_{\mathrm{te-}}) = C_{\mathrm{st}} V^i_{\mathrm{st|D}}(t) - C_{\mathrm{t-|BD}}(t)(V^i_{\mathrm{t-|BD}}(t) - V_{\mathrm{te-}})$$

$$V^i_{\mathrm{t+|BD}}(t) = V^i_{\mathrm{t-|BD}}(t) + V^i_{\mathrm{st|BD}}(t) - \Delta \mathrm{V}$$

Because we have already defined the terminating voltages at relevant points, from these equations we can derive and shape of the charge exchange in each capacitor which can be observed through TENG's voltage equations.

$$V_{t+}(t|_{B\to D}) = \frac{C_{\max}(V^i_{t|A} - V_{\mathsf{te}+}) + C_{\min}(V^i_{t|A} - V_{\mathsf{te}-}) + C_{t-}(t|_{B\to D}) + C_{t+}(t|_{B\to D})}{C_{t-}(t|_{B\to D}) + C_{t+}(t|_{B\to D})}$$

$$\begin{aligned} V_{t-}(t|_{B\to D}) = \frac{1}{(C_{\mathsf{st}} + C_{t-}(t|_{B\to D}))(C_{t-}(t|_{B\to D}) + C_{t+}t)}[C_{\max}C_{\mathsf{st}}(V^i_{t|A} - V_{\mathsf{te}+}) \\ + C_{\mathsf{st}}V_{\mathsf{te}+}C_{t-}(t|_{B\to D}) + 2C_{\mathsf{st}}V_{\mathsf{te}-}C_{t-}(t|_{B\to D}) - C_{\mathsf{st}}V^i_{t+|A}C_{t-}(t|_{B\to D}) + V_{\mathsf{te}-}{C_{t-}}^2(t|_{B\to D}) \\ + 2C_{\mathsf{st}}V_{\mathsf{te}+}C_{t+}t + C_{\mathsf{st}}V_{\mathsf{te}-}C_{t+}t - C_{\mathsf{st}}V^i_{t+|A}C_{t+}t + V_{\mathsf{te}-}C_{t-}(t|_{B\to D})C_{t+}t + C_{\min}(V^i_{t+|A} - V_{\mathsf{te}-}) \\ (C_{\mathsf{st}} + C_{t+}t + C_{t-}(t|_{B\to D}))] \end{aligned}$$

Based on the relationship between charge, voltage and capacitance $Q = VC$, the expressions for the $Qt{+}(t|_{B\to D})$ and $Qt{-}(t|_{B\to D})$ can be easily derived and are:

$$\begin{aligned} Q_{t+}(t|_{B\to D}) = C_{t+}(t|_{B\to D})\frac{C_{\max}(V^i_{t|A} - V_{\mathsf{te}+}) + C_{\min}(V^i_{t|A} - V_{\mathsf{te}-})}{C_{t-}(t|_{B\to D}) + C_{t+}(t|_{B\to D})} \\ + \frac{)V_{\mathsf{te}-}C_{t-}(t|_{B\to D}) + V_{\mathsf{te}+}C_{t+}(t|_{B\to D}}{C_{t-}(t|_{B\to D}) + C_{t+}(t|_{B\to D})} \end{aligned}$$

$$\begin{aligned} Q_{t-}(t|_{B\to D}) = \frac{C_{t-}(t|_{B\to D})}{(C_{\mathsf{st}} + C_{t-}(t|_{B\to D}))(C_{t-}(t|_{B\to D}) + C_{t+}t)}[C_{\max}C_{\mathsf{st}}(V^i_{t|A} - V_{\mathsf{te}+}) \\ + C_{\mathsf{st}}V_{\mathsf{te}+}C_{t-}(t|_{B\to D}) + 2C_{\mathsf{st}}V_{\mathsf{te}-}C_{t-}(t|_{B\to D}) - C_{\mathsf{st}}V^i_{t+|A}C_{t-}(t|_{B\to D}) + V_{\mathsf{te}-}{C_{t-}}^2(t|_{B\to D}) \\ + 2C_{\mathsf{st}}V_{\mathsf{te}+}C_{t+}t + C_{\mathsf{st}}V_{\mathsf{te}-}C_{t+}t - C_{\mathsf{st}}V^i_{t+|A}C_{t+}t + V_{\mathsf{te}-}C_{t-}(t|_{B\to D})C_{t+} \\ + C_{\min}(V^i_{t+|A} - V_{\mathsf{te}-})(C_{\mathsf{st}} + C_{t+}t + C_{t-}(t|_{B\to D}))] \end{aligned}$$

From D^i to E^i

$$\begin{aligned} Q^i_{\mathrm{t+|D}} &= Q^i_{\mathrm{t+|E}} \\ C_{\mathrm{t+|D}}\left({V_{\mathrm{t+|D}}}^i - V_{\mathrm{te+}}\right) &= C_{\mathrm{t+|E}}\left(V^i_{\mathrm{t+|E}} - V_{\mathrm{te+}}\right) \\ Q^i_{t-|D} &= Q^i_{t-|E} \end{aligned} \tag{85}$$

$$C_{t-|D}\left({V_{t-|D}}^{i}-V_{\mathrm{te}-}\right)=C_{t-|E}\left(V_{t-|E}^{i}-V_{\mathrm{te}-}\right) \tag{86}$$

The charge equation are sourcing the expressions for either a capacitance or voltage at the extreme E^{i} :

$$(85)\rightarrow C_{t+|E}=C_{t+|D}\frac{V_{t+|D}^{i}-V_{\mathrm{te}+}}{V_{t+|E}^{i}-V_{te+}}=C_{\min}\frac{V_{t+|D}^{i}-V_{te+}}{V_{t+|E}^{i}-V_{te+}}=C^{**}$$

$$(85)\rightarrow V_{t+|E}^{i}=\left({V_{t+|D}}^{i}-V_{\mathrm{te}+}\right)\frac{C_{\min}}{C_{t+|E}}+V_{\mathrm{te}+}$$

$$(86)\rightarrow C_{t-|E}=C_{t-|D}\frac{{V_{t-|D}}^{i}-V_{\mathrm{te}-}}{V_{t-|E}^{i}-V_{\mathrm{te}-}}=C_{\max}\frac{V_{t-|D}^{i}-V_{\mathrm{te}-}}{V_{t-|E}^{i}-V_{\mathrm{te}-}}=C^{*}$$

$$(86)\rightarrow V_{t-|E}^{i}=\left({V_{t-|D}}^{i}-V_{\mathrm{te}-}\right)\frac{C_{\max}}{C_{t-|E}}+V_{\mathrm{te}-}$$

From E^{i} to F^{i}

$$Q_{tot|E}=Q_{tot|F}$$

$$Q_{t+|E}+Q_{t-|E}=Q_{t+|F}+Q_{t-|F}$$

$$(V_{t+|E}-V_{te+})C_{t+|E}+(V_{t-|E}-V_{te-})C_{t-|E}=(V_{t+|F}-V_{te+})C_{t+|F}+(V_{t-|F}-V_{te-})C_{t-|F} \tag{87}$$

The contour of the circuit's formed closed loop constructs Kirchhoff's voltage law which helps determine final expressions for this period.

$$-V_{te+}+V_{t+|F}-V_{t-|F}+V_{te-}=0 \tag{88}$$

Equations 87 and 88 give a base for voltage equation derivations which are as follows:

$$V_{t+|F}=V_{t-|F}=\frac{C_{t-|F}V_{te+}-C_{t+|E}V_{te+}+C_{t+|F}V_{te+}-C_{t-|E}V_{te-}+C_{t-|E}V_{t-|E}+C_{t+|E}V_{t+|E}}{C_{t-|F}+C_{t+|F}}$$

$$V_{\mathrm{t}\mp}(t|_{\mathrm{E}\rightarrow\mathrm{F}})=\frac{C_{\mathrm{t}-|\mathrm{F}}V_{te+}-C_{\mathrm{t}+|\mathrm{E}}V_{\mathrm{te}+}+C_{\mathrm{t}+|\mathrm{F}}V_{\mathrm{te}+}-C_{\mathrm{t}-|\mathrm{E}}V_{\mathrm{te}-}}{C_{\mathrm{t}-|\mathrm{F}}+C_{\mathrm{t}+|\mathrm{F}}}+\frac{C_{\mathrm{t}-|\mathrm{E}}V_{\mathrm{t}-}(t|_{\mathrm{E}\rightarrow\mathrm{F}})+C_{\mathrm{t}+|\mathrm{E}}V_{\mathrm{t}+}(t|_{\mathrm{E}\rightarrow\mathrm{F}})}{C_{\mathrm{t}-|\mathrm{F}}+C_{\mathrm{t}+|\mathrm{F}}}$$

From F^{i} to A^{i+1}

$$Q_{\mathrm{tot}|\mathrm{F}}=Q_{\mathrm{tot}|\mathrm{A}^{\mathrm{i}+1}}$$

$$Q_{\mathrm{t}+|\mathrm{F}}+Q_{\mathrm{t}-|\mathrm{F}}+Q_{\mathrm{st}}=Q_{\mathrm{t}+|\mathrm{A}^{\mathrm{i}+1}}+Q_{\mathrm{t}-|\mathrm{A}^{\mathrm{i}+1}}+Q_{\mathrm{st}|\mathrm{A}^{\mathrm{i}+1}}$$

$$C_{\mathrm{t+|F}}(V_{\mathrm{t+|F}} - V_{\mathrm{te+}}) + C_{\mathrm{t-|F}}(V_{\mathrm{t-|F}} - V_{\mathrm{te-}}) + C_{\mathrm{st}}V_{\mathrm{st|F}} = C_{\mathrm{max}}(V_{\mathrm{t+|A^{i+1}}} - V_{\mathrm{te+}}) + C_{\mathrm{min}}(V_{\mathrm{t-|A^{i+1}}} - V_{\mathrm{te-}}) + C_{\mathrm{st}}V_{\mathrm{st|A_{i+1}}}$$

From the fact that the three capacitors are now connected in parallel, we can conclude that they are at the equipontential point.

$$V_{\mathrm{t+|A^{i+1}}} = V_{\mathrm{t-|A^{i+1}}} = V_{\mathrm{st|A^{i+1}}} = V_{\mathrm{A^{i+1}}}$$

Finally, the expression of the terminal voltage of the i^{th} QV cycle and the initial voltage of the $i+1^{st}$ cycle, that characterises all the capacitors can be developed as:

$$V_{\mathrm{A^{i+1}}} = \frac{C_{\mathrm{t+|F}}(V_{\mathrm{t+|F}} - V_{\mathrm{te+}}) + C_{\mathrm{t-|F}}(V_{\mathrm{t-|F}} - V_{\mathrm{te-}}) + C_{\mathrm{st}}V_{\mathrm{st|F}} + C_{\mathrm{max}}V_{\mathrm{te+}} + C_{\mathrm{min}}V_{\mathrm{te-}}}{C_{\mathrm{max}} + C_{\mathrm{min}} + C_{\mathrm{st}}}$$

The total charge at the moment A^{i+1} is equal to the sum of the individual charges over each capacitor. The expression for individual charge levels are:

$$Q_{\mathrm{t+|A^{i+1}}} = C_{\mathrm{max}}\frac{C_{\mathrm{t+|F}}(V_{\mathrm{t+|F}} - V_{\mathrm{te+}}) + C_{\mathrm{t-|F}}(V_{\mathrm{t-|F}} - V_{\mathrm{te-}}) + C_{\mathrm{st}}V_{\mathrm{st|F}} + C_{\mathrm{max}}V_{\mathrm{te+}} + C_{\mathrm{min}}V_{\mathrm{te-}}}{C_{\mathrm{max}} + C_{\mathrm{min}} + C_{\mathrm{st}}} - C_{\mathrm{max}}V_{\mathrm{te+}}$$

$$Q_{\mathrm{t-|A^{i+1}}} = C_{\mathrm{min}}\frac{C_{\mathrm{t+|F}}(V_{\mathrm{t+|F}} - V_{\mathrm{te+}}) + C_{\mathrm{t-|F}}(V_{\mathrm{t-|F}} - V_{\mathrm{te-}}) + C_{\mathrm{st}}V_{\mathrm{st|F}} + C_{\mathrm{max}}V_{\mathrm{te+}} + C_{\mathrm{min}}V_{\mathrm{te-}}}{C_{\mathrm{max}} + C_{\mathrm{min}} + C_{\mathrm{st}}} - C_{\mathrm{min}}V_{\mathrm{te-}}$$

$$Q_{\mathrm{st|A^{i+1}}} = C_{\mathrm{st}}\frac{C_{\mathrm{t+|F}}(V_{\mathrm{t+|F}} - V_{\mathrm{te+}}) + C_{\mathrm{t-|F}}(V_{\mathrm{t-|F}} - V_{\mathrm{te-}}) + C_{\mathrm{st}}V_{\mathrm{st|F}} + C_{\mathrm{max}}V_{\mathrm{te+}} + C_{\mathrm{min}}V_{\mathrm{te-}}}{C_{\mathrm{max}} + C_{\mathrm{min}} + C_{\mathrm{st}}}$$

And finally, $Q_{\mathrm{tot|A^{i+1}}}$ is defined by the following expression

$$Q_{\mathrm{tot|A^{i+1}}} = \frac{C_{\mathrm{t+|F}}(V_{\mathrm{t+|F}} - V_{\mathrm{te+}}) + C_{\mathrm{t-|F}}(V_{\mathrm{t-|F}} - V_{\mathrm{te-}}) + C_{\mathrm{st}}V_{\mathrm{st|F}} + C_{\mathrm{max}}V_{\mathrm{te+}} + C_{\mathrm{min}}V_{\mathrm{te-}}}{C_{\mathrm{max}} + C_{\mathrm{min}} + C_{\mathrm{st}}} (C_{\mathrm{max}} + C_{\mathrm{min}} + C_{\mathrm{st}}) - C_{\mathrm{min}}V_{\mathrm{te-}} - C_{\mathrm{max}}V_{\mathrm{te+}}$$

The moment A^{i+1} is at the same time the terminal point of the i^{th} cycle and the starting point of the $i+1^{st}$ cycle. Each cycle starts at predefined voltage and charge levels based on the previous cycle and at its end it sets values for the next cycle. The increase from start to the end of the mechanical and QV cycles provides the proof of the fundamental principle of Bennet's charge doubler. By examining derived equations and principles of Bennet's charge doubler,

there is no limit or, so called, saturation point by which cycle-to-cycle energy conversion increase would be restricted.

Capacitance ratio condition for the circuit

$$V^i_{\mathrm{t+|B}} = V^i_{\mathrm{t-|B}} + V^i_{\mathrm{st|B}}$$

Substituting $V^i_{\mathrm{t+|B}}$ and $V^i_{\mathrm{t-|B}}$ with the expressions derived previously at subsection 2.1.

$$\frac{C_{\max}}{C^i_{\mathrm{t+|B}}}(V^i_{\mathrm{t+|A}} - V_{\mathrm{te+}}) - V_{\mathrm{te+}} = \frac{C_{\min}}{C^i_{\mathrm{t-|B}}}(V^i_{\mathrm{t+|A}} - V_{\mathrm{te+}}) - V_{\mathrm{te-}} + V^i_{\mathrm{t+|A}}$$

$$\frac{C_{\max}}{C^i_{\mathrm{t+|B}}}(V^i_{\mathrm{t+|A}} - V_{\mathrm{te+}}) - \frac{C_{\min}}{C^i_{\mathrm{t-|B}}}(V^i_{\mathrm{t+|A}} - V_{\mathrm{te+}}) = V^i_{\mathrm{t+|A}} + V_{\mathrm{te+}} - V_{\mathrm{te-}}$$

If we consider that $V_{\mathrm{te+}} = V_{\mathrm{te-}} = V_{\mathrm{te}}$ the above equation can be simplified.

$$(V^i_{\mathrm{t+|A}} - V_{\mathrm{te}})(\frac{C_{\max}}{C^i_{\mathrm{t+|B}}} - \frac{C_{\min}}{C^i_{\mathrm{t-|B}}}) = V^i_{\mathrm{t+|A}} + V_{\mathrm{te+}} - V_{\mathrm{te-}}$$

$$\frac{C_{\max}}{C^i_{\mathrm{t+|B}}} - \frac{C_{\min}}{C^i_{\mathrm{t-|B}}} = \frac{V^i_{\mathrm{t+|A}}}{V^i_{\mathrm{t+|A}} - V_{\mathrm{te}}}$$

$$\frac{C_{\max}}{C^*} - \frac{C}{C^{**}} = \frac{V^i_{\mathrm{t+|A}}}{V^i_{\mathrm{t+|A}} - V_{\mathrm{te}}}$$

$$\frac{\frac{C_0}{1-\alpha}}{\frac{C_0}{1-\alpha\cos(\omega t_{\mathrm{B}})}} - \frac{\frac{C_0}{1+\alpha}}{\frac{C_0}{1+\alpha\cos(\omega t_{\mathrm{B}})}} = \frac{V^i_{\mathrm{t+|A}}}{V^i_{\mathrm{t+|A}} - V_{\mathrm{te}}}$$

$$\frac{1-\alpha\cos(\omega t_{\mathrm{B}})}{1-\alpha} - \frac{1+\alpha\cos(\omega t_{\mathrm{B}})}{1+\alpha} = \frac{V^i_{\mathrm{t+|A}}}{V^i_{\mathrm{t+|A}} - V_{\mathrm{te}}}$$

$$\frac{2\alpha - 2\alpha\cos(\omega t_{\mathrm{B}})}{1-\alpha^2} = \frac{V^i_{\mathrm{t+|A}}}{V^i_{\mathrm{t+|A}} - V_{\mathrm{te}}}$$

$$V^i_{\mathrm{t+|A}}(1-\alpha^2) = (V^i_{\mathrm{t+|A}} - V_{te})(2\alpha - 2\alpha\cos(\omega t_{\mathrm{B}}))$$

$$cos(\omega t_{\mathrm{B}}) = 1 + \frac{V^i_{\mathrm{t+|A}}}{V^i_{\mathrm{t+|A}} - V_{\mathrm{te}}}\frac{1-\alpha^2}{2\alpha}$$

To ensure the integrity of the QV cycle it is necessary to set conditions on α and, therefore $cos(\omega t_{\mathrm{B}})$ which has to be greater than -1.

$$\cos(\omega t_{\mathrm{B}}) > -1$$

The marginal case is the one when $cos(\omega t_{\mathrm{B}})) = -1$ leading to $\alpha_{\min}$ expression.

$$\cos(\omega t_{\mathrm{B}}) = 1 + \frac{V^i_{\mathrm{t+|A}}}{V^i_{\mathrm{t+|A}} - V_{\mathrm{te}}} \frac{1 - {\alpha_{\min}}^2}{2\alpha_{\min}} = -1$$

$$\frac{1 - {\alpha_{\min}}^2}{2\alpha_{\min}} = -\frac{2}{\frac{V^i_{\mathrm{t+|A}}}{V^i_{\mathrm{t+|A}} - V_{\mathrm{te}}}}$$

The expression can be simplified by substituting

$$\frac{V^i_{\mathrm{t+|A}}}{V^i_{\mathrm{t+|A}} - V_{\mathrm{te}}} = \delta$$

which than transforms it into the following equation.

$$\frac{1 - {\alpha_{\min}}^2}{2\alpha_{\min}} = -\frac{2}{\delta}$$

$$\delta(1 - {\alpha_{\min}}^2) = -4\alpha_{\min}$$

$$-\delta{\alpha_{\min}}^2 + 4\alpha_{\min} + \delta = 0$$

From here, we can make a concluding expression of the $\alpha_{\min}$.

$$\alpha_{\min} = -\frac{2}{\delta} + \sqrt{\frac{4}{\delta^2} + 1}$$

Appendix B

Wolfram Mathematica script designed for the calculation of theoretical analysis

Integral Equations for tracing QV Cycle of double variable Bennet

This is a file containing all the equations and their derivations to obtain a QV cycle of a double variable Bennet' s doubler .
There are following sections:

- Segment form A to B
- Segment form B to D static - moment D
- Dynamic part from B to D
- First charge exchange (occurring form B to D)
- From D to E (with focus on moment E)
- From E to F (focuses on point F)
- From F to A^(i+1) (focuses on point A^(i+1))

Segment from A to B

For this interval of operation it is expected to have a constant charge and change in voltage . Specifically, increase of voltage for the positive TENG part and decrease of voltage for other capacitor of the TENG . Knowing that at the initial moments capacitances CtpA and CtmA are Cmax and Cmin, respectively, we can substitute them in equations and simplify the expressions, and obtain solutions for capacitance and voltage at point B.

```
In[ ]:= Remove["Global`*"]
Replace[Solve[CtpA ( VtpA - Vte) == CtpB (VtpB - Vte), CtpB],
 CtpA → Cmax, Infinity]
Simplify[Replace[
   Solve[CtpA ( VtpA - Vte) == CtpB (VtpB - Vte), VtpB], CtpA → Cmax, Infinity]]
Replace[Solve[CtmA (VtmA - Vtm) == CtmB (VtmB - Vtm), CtmB], CtmA → Cmin, Infinity]
Simplify[
 Replace[Solve[CtmA (VtmA - Vtm) == CtmB (VtmB - Vtm), VtmB], CtmA → Cmin, Infinity]]
```

$$\text{Out[ ]=}\quad \left\{\left\{\text{CtpB} \to \frac{\text{Cmax}\ (\text{Vte} - \text{VtpA})}{\text{Vte} - \text{VtpB}}\right\}\right\}$$

$$\text{Out[ ]=}\quad \left\{\left\{\text{VtpB} \to \text{Vte} + \frac{\text{Cmax}\ (-\text{Vte} + \text{VtpA})}{\text{CtpB}}\right\}\right\}$$

$$\text{Out[ ]=}\quad \left\{\left\{\text{CtmB} \to \frac{\text{Cmin}\ (\text{Vtm} - \text{VtmA})}{\text{Vtm} - \text{VtmB}}\right\}\right\}$$

$$\text{Out[ ]=}\quad \left\{\left\{\text{VtmB} \to \text{Vtm} + \frac{\text{Cmin}\ (-\text{Vtm} + \text{VtmA})}{\text{CtmB}}\right\}\right\}$$

Segment form B to D static - moment D

```
In[ ]:= Remove["Global`*"]
        eq1 = Cmax * α + Cmin * β == Cmin * (VtpD - Vtep) + Cmax * (VtmD - Vtem)
        eq2 = Cst * V - Cmin * β == Cst * VstD - Cmax * (VtmD - Vtem)
        eq3 = VtpD == VtmD + VstD - δV
```

$$\text{Cmax}\,\alpha + \text{Cmin}\,\beta == \text{Cmax}\,(-\text{Vtem} + \text{VtmD}) + \text{Cmin}\,(-\text{Vtep} + \text{VtpD})$$

$$\text{Cst}\,\text{V} - \text{Cmin}\,\beta == \text{Cst}\,\text{VstD} - \text{Cmax}\,(-\text{Vtem} + \text{VtmD})$$

$$\text{VtpD} == \text{VstD} + \text{VtmD} - \delta\text{V}$$

```
In[ ]:= Simplify[Solve[eq1 && eq2 && eq3, {VtpD, VtmD, VstD}]]
```

$$\left\{\left\{\text{VtpD} \to \frac{\text{Cmax Cmin Vtep} + \text{Cmax}^2\,\alpha + \text{Cmin Cst}\,(\text{Vtep} + \beta) + \text{Cmax Cst}\,(\text{V} + \text{Vtem} + \alpha - \delta\text{V})}{\text{Cmin Cst} + \text{Cmax}\,(\text{Cmin} + \text{Cst})},\right.\right.$$

$$\text{VtmD} \to \frac{\text{Cmax Cmin Vtem} + \text{Cmax Cst}\,(\text{Vtem} + \alpha) + \text{Cmin}^2\,\beta + \text{Cmin Cst}\,(-\text{V} + \text{Vtep} + \beta + \delta\text{V})}{\text{Cmin Cst} + \text{Cmax}\,(\text{Cmin} + \text{Cst})},$$

$$\left.\left.\text{VstD} \to \frac{\text{Cmax Cst V} + \text{Cmax}^2\,\alpha + \text{Cmin}\,(\text{Cst V} - \text{Cmin}\,\beta) + \text{Cmax Cmin}\,(-\text{Vtem} + \text{Vtep} + \delta\text{V})}{\text{Cmin Cst} + \text{Cmax}\,(\text{Cmin} + \text{Cst})}\right\}\right\}$$

eq1 is based on the conservation of charge at the node of theTENG
eq2 is based on the conservation at the node between the TENG and storage capacitor
eq3 is based on the Kirchhoff's voltage law for this circuit construction
To check if these equations are correct, it is easiest to compare their results with expected results for values that are most commonly used in practice.

In[ ]:=
```
α = V - Vte;
β = V - Vtem;
δV = Vte - Vtem;
d = 50 * 10^-6;
x = 30 * 10^-6;
e = 2.1;
ϵ = 8.854 * 10^-9;
Cmax = 929.67 * 10^-12;
Cmin = 411.358 × 10^-12;
Cst = 10 * 10^-9;
Vtep = 26.89;
Vtem = 26.89;
V = 16;
s = 0.0025;
VtpD = (Cmax Cmin Vtep + Cmax^2 α + Cmin Cst (Vtep + β) + Cmax Cst (V + Vtem + α - δV)) / (Cmin Cst + Cmax (Cmin + Cst))
VtmD = (Cmax Cmin Vtem + Cmax Cst (Vtem + α) + Cmin^2 β + Cmin Cst (-V + Vtep + β + δV)) / (Cmin Cst + Cmax (Cmin + Cst))
VstD = (Cmax Cst V + Cmax^2 α + Cmin (Cst V - Cmin β) + Cmax Cmin (-Vtem + Vtep + δV)) / (Cmin Cst + Cmax (Cmin + Cst))
```

Out[ ]= 26.404

Out[ ]= 11.3965

Out[ ]= 15.0076

Dynamic B to D - the charge exchange curve

A similar set of equations as in previous subsection is used with the difference that following lines are not just expressions that are combinations of multiple variables, but functions . As per QV cycle the evolution of charge and capacitance and their mutual relationship, both of them are time dependent . Therefore, the following functions are time dependent and containing variables that are time dependent.

In[ ]:=
```
Remove["Global`*"]
A[t_] := C_max * (V_t|A^i - V_te) + C_min * (V_t|A^i - V_tem) ==
  C_p[t] * (V_tp[t] - V_te) + C_m[t] * (V_tp[t] - V_tem)
B[t_] := C_st * V_t|A^i - C_min * (V_t|A^i - V_tem) ==
  C_st * (V_te + V_tem - V_tm[t] + V_tp[t]) - C_m[t] * (V_tm[t] - V_tem)
F[t_] := V_tp[t] == V_tm[t] + V_st[t] - V_te - V_tem
```

In[ ]:=
```
Solve[V_tp[t] == V_tm[t] + V_st[t] - V_te - V_tem, {V_st[t]}]
```

Out[ ]= $\{\{V_{st}[t] \to V_{te} + V_{tem} - V_{tm}[t] + V_{tp}[t]\}\}$

In[•]:=
```
Simplify[Solve[Cmax * (Vt|A^i - Vte) + Cmin * (Vt|A^i - Vtem) == Cp[t] * (Vtp[t] - Vte) +
    Cm[t] * (Vtp[t] - Vtem) && Cst * Vt|A^i - Cmin * (Vt|A^i - Vtem) ==
   Cst * (Vte + Vtem - Vtm[t] + Vtp[t]) - Cm[t] * (Vtm[t] - Vtem), {Vtp[t], Vtm[t]}]]
```

Out[•]=
$$\left\{\left\{V_{tp}[t] \to \frac{C_{max}\left(-V_{te}+V_{t|A}^{i}\right)+C_{min}\left(-V_{tem}+V_{t|A}^{i}\right)+V_{tem}\,C_m[t]+V_{te}\,C_p[t]}{C_m[t]+C_p[t]},\right.\right.$$
$$V_{tm}[t] \to \left(C_{max}\,C_{st}\left(-V_{te}+V_{t|A}^{i}\right)+C_{st}\,V_{te}\,C_m[t]+2\,C_{st}\,V_{tem}\,C_m[t]-C_{st}\,V_{t|A}^{i}\,C_m[t]+\right.$$
$$V_{tem}\,C_m[t]^2+2\,C_{st}\,V_{te}\,C_p[t]+C_{st}\,V_{tem}\,C_p[t]-C_{st}\,V_{t|A}^{i}\,C_p[t]+V_{tem}\,C_m[t]\,C_p[t]+$$
$$\left.\left.\left.C_{min}\left(-V_{tem}+V_{t|A}^{i}\right)\left(C_{st}+C_m[t]+C_p[t]\right)\right)\Big/\left(\left(C_{st}+C_m[t]\right)\left(C_m[t]+C_p[t]\right)\right)\right\}\right\}$$

Section fro D to E

For the interval from D to E when it is presumed that charge is constant, a general charge conservation law yields expressions for voltage and capacitance at point E for both TENG capacitors .

In[•]:=
```
Replace[Solve[CtpD ( VtpD - Vte) == CtpE (VtpE - Vte), CtpE], CtpD → Cmin, Infinity]
Simplify[Replace[
   Solve[CtpD ( VtpD - Vte) == CtpE (VtpE - Vte), VtpE], CtpD → Cmin, Infinity]]
Replace[Solve[CtmD (VtmD - Vtm) == CtmE (VtmE - Vtm), CtmE], CtmD → Cmax, Infinity]
Simplify[
 Replace[Solve[CtmD (VtmD - Vtm) == CtmE (VtmE - Vtm), VtmE], CtmD → Cmax, Infinity]]
```

Out[•]=
$$\left\{\left\{CtpE \to \frac{Cmin\,(Vte - VtpD)}{Vte - VtpE}\right\}\right\}$$

Out[•]=
$$\left\{\left\{VtpE \to Vte + \frac{Cmin\,(-Vte + VtpD)}{CtpE}\right\}\right\}$$

Out[•]=
$$\left\{\left\{CtmE \to \frac{Cmax\,(Vtm - VtmD)}{Vtm - VtmE}\right\}\right\}$$

Out[•]=
$$\left\{\left\{VtmE \to Vtm + \frac{Cmax\,(-Vtm + VtmD)}{CtmE}\right\}\right\}$$

Section From E to F

Same as in previous sections, the equations are derived from charge conservation law at nodes that are formed for that circuit construction .

In[•]:=
```
Remove["Global`*"]
EqOne = Ctpe (Vtpe - Vte) + Ctme (Vtme - Vtem) == Ctpf (Vtpf - Vte) + Ctmf (Vtmf - Vtem)
EqTwo = -Vte + Vtpf - Vtmf + Vtem == 0
EqOneM = Ctpe (Vtpe) + Ctme (Vtme) == Ctpf (Vtpf) + Ctmf (Vtmf)
EqTwoM = Vtpf - Vtmf == 0
```

- Equations EqOneM and EqTwoM exist for the case when triboelectric layer is not present, therefore there is no Vte-s to be taken in account. (Not actively used now)

Out[•]=
$$C_{tmE}\,(-V_{tem}+V_{tmE})+C_{tpE}\left(-V_{te}+V_{tpE}\right) == C_{tmF}\,(-V_{tem}+V_{tmF})+C_{tpF}\left(-V_{te}+V_{tpF}\right)$$

Out[ ]= $-V_{te}+V_{tem}-V_{tmF}+V_{tpF}==0$

Out[ ]= $C_{tmE}\,V_{tmE}+C_{tpE}\,V_{tpE}==C_{tmF}\,V_{tmF}+C_{tpF}\,V_{tpF}$

Out[ ]= $-V_{tmF}+V_{tpF}==0$

In[ ]:=
```
Solve [EqOne && EqTwo, {VtpF, VtmF}]
```

Out[ ]= $\left\{\left\{V_{tpF}\to -\frac{-C_{tmF}\,V_{te}+C_{tpE}\,V_{te}-C_{tpF}\,V_{te}+C_{tmE}\,V_{tem}-C_{tmE}\,V_{tmE}-C_{tpE}\,V_{tpE}}{C_{tmF}+C_{tpF}},\right.\right.$

$\left.\left.V_{tmF}\to -\frac{C_{tpE}\,V_{te}+C_{tmE}\,V_{tem}-C_{tmF}\,V_{tem}-C_{tpF}\,V_{tem}-C_{tmE}\,V_{tmE}-C_{tpE}\,V_{tpE}}{C_{tmF}+C_{tpF}}\right\}\right\}$

Dynamic Analysis of segment E to F

As for the previous nonlinear segment, functions will be employed . They are based on equations from previous section. Capacitance variation is time dependent as well as some voltages. To be specific, the ones that are varying in the specific time interval, for example VtmF which corresponds to “negative” TENG part’s voltage in this interval which is varying.

In[ ]:=
```
A[t_] := CtpE (VtpE) + CtmE (VtmE) == CtpF[t] (VtpF[t]) + CtmF[t] (VtmF[t])
B[t_] := -Vte + VtpF[t] - VtmF[t] + Vtem == 0
Solve [A[t] && B[t], {VtpF[t], VtmF[t]}]
```

Out[ ]= $\left\{\left\{\text{VtpF}[t]\to -\frac{-\text{CtmE VtmE}-\text{CtpE VtpE}-\text{Vte CtmF}[t]+\text{Vtem CtmF}[t]}{\text{CtmF}[t]+\text{CtpF}[t]},\right.\right.$

$\left.\left.\text{VtmF}[t]\to -\frac{-\text{CtmE VtmE}-\text{CtpE VtpE}+\text{Vte CtpF}[t]-\text{Vtem CtpF}[t]}{\text{CtmF}[t]+\text{CtpF}[t]}\right\}\right\}$

Segment form F to A (i + 1)

- The two equations that are necessary to be resolved for this time interval are:
  - Charge conservation law - sum of all the charge in the circuit at the moment F has to be equal to sum of all the charge in the circuit at the moment A(i+1)
  - Because of the topology of the circuit at this time interval (all three capacitors are in parallel), voltages across all three capacitors at the moment A(i+1) are equal

In[ ]:=
```
Refine[Solve[CtpF (VtpF - P) + CtmF (VtmF - M) + Cst VstF ==
    Cmax (VtpA - P) + Cmin (VtpA - M) + Cst VtpA, {VtpA}]]
```

Out[ ]= $\left\{\left\{V_{tpA}\to \frac{P\,C_{max}+M\,C_{min}-M\,C_{tmF}-P\,C_{tpF}+C_{st}\,V_{stF}+C_{tmF}\,V_{tmF}+C_{tpF}\,V_{tpF}}{C_{max}+C_{min}+C_{st}}\right\}\right\}$

Calculate Maximum Voltage

- To find maximum voltage of one QV cycle, it is necessary to take a parametric derivative of the curve. Because all the expressions are time dependent, it is necessary to go back to the initial forms of voltage and charge for this time interval.

In[•]:=
```
Remove["Global`*"]
Vtp[t_] := (Cmin Cst (VA - Vtem) + Cst VA Ctm[t] - Cst Vte Ctm[t] + 2 Cst Vtem Ctm[t] +
    Cmax (VA - Vte) (Cst + Ctm[t]) + Cst Vte Ctp[t] + Vte Ctm[t] Ctp[t]) /
  (Ctm[t] Ctp[t] + Cst (Ctm[t] + Ctp[t]))
z[t_] := Replace[Vtp[t],
  {Ctm[t] → ϵ s / (d/e + x/2 + x/2 Cos[2 Pi f t]), Ctp[t] → ϵ s / (d/e + x/2 - x/2 Cos[2 Pi f t])}, Infinity]
Qtp[t_] := Ctp[t] Vtp[t]
j[t_] := Replace[Qtp[t],
  {Ctm[t] → ϵ s / (d/e + x/2 + x/2 Cos[2 Pi f t]), Ctp[t] → ϵ s / (d/e + x/2 - x/2 Cos[2 Pi f t])}, Infinity]
G[t_] := z'[t] / j'[t]
sol = Simplify[Solve[G[t] == 0, t]]
```

- parametric derivative of the curve according to y-axis is actually equal to derivative of voltage divided by derivative of charge.The point at which the derivative is equal to zero corresponds to the point of maximum voltage

Out[•]=

$$\left\{\left\{t \to \frac{\text{ArcTan}\left[1+\frac{2\,d}{e\,x},\ -\frac{2\sqrt{-d\,(d+e\,x)}}{e\,x}\right]+2\,\pi\,c_1}{2\,f\,\pi}\ \text{if}\ c_1 \in \mathbb{Z}\right\},\right.$$

$$\left\{t \to \frac{\text{ArcTan}\left[1+\frac{2\,d}{e\,x},\ \frac{2\sqrt{-d\,(d+e\,x)}}{e\,x}\right]+2\,\pi\,c_1}{2\,f\,\pi}\ \text{if}\ c_1 \in \mathbb{Z}\right\},\ \left\{t \to \frac{1}{2\,f\,\pi}\left(\text{ArcTan}\left[-\frac{s \in \left(C_{max}\,\left(V_A - V\right.\right.\right.\right.$$

$$\left.\left.\left.\left.x\,C_{st}\,\left(C_{max}\,\left(V\right.\right.\right.\right.\right.$$

$$-\left(\left(\sqrt{\left(-C_{max}^2\,\left(s^2\,\in^2 - x^2\,C_{st}^2\right.\right.\right.\right.$$

$$\left.\left.\left.\left.\left(s^2\,\in^2 - x^2\,C_{min}\right.\right.\right.\right.$$

$$\left.\left.\left.\left.C_{st}^2\,\left(\left(-s^2\,\in^2 + x^2\right.\right.\right.\right.\right.$$

$$\left.\left.\left.\left.V_{tem}^2 + V_A\,\left(4\right.\right.\right.\right.\right.$$

$$\left.\left.\left.\left.\left(\sqrt{x^2\,C_{st}^2\,\left(C_{max}\,\left(V_A - V_t\right.\right.\right.\right.\right.\right.$$

$$\frac{1}{2\,f\,\pi}\left(\text{ArcTan}\left[-\frac{s \in \left(C_{max}\,\left(V_A - V_{te}\right) + C_{st}\,\left(V_A - 2\,V_{te} + 2\,V_{tem}\right)\right)}{x\,C_{st}\,\left(C_{max}\,\left(V_A - V_{te}\right) + C_{min}\,\left(V_A - V_{tem}\right)\right)},\right.\right.$$

$$\left(\sqrt{\left(-C_{max}^2\,\left(s^2\,\in^2 - x^2\,C_{st}^2\right)\,\left(V_A - V_{te}\right)^2 - 2\,C_{max}\,C_{st}\,\left(V_A - V_{te}\right)\right.\right.}$$

$$\left(\left(s^2\,\in^2 - x^2\,C_{min}\,C_{st}\right)\,V_A - 2\,s^2\,\in^2 V_{te} + \left(2\,s^2\,\in^2 + x^2\,C_{min}\,C_{st}\right)\,V_{tem}\right) +$$

$$C_{st}^2\,\left(\left(-s^2\,\in^2 + x^2\,C_{min}^2\right)\,V_A^2 - 4\,s^2\,\in^2 V_{te}^2 + 8\,s^2\,\in^2 V_{te}\,V_{tem} +\right.$$

$$\left.\left.\left.\left(-4\,s^2\,\in^2 + x^2\,C_{min}^2\right)\,V_{tem}^2 + V_A\,\left(4\,s^2\,\in^2 V_{te} - 2\,\left(2\,s^2\,\in^2 + x^2\,C_{min}^2\right)\,V_{tem}\right)\right)\right)\Big/$$

$$\left.\left.\left.\left(\sqrt{x^2\,C_{st}^2\,\left(C_{max}\,\left(V_A - V_{te}\right) + C_{min}\,\left(V_A - V_{tem}\right)\right)^2}\right)\right] + 2\,\pi\,c_1\right)\ \text{if}\ c_1 \in \mathbb{Z}\right\}$$

$$\left.\right\}$$

- As the derivation is complex, it yielded a few solutions for the possible times at which maximum voltage occurs. Based on the logical conclusions like that time can not be negative and that the system has to be causal, there is only one possibility for the time expression, which is obtained by inputting realistic values from one of the experiments/simulations . Once a correct time expression is selected, it can be substituted into voltage equation and the expression for maximum voltage is obtained.

In[]:=
```
d = 50 * 10^-6;
x = 30 * 10^-6;
e = 2.1;
ϵ = 8.854 * 10^-9;
C_max = 929.67 * 10^-12;
C_min = 411.358 × 10^-12;
C_st = 10 * 10^-9;
V_te = 26.89;
V_tem = 26.89;
V_A = 10;
s = 0.0025;
sol
```

Out[]=
$$\left\{\left\{t \to \frac{(0. - 1.60413\,i) + 2\,\pi\,C_1}{2\,f\,\pi} \text{ if } C_1 \in \mathbb{Z}\right\}, \left\{t \to \frac{(0. + 1.60413\,i) + 2\,\pi\,C_1}{2\,f\,\pi} \text{ if } C_1 \in \mathbb{Z}\right\},\right.$$
$$\left.\left\{t \to \frac{(0. - 6.30848\,i) + 2\,\pi\,C_1}{2\,f\,\pi} \text{ if } C_1 \in \mathbb{Z}\right\}, \left\{t \to \frac{(0. + 6.30848\,i) + 2\,\pi\,C_1}{2\,f\,\pi} \text{ if } C_1 \in \mathbb{Z}\right\}\right\}$$

In[]:=
$$t\,(V_{max}) = \frac{\tan^{-1}\left(1 + \frac{2\,d_{die}}{\epsilon_r\,X_{max}}, -\frac{2\,\sqrt{-d_{die}\,(d_{die}+\epsilon_r\,X_{max})}}{\epsilon_r\,X_{max}}\right)}{2\,f\,\pi}$$

$$V_{t+}\,(V_{max}) = -\frac{-2\,C_{max}\,V_A + 2\,C_{max}\,V_{te} - C_{min}\,V_{te+} - V_{te+}\,\frac{\epsilon_0\,s}{\frac{d_{die}}{\epsilon_r} + \frac{X_{max}}{2} - \frac{X_{max}}{2}\,\text{Cos}[2\,\text{Pi}\,f\,t]}}{C_{min} + \frac{\epsilon\,s}{\frac{d_{die}}{\epsilon_r} + \frac{X_{max}}{2} - \frac{X_{max}}{2}\,\text{Cos}[2\,\text{Pi}\,f\,t]}}$$

Appendix C

:

LTspice netlist used for simulations

```
1
2  ;Simulation of a gap-closing TENG with Bennet circuit
3  ; TENG PARAMETERS
4  .param eps0=8.854p er=2.1 ddie=300u ro=-10u s=0.0081
5  .param Xmax=1.2m
6
7  ;Cmin value change
8  ;.param a={a}
9  ;.step param a 0 1 0.1
10
11 Cteng+  Vteng Vte+   Q=(eps0*S/(ddie/er+Xmax/2-Xmax/2*cos(2*pi*Freq*
       time)))*x    ; Ct+
12 Cteng- Vteng Vte-  Q=(eps0*S/(ddie/er+Xmax/2-Xmax/2*(-cos(2*pi*Freq*
       time))))*x ; Ct-
13
14 ; VOLTAGE OF TRIBOELECTRIC LAYER
15 B Vte+  Vte+  0  V=ro*ddie/(eps0*er)
16 B Vte- Vte- N1 V=ro*ddie/(eps0*er)
17
18 ; BENNET CIRUCIT
19 D1 0 N1 diode
20 D2 N1 Vout diode
21 D3 Vout Vteng diode
22 Cout Vout 0 10n
23
24 ;DIODE MODELS
25 .model diode D (Vfwd=0.1)
26 ;.model diode D(Is=0.2n)
27 ;.model diode D(Is=25n N=2.81 Rs=.568 Ikf=0 Cjo=20p M=.3185 Vj=.75 Nr
       =2.08 Bv=835 Iave=0.400 Vpk=200 Ibv=5.000u mfg=Fair type=silicon) ;1
       n649
28
29 ;SIMULATION PARAMETERS
30 .param Freq=3 ; Frequency of the TENG
31 .tran 0 6.334 6 5us ; transient simulation
32
33 ; CHARGE THROUGH TRANSDUCER
34 BQteng+ Qteng+ 0 V= 81n + idt(I(Cteng+))
35 BQteng- Qtengm- 0 V= 81n + idt(I(Cteng-))
36
37 ; VISUALIZATION OF DISPLACEMENT
38 BXgap+  Xgap+  0   V=( S/2 -(S/2)*  cos(2*pi*Freq*time) )
39 BXgap- Xgap- 0   V=( S/2 -(S/2)* (-cos(2*pi*Freq*time)))
40
41 ; VISUALISATION OF CAPACITANCE
42 BCteng+  Cteng+  0 V =33p+ eps0*S/(ddie/er+Xmax/2-Xmax/2*cos(2*pi*Freq*
       time))
43 BCteng- Cteng- 0 V =33p+ eps0*S/(ddie/er+Xmax/2-Xmax/2*(-cos(2*pi*Freq*
```

```
   time)))

; ENERGY PER CYCLE
BWacc Wacc 0 V=10n*V(Vout)*V(Vout)/2

;Find the Cmax to Cmin ratio for the capacitance sweep of Cmin
;.PROBE V(cteng-).PLOT  TRAN V(ctengmoins)
;.MEAS TRAN cminus_maximum max V(cteng-)
;.MEAS TRAN cminus_manimum min V(cteng-)

;Find the Cmax to Cmin ratio of Ctengplus for the xmax sweep
;.PLOT  TRAN V(ctengplus) time
;.MEAS TRAN c_plus_maximum max V(ctengplus)
;.MEAS TRAN c_plus_manimum min V(ctengplus)
;.MEAS TRAN Vt min V(vout)

;Find the Cmax to Cmin ratio of Ctengplus for the xmax sweep
;.PROBE V(ctengplus)
;.PLOT  TRAN V(qtengplus) time
;.MEAS TRAN q_cplus_maximum max V(qtengplus)
;.MEAS TRAN q_cplus_manimum min V(qtengplus)

;.option plotwinsize=0 numdgt=15
.backanno
.end
```

Appendix D

:

PCB design of automatic measurement card

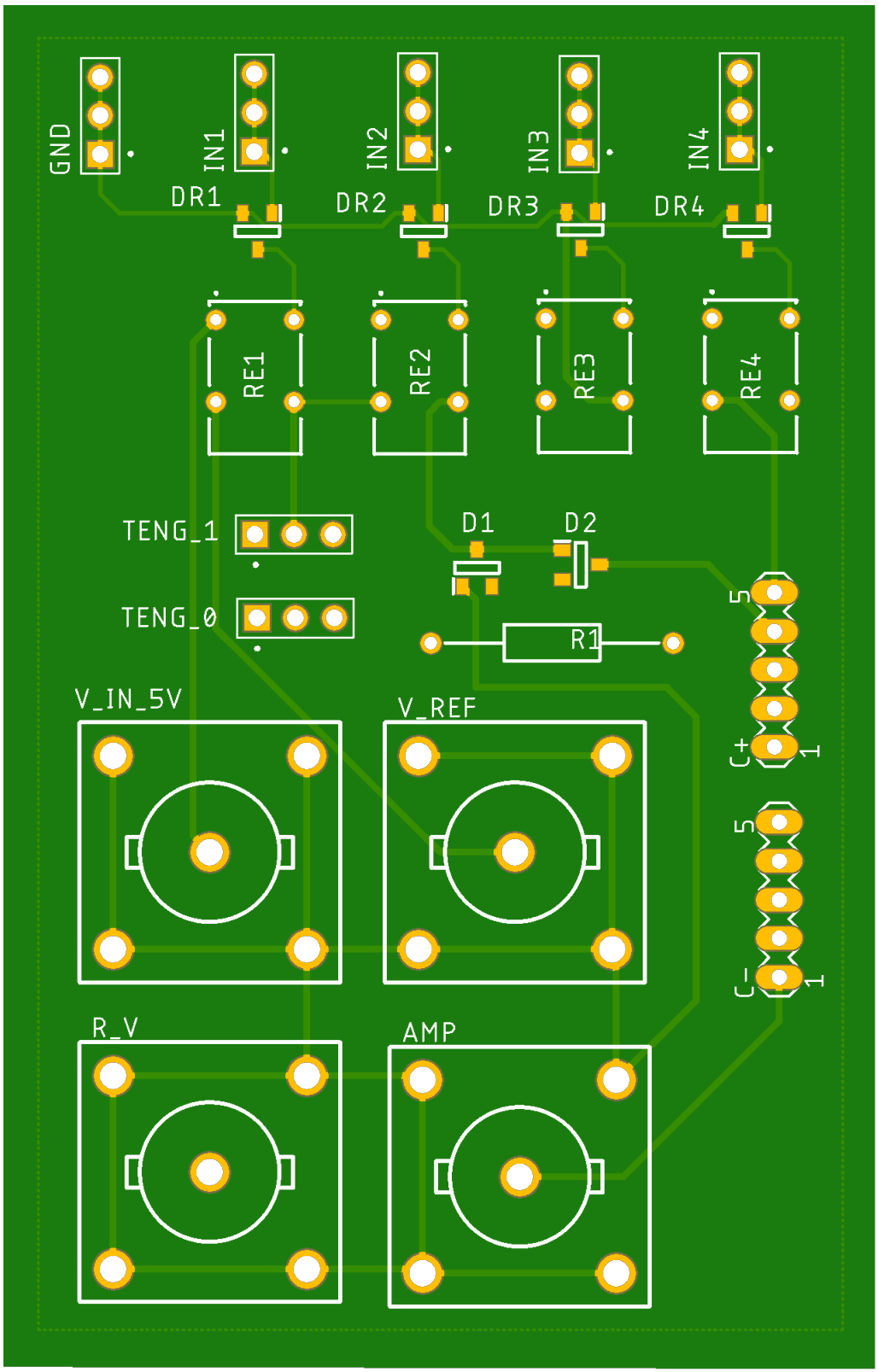
GND
IN1
IN2
IN3
IN4
DR1
DR2
DR3
DR4
RE1
RE2
RE3
RE4
TENG_1
TENG_0
D1
D2
R1
V_IN_5V
V_REF
R_V
AMP
C+
C-
5
1
5
1